

# The Blume-Capel model for spins $S = 1$ and $3/2$ in dimensions $d = 2$ and $3$

P. Butera\*

*Dipartimento di Fisica Università' di Milano-Bicocca  
and  
Istituto Nazionale di Fisica Nucleare  
Sezione di Milano-Bicocca  
3 Piazza della Scienza, 20126 Milano, Italy*

M. Pernici†

*Istituto Nazionale di Fisica Nucleare  
Sezione di Milano  
16 Via Celoria, 20133 Milano, Italy  
(Dated: November 4, 2018)*

Expansions through the 24th order at high-temperature and up to 11th order at low-temperature are derived for the main observables of the Blume-Capel model on bipartite lattices (*sq, sc* and *bcc*) in  $2d$  and  $3d$  with various values of the spin and in presence of a magnetic field. All expansion coefficients are computed exactly as functions of the crystal and magnetic fields. Several critical properties of the model are analyzed in the two most studied cases of spin  $S = 1$  and  $S = 3/2$ .

PACS numbers: 03.70.+k, 05.50.+q, 64.60.De, 75.10.Hk, 64.70.F-, 64.10.+h  
Keywords: Ising model, Blume-Capel model, tricritical phenomena

## I. INTRODUCTION

The Ising system with spin  $S = 1$ , subject to a uniform “single-ion-splitting crystal-field” (also called “anisotropy field”)<sup>1,2</sup>, in absence of magnetic field, is the simplest lattice spin-model exhibiting a tricritical<sup>3,4</sup> point (TCP), namely a point of the phase-boundary at which a smooth line of second-order phase-transitions undergoes a sudden change into a line of first-order transitions. It was originally studied by M. Blume and H.W. Capel<sup>1,2</sup> and thereby it is known as the Blume-Capel (BC) model. Extensions of the model featuring interactions of higher spins<sup>5,6</sup>, in particular of spin  $S = 3/2$ , were also considered in the literature.

The BC model has been explored in a variety of analytical approximations (mean field (MF), effective field, Renormalization Group, etc.)<sup>1,2,5–20</sup>, by transfer-matrix methods<sup>21–23</sup> and by MonteCarlo (MC) simulation methods<sup>14,20,24–39</sup>, but only in a handful of papers<sup>40–45</sup> extrapolations of series-expansions were employed, in spite of the potential reliability and accuracy of this technique. The high-temperature (HT) and the low-temperature (LT) expansions have been jointly used<sup>43</sup> to map out the phase diagram, (the former being generally sufficient to locate the second-order part of the phase-boundary and to determine its universal parameters, the latter being helpful for the first-order part).

This work fills a gap in the literature by contributing *exact* HT expansions (based on the computations of Ref. [46–48]), that reach the 24th order for the square (*sq*), simple cubic (*sc*) and body-centered cubic (*bcc*) lattices, *in presence of a magnetic field*, in the two most representative cases of the BC model with spin  $S = 1$  and  $S = 3/2$ . In the spin  $S = 1$  case, we have also computed *exact* LT expansions for the *sq* and the *sc* lattices through the 11th order, while our LT results reach only the 10th order for the *bcc* lattice. In the spin  $S = 3/2$  case, the LT expansions extend through the 9th order. All series coefficients, both at HT and LT, are expressed in a closed form as *explicit* functions of the crystal and magnetic fields. The analysis of these expansions leads to results directly comparable with those of the modern simulation studies, generally carried out on the simple cubic lattices in  $2d$  and  $3d$ . Moreover this work makes now possible to achieve high accuracy in the determination of the phase-boundaries, in the tests of universality of the critical exponents as well as of appropriate combinations of critical amplitudes, and to describe the dependence of the observables on the magnetic field, in regions of the model’s parameter-space that are wider than those covered by other numerical approaches.

The longest series expansions so far available, that date back to long ago, were limited to systems with spin  $S = 1$  on the (close-packed) face-centered-cubic (*fcc*) lattice<sup>40,41,43</sup>, *in absence* of magnetic field. At best<sup>43</sup>, the HT expansions extended only through the 12th order while the LT expansions reached the 7th. The results of their analysis are not comparable with those of the modern MC studies for the non-universal features such as the phase-contours, but are relevant only for the universal critical parameters. The *fcc* lattice was chosen because its non-bipartite nature entails

the absence of a nearby antiferromagnetic singularity in the complex plane of the inverse temperature and together with its large coordination-number  $q = 12$ , ensures smooth expansion-coefficient sequences. It was therefore hoped that reasonable series extrapolations might be performed in spite of the short order of the expansions.

Also for the bipartite lattices, at the time of Ref. [43], by employing essentially the same code, expansions might be derived with the same extension as for the *fcc* lattice and with the same limitations, but they were not. Only shorter expansions<sup>44</sup> through the 8th order were obtained in  $2d$  and  $3d$  for these lattices, but were not analyzed. In Ref.[42], HT expansions up to the 5th-order, valid for general spin on the *sc* and the *bcc* lattices, were briefly discussed, yielding qualitative indications. In conclusion, the state of the expansions for the *sq*, the *sc* and the *bcc* lattices has been so far inadequate, while substantial extensions and updates of the *fcc* lattice study remain desirable, but not as urgent.

The paper is organized as follows. Section II introduces the BC model with general spin  $S$  and sketches its main features. The following subsections recall the established results of the MF approximation, and contain a few comments on recent numerical studies to be later compared with ours. The following subsections describe some details of the algebraic structure of the HT and LT expansion coefficients and state the expected singular asymptotic behaviors of the thermodynamical quantities under scrutiny, to which reference is made in discussing the estimates of the critical parameters. This Section is supplemented by the Appendices A and B, the first one being a very detailed pedagogical reminder of the known methods and results of the MF approximation for each value of the spin considered in our study while the second one recalls known arguments about the tricritical scaling.

Section III contains a few general remarks on the analysis of the expansions, valid independently of the structure and dimension of the lattices considered, while the main properties of the numerical tools such as “modified ratio approximants”(MRA), “Padé approximants”(PA) and “differential approximants”(DA) employed to estimate the critical parameters of the model, are recalled in Appendix C.

In the Sections IV-VII, we discuss the results of our series analyses in dimension  $d = 2$ , and  $d = 3$  for spin  $S = 1$  and  $S = 3/2$  and compare them with the known closed-form expressions for the phase-boundaries in the MF approximation and with numerical results obtained by transfer-matrix in  $2d$  and/or by MC methods both in  $2d$  and in  $3d$ . In the Section VIII, we summarize our work and draw some conclusions.

## II. THE BC MODEL WITH SPIN $S$

An extensive discussion of tricriticality, covering a wide range of the physical situations in which it occurs and a thorough account of the numerous experimental and theoretical investigations of the BC model before 1984 can be found in the review paper[49], from which we have largely drawn throughout the paper.

The BC model is a simple representative<sup>49</sup> of a class of pure or disordered spin models capable of describing the phenomenology of a variety of physical systems, that includes liquid mixtures of  ${}^3\text{He}-{}^4\text{He}$ , many-component classical solutions<sup>3,4</sup>, antiferromagnets and metamagnets<sup>50</sup>, alloys of magnetic and non-magnetic materials<sup>51</sup>, ferroelectrics, liquid crystals and several others.

The BC model with spin  $S$  is defined by the reduced Hamiltonian

$$\frac{1}{k_B T} \mathcal{H}_N[s] = -\frac{K}{S^2} \sum_{\langle ij \rangle} s_i s_j + \frac{D}{S^2} \sum_i s_i^2 - \frac{h}{S} \sum_i s_i \quad (1)$$

The Hamiltonian  $\mathcal{H}_N[s]$  is evaluated in a finite lattice of volume  $N$ . The first sum on the right hand side, describing the nearest-neighbor spin-pair interaction, runs over all ordered links, while the second and third extend to all sites. If  $S = 1$ , the spin  $s_i$  at the site  $i$  can take the values  $s_i = \pm 1, 0$ . In the  $S = 3/2$  case also discussed here, the spins can take the values  $s_i = \pm 1/2, \pm 3/2$ .

The natural variables appearing in Eq. (1) are defined as follows:  $K = J/k_B T$ , with  $T$  the temperature,  $k_B$  the Boltzmann constant (set to 1 in what follows) and  $J > 0$  the exchange-interaction energy, is an adimensional quantity such that  $K/S^2$  can be taken as HT expansion parameter; the quantity  $h$  represents the reduced magnetic field  $h = -KH/J$  with  $H$  the external uniform magnetic field, and finally  $D = K\Delta/J$  called “reduced crystal-field” (also “reduced anisotropy field”), with  $\Delta$  the “crystal field” (also “anisotropy field”). A further generalization of the BC model, called the BEG model<sup>7,52</sup> includes an additional biquadratic exchange-coupling interaction between nearest-neighbor spins.

The thermodynamics of the model is described in terms of three conjugate pairs of field-density variables: the temperature and the specific entropy; the magnetic field  $H$  and the specific magnetization  $M$  (“order parameter”); the crystal field  $\Delta$  and its conjugate density  $X$  called “concentration” (or “non-ordering parameter”). For systems with spin  $S = 1$ , the concentration (of the spins with  $s_i = 0$ ) is usually defined as  $X = 1 - \langle s_0^2 \rangle$ . In the case of spin  $S = 3/2$ , the concentration (of the spins with  $s_i = \pm 1/2$ ) defined as  $X = 1/2(9/4 - \langle s_0^2 \rangle)$ , retains the same range

$[0, 1]$  of variation. The main thermodynamic observables of the model are the response functions, e.g. the specific-heat, the derivative of  $X$  with respect to  $\Delta$ , denoted by  $Y$  and called “concentration susceptibility” (or “quadrupolar susceptibility”), and the derivatives of  $M$  with respect to  $H$ , for example the ordinary magnetic susceptibility, as well as the other higher-order derivatives.

We can intuitively figure out what the critical behavior of the BC system will be in zero magnetic field, as follows. For  $D = 0$ , the model reduces to the Ising model with spin  $S$ , that, in a vanishing magnetic field, displays a power-law critical transition from a disordered HT phase to an ordered LT phase at a temperature  $T_c(0)$ . When  $D$  is switched on to a small enough positive (negative) value, it raises (lowers) slightly the energy of the spins with  $s_i = \pm S$  above (below) that of the spins with  $s_i < S$ . The field  $D$  does not break the symmetry of the disordered phase and the exchange interaction remains dominant, so that a continuous transition still occurs, though at a slightly smaller (higher) temperature  $T_c(D)$ , since by increasing (decreasing)  $D$ , the onset of order is disfavored (favored). Thus, over some range of nonzero values of  $D$ , a line of second-order transitions  $T = T_c(D)$  will be observed. Moreover the universal features of the asymptotic critical behavior will not be affected by  $D$  and thus a single set of exponents with the Ising values<sup>3,4</sup> associated with  $D = 0$ , will characterize this line of critical points.

For large enough values of the ratio  $D/K$ , this picture might change drastically, as indicated by the emergence of a first-order transition line rooted at  $T = 0$ , which is discussed below.

### A. The main predictions of the MF approximation

A spin-dependent description of the essential features of the phase diagram of the BC model, in particular an answer to the question whether and how the above mentioned line of continuous Ising-like critical points is connected with the first-order line, can be obtained<sup>1,2,6,7</sup> in the conventional MF approximation of the Hamiltonian of Eq. (1). In what follows, we shall summarize the main indications that emerge, leaving a formalization of this approach to the Appendix A that rephrases in greater detail the general solutions of Ref. [6] for the two values of the spin examined in this paper. First, let us set

$$\tilde{\Delta} = \Delta/Jq \quad \text{and} \quad \tilde{T} = T/Jq \quad (2)$$

and sketch the main features of the BC models with *integer* spin in the MF approximation. For  $H = 0$  and  $-\infty < \Delta \leq \Delta_{tr}$ , a continuous transition line separates a ferromagnetically ordered LT phase from a paramagnetic HT phase. In the case of spin  $S = 1$ , this line terminates with a TCP of coordinates  $(\tilde{\Delta}_{tr} = \frac{2}{3}\ln 2, \tilde{T}_{tr} = \frac{1}{3})$ .

The ground-state specific energy for  $S = 1$  can be computed exactly and it is observed that its behavior changes at  $\tilde{\Delta} = 1/2$ . All spins are in the same state  $s_i = S$  for  $\tilde{\Delta} < 1/2$ , and the point  $(\tilde{\Delta} = 1/2, T = 0)$ , at which the energy becomes independent of the spin value, is the tip of a first-order transition line that joins the second-order line at the TCP. For  $\tilde{\Delta} > 1/2$ , the BC system remains paramagnetic at all temperatures.

For all integer spins  $S > 1$ , the overall phase structure remains essentially the same: in the  $H = 0$  plane, there is a second order transition line that terminates with a TCP. Various first-order transition lines, all of them rooted at  $(\tilde{\Delta} = 1/2, T = 0)$ , appear in the LT phase and only the rightmost first-order line joins the second-order line at the TCP, while the others display a branched structure and terminate with double-critical endpoints<sup>31</sup>. The structure of this phase diagram for spin  $S = 1$  is schematized in Fig. 1.

If viewed in the extended space of the fields  $T, \Delta, H$ , the TCP in the case of spin  $S = 1$  reveals a complex structure. As indicated schematically in Fig. 1, at this point three distinct critical lines (only one of which lies in the  $H = 0$  plane) and a line of first-order transitions meet together. It was this confluence that suggested<sup>3,4</sup> the name “tricritical point”. Thus we can as well say that the TCP is the end-point of a first-order line of three-phase coexistence (a line of triple-points), at which these phases become simultaneously critical. The critical lines bound three surfaces of first-order transitions, one of them in the  $H = 0$  plane and two surfaces usually called “wings”, extending symmetrically for  $H \neq 0$ .

On the other hand, the models with *half-odd* values of the spins  $S > 1$ , show the distinctive feature that the second-order line does not terminate with a TCP and does not join there with a first-order line, but extends indefinitely for  $-\infty \leq \Delta \leq \infty$ . As to the ground-state specific energy, one observes that all spins are in the same state  $s_i = S$  for  $\tilde{\Delta} < 1/2$ , while they are in the state  $s_i = 1/2$  for  $\tilde{\Delta} > 1/2$ . For  $S > 3/2$ , several first-order transition lines occur within the LT phase, all of them rooted at  $(\tilde{\Delta} = 1/2, \tilde{T} = 0)$ . As the spin gets large, they display an increasingly branched structure and terminate with double-critical endpoints.

In the spin  $S = 3/2$  case, a single first-order line appears in the LT phase, but no TCP occurs on the phase-boundary in the  $H = 0$  plane and again two wings depart, as for spin  $S = 1$ , from the first-order surface. The structure of this phase diagram is schematized<sup>31</sup> in Fig. 2. In this case, one can also say that a line of four-phase coexistence terminates at the double-critical endpoint at which these phases become simultaneously critical.

It will be interesting to compare the qualitative indications obtained from the MF closed-form expressions<sup>6</sup> with the results of a numerical analysis of the series expansions.

Also for the TCP, there exists an upper tricritical lattice dimension  $d_{tr}^*$  (the subscript *tr* will be henceforth attached to the quantities associated to the TCP). For  $d \leq d_{tr}^*$  the critical fluctuations are sufficiently strong that the TCP occurs with non-MF exponents. Thus, the MF approximation can only be a first guide to the critical behavior and its predictions must be qualitatively validated and quantitatively refined. Determining the upper critical dimension of the TCP is then a necessary step to get a complete understanding of the model. Both by renormalization-group<sup>53-55</sup> (RG) methods, as mentioned below, and by applying<sup>56</sup> the Ginzburg criterion, it was argued that  $d_{tr}^* = 2$ . At the borderline dimension  $d = 3$ , the MF critical behaviors, possibly modified by logarithmic correction factors, are expected to set in at the TCP, just as it is observed at  $d = 4$  for the ordinary critical phenomena. For  $d > 3$ , the tricritical exponents should retain  $d$ -independent values since the MF approximation becomes consistent and therefore also quantitatively reliable. In  $d = 2$  dimensions, the field theory defined by Eq. (A1) can be solved within the conformal field-theory(CFT) approach<sup>57-59</sup> yielding the exact tricritical values reported in Tab. II. The remaining exponents can be calculated by the usual scaling relations. The  $2d$  exponents are markedly different from the corresponding MF values.

Also for  $d > 4$ , the MF values of the critical exponents should change discontinuously at the TCP, into the tricritical ones indicated in Tabs. I and II.

TABLE I: The exponents of the Ising universality-class<sup>60</sup> for lattices of dimension  $d = 2$  and  $d = 3$ . We have also indicated the values of these exponents in the MF approximation, valid for  $d > 3$ .

	$\alpha$	$\beta$	$\gamma$	$\nu$
$d = 2$	0	1/8	7/4	1
$d = 3$	0.11(1)	0.326(5)	1.2371(2)	0.6299(4)
<i>MF</i>	0	1/2	1	1/2

TABLE II: The exponents of the BC model at the TCP. They are distinguished from the exponents on the critical phase-contour by the subscript *tr*. For lattices of dimension  $d = 3$ , MF values are expected, possibly modified by logarithmic correction factors.

	$\alpha_{tr}$	$\beta_{tr}$	$\gamma_{tr}$	$\nu_{tr}$	$\phi_{tr}$
$d = 2$ (CFT)	8/9	1/24	37/36	5/9	4/9
$d = 3$ (MF)	1/2	1/4	1	1/2	1/2

Along the second-order lines that border the wings, the BC model is expected to display exponents *independent* of  $D$ , retaining by universality the Ising-like values taken at  $H = D = 0$  and appropriate to the lattice dimension.

We shall return later on the emergence at the TCP, of the additional *crossover* exponent  $\phi$  reported in Tab. II.

## B. Further comments on the recent numerical studies

No exact results are known for the BC model (or even for the Ising models with spin  $S > 1/2$ ) on lattices of dimension  $d > 1$ . A number of analytic approximations of uncontrolled convergence rate were proposed to improve the MF approximation<sup>19</sup>, but so far the transfer-matrix method and the MC simulations remain the only safe alternatives to series methods.

Many MC simulations of accuracy increasing with the speed and memory of the available computers, were carried out on the  $sq$ <sup>20,24,29,38,39</sup>, on the  $sc$ <sup>30,32,33</sup>, and the  $fcc$  lattices<sup>25</sup> for the BC model with various values of the spin. In particular a very recent multicanonical simulation<sup>39</sup> for the  $sq$  lattice reaches a very high accuracy. In  $d = 2$  dimensions, for  $S = 1$ , one can take also advantage of the feasibility<sup>21-23</sup> of very accurate transfer-matrix computations.

The qualitative indications of the MF approximation were supported by a transfer-matrix calculation<sup>14</sup> also in the case of the spin  $S = 3/2$  BC model in  $2d$  and by a MC simulation<sup>13</sup> in  $3d$ . For the  $sq$  lattice, an effective-field theory with correlation was studied<sup>17</sup> for all values of the spin. Additionally, we can cite a MC simulation of the BC model on the  $sq$  lattice with quenched disorder<sup>36</sup> in which accurate data, comparable with the results of this paper, are reported also for the pure case.

So far no simulations have been carried out for the  $bcc$  lattice. An estimate for the location of the TCP came however from a calculation<sup>15</sup> in a self-consistent Ornstein-Zernike approximation.

The estimates of the critical parameters obtained in some of the cited studies will be later confronted with those from our analysis of the LT and HT expansions.

The Euclidean field theory with the potential  $V(\phi)$  of Eq. (A1) can be used as a basis for the RG based approximations, if we assume that its tricritical behavior belongs to the same universality class as the BC model. RG ideas applied<sup>3,4,53-55</sup> in  $d = 3$  suggested MF behavior with logarithmic correction factors at the TCP. The above mentioned identification of the borderline-critical-dimension was thus supported. Quantitative results came also from studies of the Landau-Ginzburg model of Eq. (A1) in  $d = 3 - \epsilon$  by forming  $\epsilon$ -expansion approximations of the exponents at the TCP and from position-space RG studies of the  $S = 1$  BC model<sup>8,9</sup> on the  $sq$  lattice.

In the case of spin  $S = 3/2$ , the first approximate RG computations<sup>11</sup> failed to confirm the MF prediction concerning the absence of a TCP, but these difficulties were overcome in a more recent<sup>18</sup> approach.

### C. Structure of the Series Expansions

For all values of the spin  $S$ , the HT expansion of the dimensionless free-energy per site of the BC model on a lattice of  $N$  sites can be written in the thermodynamical limit as

$$-(K/J)f_{HT}(K, D, h; S) = \lim_{N \rightarrow \infty} (1/N) \ln Z_N(K, D, h; S) = V_0(D, h; S) + \sum_{n=1}^{\infty} g_n(D, h; S) K^n \quad (3)$$

with  $Z_N(K, D, h; S)$  the partition function for the Hamiltonian of Eq. (1)

$$V_0(D, h; S) = -D + h + \ln \left( \sum_{s=-S}^S x^{S^2 - s^2} \mu^{S-s} \right) \quad (4)$$

and

$$\mu = \exp\left(-\frac{h}{S}\right) \quad x = \exp\left(\frac{D}{S^2}\right) \quad (5)$$

Using the HT linked-cluster expansion<sup>46-48,61,62</sup> method, the coefficients  $g_n(D, h; S)$  of the expansion in powers of  $K$  can be computed *exactly in*  $D/S^2$  and  $h/S$  as multivariate polynomials in appropriately defined “vertex functions”  $V_i(D, h; S)$ , with rational coefficients depending on the lattice structure and dimension.

If the dependence of the HT series on the magnetic field is analytically known, the LT expansions can be derived by a transformation of variables and a direct graphical analysis is not necessary.

The structure of the LT expansion for the free-energy density is

$$-(K/J)f_{LT}(u, D, h; S) = \frac{1}{2}qK + h - D + \sum_{n=1}^{\infty} L_n(u, x; S) \mu^n. \quad (6)$$

Here  $u = \exp(-K/S^2)$ , while  $\mu$  plays a role of high-field expansion variable. For large magnetic fields, i.e. around  $\mu = 0$ , the quantity  $-\frac{K}{J}f_{LT} - h$  is a convergent series in  $\mu$ , with expansion coefficients  $L_k(u, x; S)$  that are polynomials in  $u$  and  $x$ . Below the critical line, this expansion is convergent also for  $\mu = 1$ , hence the name LT expansion.

From our series, either at HT or at LT, we can obtain all “mixed susceptibilities”, i.e. the derivatives of the free-energy density with respect to the ordering field  $h$  and/or to the “non-ordering” field  $D$ .

$$\chi_{(r;p)}(K, D, h; S) = (-1)^{p+1} \frac{K}{J} S^{r+2p} \frac{\partial^{r+p} f(K, D, h; S)}{\partial h^r \partial D^p} = \sum_{i_2, \dots, i_{r+p}} \langle s_0 s_{i_2} \dots s_{i_r} s_{i_{r+1}}^2 \dots s_{i_{r+p}}^2 \rangle_c \quad (7)$$

In particular for  $S = 1$ , the density  $X(K, D; 1)$  conjugated to the reduced crystal-field, namely the concentration, is

$$X(K, D; 1) = 1 - \frac{K}{J} \frac{\partial f(K, D; 1)}{\partial D} = 1 - \chi_{(0;1)}(K, D; 1) = 1 - \langle s_0^2 \rangle \quad (8)$$

The response function with respect to  $\Delta$ , namely the concentration susceptibility, is the  $D$ -derivative of  $X(K, D; 1)$

$$Y(K, D; 1) = \frac{\partial X(K, D; 1)}{\partial D} = -\frac{K}{J} \frac{\partial^2 f(K, D; 1)}{\partial D^2} = \chi_{(0;2)}(K, D; 1) = \sum_i \langle s_0^2 s_i^2 \rangle_c \quad (9)$$

For  $H = 0$ , only the susceptibilities  $\chi_{(r;p)}(K, D, h; S)$  of even order  $r$  are non-trivial at HT, whereas all field-derivatives are non-trivial at LT, in particular the specific magnetization  $M(K, D, h; S) = \chi_{(1;0)}(K, D, h; S)$ . For brevity, we shall often adopt the notations  $f(K, D; S) \equiv f(K, D, h; S)|_{h=0}$  and  $\chi_{(r;p)}(K, D; S) \equiv \chi_{(r;p)}(K, D, h; S)|_{h=0}$  ( $r = 1, 2, \dots$ ), simply dropping the  $h$ -dependence.

### D. The computation of the LT expansions

The MF approximation indicates that for spin  $S \geq 1$ ,  $\lfloor \frac{2S+1}{2} \rfloor$  ordered phases appear in the LT region. The phase in which at  $T = 0$  all spins take the value  $s_i = S$ , can be described by a LT expansion.

The HT and LT expansions of the free energy must match in the region in which  $h \rightarrow \infty$  and  $K \rightarrow 0$ , so that the following equation is valid in a vicinity of  $\mu = 0$ ,  $u = 1$

$$K \frac{q}{2} + \sum_{k \geq 1} L_k(u, x; S) \mu^k = \ln \left( \sum_{s=-S}^S x^{S^2-s^2} \mu^{S-s} \right) + \sum_{i \geq 1} g_i(h(\mu), D(x)) K(u)^i \quad (10)$$

Considering  $K$  as a function of  $z = 1 - u$ , from Eq. (10) it follows that, for  $n \geq 1$ ,

$$L_n(u, x; S) = [\mu^n] \left( \ln \left( \sum_{s=-S}^S x^{S^2-s^2} \mu^{S-s} \right) + \sum_{i \geq 1} g_i(h(\mu), D(x)) K(z)^i \Big|_{z=1-u} \right) \quad (11)$$

here  $[x^n]v$  is defined as the coefficient of the  $x^n$  term in the expansion of the function  $v(x)$  in powers of  $x$ .

Since  $K(z) = O(z)$  and  $L_n$  has order  $Sqn$  in  $u$ , only the HT coefficients  $g_i$  with  $i \leq Sqn$  contribute to  $L_n$ , in Eq. (11) so that the polynomials  $L_n$  can be computed from the HT expansion through the order  $Sqn$ .

A few more  $L_n$  can be computed from the same HT expansion, using the fact that  $L_n$  has a zero of order  $b_n$  in  $u$ . For any integer exponent  $0 \leq b \leq b_n$ ,  $u^{-b} L_n(u, x; S)$  is a polynomial in  $u$ , and hence in  $z$ , of degree  $Sqn - b$ , so that

$$u^{-b} L_n(u, x; S) = \mathcal{T}_{Sqn-b} \left\{ (1-z)^{-b} [\mu^n] \left( \ln \left( \sum_{s=-S}^S x^{S^2-s^2} \mu^{S-s} \right) + \sum_{i \geq 1} g_i(h(\mu), D(x)) K(z)^i \Big|_{z=1-u} \right) \right\} \quad (12)$$

Here the series truncation operator is defined by  $\mathcal{T}_m F = \sum_{k=0}^m z^k \frac{d^k F}{dz^k} \Big|_{z=0}$  with  $F$  is a series in the variable  $z$ .

Choosing  $b = b_n$  is the most efficient way to get  $L_n$  from Eq. (12). If  $b_n$  is not known, the RHS of Eq. (12) has to be computed for some  $b \geq b_{n-1}$ , using the heuristic observation that  $b_n \geq b_{n-1}$ . Since the lowest power in  $u$  of  $u^{-b} L_n$  must be  $b_n - b$ , the presence of a multiple zero in  $u = 0$  in the RHS of Eq. (12) indicates that the result is correct.

In the case of spin  $S = 1$ , the  $b_n$  are known<sup>63-65</sup> for  $D = 0$ , namely for the Ising model with spin  $S = 1$ . Thus, we can take  $b = b_n$  and derive the  $L_n$  through  $n = 11$  for the  $sq$  and  $sc$  lattices, and through  $n = 10$  in the  $bcc$  case. For spin  $S = 3/2$ , in the case of the  $sq$ ,  $sc$  and  $bcc$  lattices, we can compare our results with the polynomials  $L_n$  obtained in Ref. [66] through  $n = 7$ . For  $n = 8, 9$ , we have used in Eq. (12) values of  $b$  such that there are at least zeros of multiplicity 4 in the above procedure, so that we are confident that the expressions obtained for  $L_8$  and  $L_9$  are correct.

The arrangement of the LT expansion as a series of powers of  $\mu$  with coefficients polynomial in  $u$  and  $x$ , is called ‘‘field grouping’’. However the LT series can be as well thought of as an expansion in powers of  $u$ , with coefficients that are polynomials in  $x$  and  $\mu$  (‘‘temperature grouping’’). In numerical use at moderate orders, the approximations obtained in the two cases may show some difference.

As an example of the results of this procedure, for any lattice and spin the two lowest-order LT polynomials  $L_n(u, x; S)$  are

$$L_1(u, x; S) = u^{qS} x^{2S-1} \quad (13)$$

$$L_2(u, x; S) = u^{2qS} x^{4S-4} + \left( \frac{q}{2} u^{2qS-1} - \frac{q+1}{2} u^{2qS} \right) x^{4S-2} \quad (14)$$

Some properties of the LT polynomials thus obtained provide a useful partial check of the computation. For example, in the case of spin  $S = 1$ , the polynomials have the structure  $L_n(u, x; 1) = \sum_{m=0}^n L_{n,m}(u) x^m$  where the quantities  $L_{n,m}(u)$  are nonvanishing only if  $n$  and  $m$  are both even or both odd<sup>43</sup>. Moreover, as  $D \rightarrow -\infty$  the polynomials  $L_{2n+1}(u, x; 1) \rightarrow 0$ , while the  $L_{2n}(u, x; 1)$  reduce to the polynomials  $L_n$  of the Ising model with  $S = 1/2$  on the same lattice i.e.  $L_{2n}(u, x; 1) \rightarrow L_n(u^{1/4}; 1/2)$ . Similar properties are valid in the case of spin  $S = 3/2$ .

In addition, in the  $S = 1$  case, dividing out the highest power of  $x^n$  in  $L_n(u, x; 1)$  and taking the  $D \rightarrow \infty$  limit, a polynomial in  $u$  is obtained containing the powers  $u^{6n}$ ,  $u^{6n-1}$ ,  $u^{6n-2}$ , ..., whose coefficients reproduce orderly the coefficients of  $u^{3n}$ ,  $u^{3n-1}$  ... of the polynomials  $L_n(u; 1/2)$  of the Ising model with  $S = 1/2$  on the same lattice. An analogous property is observed for  $S = 3/2$ .

As an example of our results for the LT expansions for the BC model, in the Table VII we have reported the first 11 LT polynomials for the  $sc$  lattice in the case of spin  $S = 1$ .

### E. The computation of the HT expansions

The HT expansion coefficients  $g_n(D, h; S)$  Eq. (3), are polynomials with rational coefficients<sup>62</sup> in the bare vertices  $V_j(D, h; S) = \frac{d^j}{dh^j} V_0(D, h; S)$  (for  $j \geq 1$ ), that are the successive  $h$ -derivatives of the vertex generating-function  $V_0(D, h; S)$  defined by Eq. (4).

They are evidently independent of the lattice structure and dimensionality, but depend on the value  $S$  of the spin. The coefficients  $g_n$  can be computed directly by the “unrenormalized linked-cluster expansion”<sup>62</sup>. More efficiently, the quantities  $\frac{dg_i}{dh}$  can be derived using the “renormalized linked-cluster expansion”. By integration with respect to  $h$ , the polynomials  $g_n$  in the bare vertices are recovered and it can be proved that the integration constant vanishes. The bare vertices are regular series in  $\mu$  and this implies that the same property is valid for the coefficients  $g_n(h(\mu), D(x))$ .

### F. The vertex functions for spin $S = 1$

For spin  $S = 1$ , all vertex functions with  $n > 0$  can also be expressed<sup>45</sup> as polynomials in *two* auxiliary functions

$$A(D, h; 1) = \frac{1 - \mu^2}{1 + x\mu + \mu^2} \quad B(D, h; 1) = \frac{1 + \mu^2}{1 + x\mu + \mu^2} \quad (15)$$

For  $g_0(D, h; 1)$ , we have

$$g_0(D, h; 1) = V_0(D, h; 1) = \ln[1 + 2 \exp(-D) \cosh(h)] = -\ln(1 - B(D, h; 1)) \quad (16)$$

The HT expansion coefficients of the free-energy density  $g_n(D, h; 1)$  with  $n > 0$  can be rewritten more simply as bivariate polynomials (with rational coefficients) in  $A(D, h; 1)$  and  $B(D, h; 1)$ . This property follows from the equations

$$\frac{\partial A(D, h; 1)}{\partial h} = B - A^2 \quad \frac{\partial B(D, h; 1)}{\partial h} = A - AB \quad (17)$$

$$\frac{\partial A(D, h; 1)}{\partial D} = AB - A \quad \frac{\partial B(D, h; 1)}{\partial D} = B^2 - B \quad (18)$$

It is also useful to remember that

$$\frac{\partial V_0(D, h; 1)}{\partial h} = A(D, h; 1), \quad \frac{\partial V_0(D, h; 1)}{\partial D} = -B(D, h; 1) \quad (19)$$

A similar remark applies to the expansion coefficients of the higher (mixed) susceptibilities  $\chi_{(r;p)}(K, D, h; 1)$ .

From Eq. (16), it is clear that, for  $D = 0$  (i.e. for  $x = 1$ ) the coefficients  $g_n(D, h; 1)$  reduce to those of an Ising system with  $S = 1$  in a magnetic field. On the other hand, in the limit  $D \rightarrow -\infty$ , the  $S = 0$  state is suppressed and we have  $B \rightarrow 1$ ,  $A \rightarrow \tanh(h)$ , so that the expansion coefficients reduce essentially to those of an  $S = 1/2$  Ising system in a field. For  $h = 0$ , we have  $T_c(D \rightarrow -\infty; 1) = T_c(1/2)$ , where  $T_c(1/2)$  denotes the critical temperature of the spin  $S = 1/2$  system.

For  $h = 0$ , the auxiliary function  $A(D, 0; 1)$  vanishes and the coefficients  $g_n(D, 0; 1)$  reduce to polynomials in the single variable<sup>43</sup>

$$\tau \equiv B(D, 0; 1) = 1/(1 + x/2) \quad (20)$$

that coincides with the variable  $\tau$  defined in Refs.[40,41,43]. Notice finally that in the limit  $D \rightarrow \infty$ , the spin  $S = \pm 1$  states are suppressed.

### G. The vertex functions for spin $S = 3/2$

The field-derivatives of the vertex-generating function  $V_0(D, h; 3/2)$  can be expressed as polynomials in the *three* auxiliary functions

$$A(D, h; 3/2) = \frac{1 - \mu^3}{1 + x^2(\mu + \mu^2) + \mu^3} \quad (21)$$

$$B(D, h; 3/2) = \frac{1 + x^2(\mu - \mu^2) - \mu^3}{1 + x^2(\mu + \mu^2) + \mu^3} \quad (22)$$

$$C(D, h; 3/2) = \frac{1 + \mu^3}{1 + x^2(\mu + \mu^2) + \mu^3} \quad (23)$$

The expansion coefficients  $g_n(D, h; 3/2)$  (with  $n > 0$ ) are polynomials in A, B and C. For  $g_0(D, h; 3/2)$ , we have

$$g_0(D, h; 3/2) = V_0(D, h; 3/2) = \ln 2 - D - h - \ln\left(C(D, h; 3/2) - A(D, h; 3/2)\right) \quad (24)$$

Similar remarks as for the spin  $S = 1$  case are valid also for the derivatives of A, B and C with respect to  $D$  and  $h$ , so that the expansions of the mixed susceptibilities are polynomials in these variables. This property follows from the equations

$$\frac{\partial A(D, h; 3/2)}{\partial h} = \frac{2}{3}\left(\frac{3}{2}C - A^2 - \frac{AB}{2}\right) \quad (25)$$

$$\frac{\partial B(D, h; 3/2)}{\partial h} = \frac{2}{3}\left(\frac{1}{2} + C - AB - \frac{B^2}{2}\right) \quad (26)$$

$$\frac{\partial C(D, h; 3/2)}{\partial h} = \frac{2}{3}\left(\frac{3A}{2} - AC - \frac{BC}{2}\right) \quad (27)$$

$$\frac{\partial A(D, h; 3/2)}{\partial D} = \frac{8}{9}(-A + AC) \quad (28)$$

$$\frac{\partial B(D, h; 3/2)}{\partial D} = \frac{8}{9}(-A + BC) \quad (29)$$

$$\frac{\partial C(D, h; 3/2)}{\partial D} = \frac{8}{9}(-C + C^2) \quad (30)$$

and

$$\frac{\partial V_0(D, h; 3/2)}{\partial h} = \frac{1}{3}(2A + B) \quad \frac{\partial V_0(D, h; 3/2)}{\partial D} = -\frac{1}{9}(1 + 8C) \quad (31)$$

The polynomial in the variables A, B and C representing the  $n$ th coefficient of the expansion of  $\chi_{(r;p)}(K, D, h; 3/2)$  in powers of  $K$ , has order  $2n + r + p$ , irrespectively of the lattice dimensionality and structure.

From Eqs. (21-23), it follows that in the limit  $D \rightarrow -\infty$ , the set of the auxiliary functions simplifies ( $A = B$  and  $C \rightarrow 1$ ) and the  $s = \pm 1/2$  states are suppressed. Analogously the  $s = \pm 3/2$  states are suppressed in the  $D \rightarrow +\infty$  limit. Thus in both limits, the series expansions essentially reduce to those of the spin  $S = 1/2$  Ising model in a field.

For  $h = 0$ , we have  $T_c(D = -\infty; 3/2) = T_c(1/2) = 9T_c(D = +\infty; 3/2)$ . For  $D = 0$ , the series reduce to those of an Ising system with spin  $S = 3/2$  in a field. For  $h = 0$ , the auxiliary functions  $A(D, 0; 3/2)$  and  $B(D, 0; 3/2)$  vanish and the coefficients  $g_n(D, h; 3/2)$  become polynomials in the single variable

$$\tilde{\tau} \equiv C(D, 0; 3/2) = 1/(1 + x^2). \quad (32)$$

Let us add that for higher spin values, the HT coefficients can be expressed polynomially in terms of larger sets of auxiliary functions and simplifications analogous to those indicated above still occur in the same limits of  $D$  and  $h$ . These properties can be used for a partial (but non-trivial) check of the correctness of the series derivation. In particular, for all half-odd spin systems, the series expansions essentially reduce to those of the spin  $S = 1/2$  Ising model in a field, in both limits  $D \rightarrow \pm\infty$ .

To give an idea of the structure of the HT expansions that we have computed, we have shown in Table IX the first nine coefficients  $g_n(D, h; 1)$  of the free-energy expansion for the  $sc$  lattice in the spin  $S = 1$  case. When  $h \neq 0$ , the



complexity of the polynomial structure of  $g_n(D, h; 1)$  in A and B increases so rapidly with the order of expansion, that the set of series coefficients becomes very cumbersome beyond the 9th order. The expression of the 10th-order HT coefficient is as long as the whole set of the preceding ones shown in the table. Therefore an extensive tabulation of our series data does not fit the format of this paper and requires a separate report<sup>67</sup>.

Our derivation<sup>46-48</sup> of the HT expansions for any value of the spin, was made possible by an efficient coding of the linked-cluster<sup>61-63</sup> graphical computation algorithms and by an extensive use of the symbolic manipulation softwares *Sagemath*<sup>68</sup> and *Python*. At the order of expansion we have reached, the performance of the current personal computers is still adequate to face the exponential growth of the computational complexity with the order of series expansion.

No software for symbolic manipulation and multiprecision arithmetic was available at the time of the pioneering series-study of Ref.[43], so that an exact calculation of the expansion coefficients (always rational numbers) as functions of  $D$  and  $h$  was not easy. Thus in these studies, approximate numerical procedures giving rise to sizable rounding errors, even at relatively low orders, were used<sup>43</sup> to evaluate the series coefficients. On the contrary, in our work this source of error is eliminated by an extensive use of the softwares for exact symbolic computation.

## H. The critical behaviors of the main observables

If we define  $t(K, D; S) \equiv (K_c(D; S)/K - 1)$ , the critical behaviors as  $K \rightarrow K_c(D; S)$  at fixed  $D$ , of the mixed susceptibilities in zero magnetic field, expected from the scaling laws, are

$$\chi_{(r;p)}(K, D; S) \approx A_{(r;p)}(D; S) |t(K, D; S)|^{-\gamma^{(r;p)}(D; S)} \left[ 1 + a_{(r;p)}(D; S) t^\theta \dots \right] \quad (33)$$

Here  $\gamma^{(r;p)}(D; S)$  denotes the leading critical exponent of the mixed susceptibility of order  $(r; p)$ , while  $\theta$  is the exponent of the leading correction-to-scaling. A priori,  $\gamma^{(r;p)}(D; S)$  might depend on  $D$  and  $S$ , but to keep notation simpler we shall often drop this dependence. The values of the critical amplitudes  $A_{(r;p)}(D; S)$  and  $a_{(r;p)}(D; S)$  obtained approaching the critical line from the HT side will differ from those obtained on the LT side. We might distinguish them by appropriate superscripts, which however we shall omit to avoid overloading the notation, whenever it is clear from the context which is the relevant limit.

For  $d \leq 4$  (or  $d \leq 3$  in the case of the TCP), the hyperscaling relation is

$$\gamma^{(r;p)} = p + \gamma^{(2;0)} + (r - 2)\hat{\Delta} \quad (34)$$

with  $\hat{\Delta} = \beta + \gamma^{(2;0)}$ .

The asymptotic form<sup>53,54,69,70</sup> on the tricritical path, i.e. as  $T \rightarrow T_{tr}$  at fixed  $D = D_{tr}$ , of the density  $X(K, D; S)$  conjugated to the crystal field, is

$$X(K, D; S) \approx X_c(D_{tr}; S) + A_X(D_{tr}; S) |t(K, D_{tr}; S)|^\omega \quad (35)$$

Eq. (B5) implies  $\omega = 1 - \alpha_{tr}$ . In the same limit, the concentration susceptibility, namely the derivative of  $X(K, D; S)$  with respect to  $D$ , behaves<sup>53,54,69</sup> as

$$Y(K, D; S) \approx A_Y(D_{tr}; S) |t(K, D_{tr}; S)|^{-\lambda} \quad (36)$$

with  $\lambda = \alpha_{tr}$ .

The critical parameters defined by the asymptotic form Eq. (33) are calculable by series extrapolations and depend on the lattice dimension  $d$  and (as far as the amplitudes are concerned) on the lattice structure, although we have not explicitly indicated this fact. The critical amplitudes  $A_{(r;p)}(D; S)$  of the susceptibilities  $\chi_{(r;p)}(K, D; S)$  with  $r = 1, 2, \dots$ , can be obtained by forming the expansions of the *effective amplitudes* biased with the estimated values of  $K_c(D; S)$  and the expected values of  $\gamma^{(r;p)}$

$$A_{(r;p)}^{eff}(K, D; S) = |t(K, D; S)|^{\gamma^{(r;p)}} \chi_{(r;p)}(K, D; S) \quad (37)$$

and extrapolating them to  $K = K_c(D; S)$  from the appropriate side of the critical line, namely  $A_{(r;p)}(D; S) = A_{(r;p)}^{eff}(K_c; D; S)$ .

The validity of the universality property along all the critical line for the main and the correction exponents, (while the single amplitudes are non-universal), can be confirmed by simply checking that they keep the Ising model values expected for the given lattice dimensionality.

All over the critical line, we can also evaluate a few appropriate ratios of higher susceptibilities, expected to be universal, such as the lowest order terms in the sequences  $\mathcal{I}_{2r+4}^+(D; S)$  and  $\mathcal{J}_{2r+4}^+(D; S)$  defined<sup>71</sup> by

$$\mathcal{I}_{2r+4}^+(D; S) = \lim_{K \rightarrow K_c^-} \frac{\chi_{(2;0)}(K, D; S)^r \chi_{(2r+4;0)}(K, D; S)}{\chi_{(4;0)}(K, D; S)^{r+1}} = \frac{A_{(2;0)}(D; S)^r A_{(2r+4;0)}(D; S)}{A_{(4;0)}(D; S)^{r+1}} \quad (38)$$

$$\mathcal{J}_{2r+4}^+(D; S) = \lim_{K \rightarrow K_c^-} \frac{\chi_{(2r;0)}(K, D; S) \chi_{(2r+4;0)}(K, D; S)}{\chi_{(2r+2;0)}(K, D; S)^2} = \frac{A_{(2r;0)}(D; S) A_{(2r+4;0)}(D; S)}{A_{(2r+2;0)}(D; S)^2} \quad (39)$$

for  $r > 0$ . (Observe that for  $r = 1$ , we have  $\mathcal{I}_6^+ \equiv \mathcal{J}_6^+$ ). These amplitude ratios, along with additional ones involving also the susceptibilities  $\chi_{(r;0)}(K; D; S)$  with odd indices, can also be studied for  $H = 0$  on the LT side of the critical point, i.e. in the limit  $K \rightarrow K_c(D; S)^+$ . Analogous ratios can be defined in terms of the susceptibilities with  $p > 0$ . Of course, they do not reduce to known Ising quantities for  $D = 0$ .

### III. NUMERICAL ANALYSIS OF THE EXPANSIONS

In the following subsections, we shall make a general discussion of our analyses of the HT and LT series, valid for all lattices under study.

#### A. The variables

As already observed, in the  $H = 0$  plane, the HT series analyses are performed in terms of the “natural” variables  $\tau$  (or equivalently  $D$ ) and  $K$ , namely along lines of constant  $\tau$  in the  $(\tau, \tilde{T})$  plane. When comparing our estimates of the critical phase-boundaries with those from simulation methods, it should be remarked that the simulations are carried out at fixed  $\Delta$  (or  $T$ ) so that the uncertainties (reported in Tabs. III, IV and V) affect only the corresponding  $T_c$  (or  $\Delta_c$ ), while our results are obtained at fixed  $D$  (or  $\tau$ ) so that uncertainties should affect both  $T_c$  and  $\Delta_c = DT_c$ . However, for convenience in the comparison with the estimates from other sources, we can give either results at fixed  $\Delta$  and shift the uncertainty in this variable into sufficiently enlarged error bars for  $T_c$  or results at fixed  $T$ . Analogous remarks apply for the LT series.

For the systems under scrutiny, we shall map out the phase-diagrams in the  $(\tilde{\Delta}, \tilde{T})$  plane (or in the  $(\tau, \tilde{T})$  plane) and in most cases shall obtain the critical phase-contour from the HT expansion of the ordinary susceptibility. Then we shall be able also to estimate the exponents and the critical amplitudes of a few other susceptibilities (including those of higher (mixed) orders  $\chi_{(2r;p)}(K, D; S)$ ). Our *unbiased* HT series estimates for the *sq*, the *sc* and the *bcc* lattices in the case of spin  $S = 1$ , produce the phase diagrams of Figs. 3, 10, and 23 respectively. For comparison, in all these figures we have also drawn the phase-boundary in the MF approximation, which is independent of the lattice dimension and structure, due to the choice of the plotting variables. Generally the MF approximation is qualitatively correct but, for a given  $D$ , it leads to a phase-contour systematically higher in temperature than those from the series or other approximation methods. The phase diagrams in the  $(\tau, \tilde{T})$  plane, are particularly suggestive, not only because for spin  $S = 1$ , the MF critical phase-contour reduces exactly (see the Appendix A) to the straight line between the points  $(1/3, 1/3)$  and  $(1, 1)$ , but also because the critical boundaries computed by series remain nearly straight lines although shifted to lower temperatures with respect to the MF approximation and with smaller slopes, except very near the TCP. As an example, we shall show only Fig. 12 for the *sc* lattice. The phase-contours in the  $(\tau, \tilde{T})$  plane obtained for the *sq* and the *bcc* lattices are completely similar and are not reported for brevity. For the spin  $S = 3/2$  systems the MF critical boundary in the  $(\tilde{\tau}, \tilde{T})$  plane is the straight line  $\tilde{T} = 8\tilde{\tau}/9 + 1/9$  with  $0 \leq \tilde{\tau} \leq 1$  and also the phase-contours obtained from the series for the *sq*, *sc* and *bcc* lattices do not show a pronounced curvature except in the range  $0 \leq \tilde{\tau} \lesssim 0.1$  in which the infinite region  $\tilde{\Delta} \gtrsim 0.4$  is mapped. For brevity, we shall generally show only the phase diagram in the  $(\tilde{\Delta}, \tilde{T})$  plane (see Fig. 27).

For each value of  $D$ , our unbiased estimates of the points of the critical boundaries are obtained fitting the asymptotic form Eq. (C6) to the last few terms of the MRA estimator-sequences introduced in Appendix C and formed in most cases with the HT expansions of the susceptibility. As a rule, we have extrapolated only the estimator-sequences that appear to have settled down in their expected asymptotic forms (see the Appendix C), always after making sure that the final estimates are consistent with those from unbiased second-order DAs.

## B. The LT expansions

In the analysis of the LT expansions, both simple ratio-methods and their extensions<sup>72,73</sup>, such as the MRAs introduced in the Appendix C, are unfit to locate the critical points and estimate the exponents, because generally the large-order behavior of the LT expansion coefficients is dominated by nonphysical complex singularities closer to the origin than the critical singularity. For these analyses, only the PA and DA techniques are useful.

All methods described in the Appendix C fail to map the first-order lines which are associated with singularities too weak to be detected by the MRAs, PAs or DAs. In the study of the spin  $S = 1$  BC model on the  $fcc$  lattice, the LT series have been employed<sup>43</sup> jointly with the HT series to map the first-order part of the phase-boundary. It is expected that the free-energy is continuous across the phase-boundary and that also its temperature- (or field-) derivatives are continuous across the second-order line, while they are discontinuous across the first-order line. Thus, at fixed  $D$ , the values of the free-energy computed by HT and LT expansions should intersect, *if* these expansions share a common region of approximate numerical validity. This makes it possible to locate the first-order phase-boundary. This intersection-method is controversial<sup>74,75</sup> to some extent since the features of the singularity associated to the first-order transition are not known in detail and anyway one is evaluating the two series near the borders of their convergence regions. Using the intersection method, whenever we have observed that the curve of the LT free-energy shows two nearby intersections with the HT curve, as a rule we have chosen the lowest temperature one.

We should finally add that in our case this procedure unfortunately does not lead to reliable results in some small range of temperatures  $T \lesssim T_{tr}$ , but otherwise it appears to work reasonably well. The method can be applied also for  $T > T_{tr}$ , by looking for tangency points, (since the free energy is continuous across the second-order line) instead of intersections. The resulting critical phase-boundary generally lies at a temperature slightly smaller than that determined by the MRAs of the HT susceptibility, as it was already observed<sup>43</sup> in the  $fcc$  lattice analysis.

In Figs. 4, 13, 24, the phase diagram is shown at  $h = 0$ , in the concentration-temperature plane  $(X, \tilde{T})$  for the  $sq$ , the  $sc$  and the  $bcc$  lattices, in the case of spin  $S = 1$ . These critical phase-contours are obtained evaluating the expansions of  $X(K, D; S)$  along the curves  $T_c = T_c(D; S)$  that represent the critical phase-boundary in the anisotropy-temperature plane as obtained from the HT susceptibility expansions, while the first order branches are determined using the intersections of the HT-LT free-energy expansions (and/or the simulation data when they exist, as in 2d).

## C. Determination of the exponents along the critical boundaries

It is expected that by universality, along the second-order part of the phase-boundary the exponents of the ordinary susceptibility  $\chi_{(2;0)}(K, D; 1)$ , of the fourth-order susceptibility  $\chi_{(4;0)}(K, D; 1)$ , of the correlation-length, etc. should retain the known Ising values reported in Table I. As the TCP is reached, these exponents must change discontinuously into the sharply different tricritical values of Table II. Series of finite length cannot possibly reproduce such a step-like change of the exponents, but only approximate it by a smooth transition extending over some interval of values of  $D < D_{tr}$ , whose width depends on the extension of the available series. From a numerical point of view, the smooth exponent change and the crossover phenomenology, that occur in a left-hand neighborhood of  $D_{tr}$  may be related to an increasingly complex pattern of corrections to scaling near the TCP. This makes the (unbiased) MRA estimates of the exponents by Eq. (C4) a delicate issue, particularly so in the analysis of spin  $S = 1$  on the  $sq$  lattice.

So far, the crossover behavior of the exponent approximations was not described systematically in the series context. In a somewhat simplified RG model<sup>53,54</sup>, that made possible to study the competition between a tricritical and a critical fixed point, the crossover was illustrated by forming “effective exponents”<sup>76</sup>, that measure the exponents as they are “locally felt” by the singular observables at the point  $(D, K)$ . These local quantities are studied as functions of  $K$  for  $K < K_c(D)$ , at fixed values of  $D$  close to  $D_{tr}$ . As  $K \rightarrow K_c(D)$ , they tend to the asymptotic critical exponents. For example, for the ordinary susceptibility, an effective exponent can be defined by

$$\gamma_{eff}^{(2;0)}(K, D) = (K_c(D) - K) \frac{d \ln \chi_{(2;0)}(K, D; S)}{dK} \quad (40)$$

It is observed<sup>53,54</sup> that, for small  $(K_c(D) - K)$  in the crossover region, the quantity  $\gamma_{eff}^{(2;0)}(K; D)$  initially appears to tend to  $\gamma^{(2;0)}(D_{tr}; 1)$  and then approaches  $\gamma^{(2;0)}(D; S)$  only as  $(K_c(D) - K) \rightarrow 0$ . In other words, initially the renormalized Hamiltonian is attracted by the tricritical fixed point and only eventually it feels the attraction of the ordinary critical fixed point. A calculation of this kind can be repeated in the series context using PAs to resum the HT expansions of the effective exponents. The procedure is biased, and might be sensitive to the accuracy of the estimate of  $K_c(D)$ .

Alternatively, the crossover can also be studied, for example by plotting vs  $1/n^\theta$  the MRA estimator-sequences for the exponent  $\gamma^{(2;0)}(D; 1)$  formed with the HT coefficients of the susceptibility, at fixed values of  $D$ . This procedure is not biased by  $K_c(D)$ , unlike that for the calculation of the effective exponent.

#### D. Accuracy problems near the TCP

The numerical accuracy of the MRAs and the PAs or DAs, formed with the ordinary susceptibilities to determine either the critical contour in the anisotropy-temperature plane or the critical exponents, varies greatly along the critical phase-boundary. A marked worsening of the accuracy is observed when entering in the crossover region. This shortcoming of the series approach had been pointed out already in the pioneering analyses for the *fcc* lattice<sup>43</sup>, but remained unexplained. We conjecture that it might be related to a clustering of unphysical singularities nearby the border of the convergence disk of the series, accompanied by the vanishing of the strength of the physical singularities as  $D \rightarrow D_{tr}$ , that gradually enhances the relative strength of the unphysical singularities as the TCP is approached. Then, the pattern of corrections to scaling, that rules the rate of convergence of all approximants, becomes increasingly complex and makes the analysis of limited-order expansions problematic. Such a mechanism might explain why, in these conditions, pronounced oscillations appear in the MRA estimator-sequences and at the same time both the PAs and the DAs loose precision or even miss altogether the physical singularities. (The weakening of the amplitudes of the physical singularities is prescribed by the tricritical-scaling property discussed in Appendix B and the behavior of the amplitudes of  $\chi_{(2,0)}(K, D; S)$  and of  $-\chi_{(4,0)}(K, D; S)$  as  $D \rightarrow D_{tr}$  is outlined in the Figs. 9, 19 and 25. The clustering of the unphysical singularities is indicated by inspection of PA maps of the singularities in the complex  $K$  plane.)

This effect, especially evident in the analysis of the *sq* lattice, is less important in  $3d$ . A similar phenomenon is observed also in the case of the BC system with spin  $S = 3/2$ , in a neighborhood of  $\tilde{\Delta} = 1/2$ , in spite of the absence of a TCP, for reasons probably similar to those explained for the spin  $S = 1$ . We must add that by itself, the weakening of the critical amplitudes does not hinder the efficiency of the MRAs and we cannot remedy to the problem considering quantities that should be explicitly independent of these amplitudes, such as for example the log-derivative of the susceptibilities, because the effect of the unphysical singularities clustering remains unmodified. However, one can extend the range of values of  $D$  in which the estimates of the parameters of the critical singularity are still reasonably accurate, by analyzing the expansions of a  $D$ - or  $K$ -derivative of the susceptibilities instead of the ordinary susceptibilities, because generally these quantities have different unphysical singularities and their critical singularities are sharper. Sometimes, also smoothing out the oscillations of the MRA sequences, for example by computing “weighted moving-averages” over several terms, might be helpful. Anyway, we have to conclude that in some small left-hand vicinity of the TCP, our simple extrapolations of the HT (and LT) expansions, might be unable to improve the precision of the best present MC simulations or transfer-matrix methods in the determination of the critical boundary.

#### IV. THE BC MODEL WITH SPIN $S = 1$ ON THE *sq* LATTICE

The earliest MC and transfer-matrix calculations on the *sq* lattice determined<sup>20,21,24,29,35</sup> the tricritical value of the crystal field  $\tilde{\Delta}_{tr}$  between 0.4912 and 0.4915, with uncertainties of a few units in the last figure. The values of the tricritical temperature  $\tilde{T}_{tr}$  ranged between 0.1520 and 0.1525, with similar uncertainties. More recently, a Wang-Landau simulation<sup>37</sup> determined  $\tilde{\Delta}_{tr} = 0.49151(1)$  at  $\tilde{T}_{tr} = 0.152$  and a sparse transfer-matrix technique of higher estimated accuracy<sup>22</sup> yielded  $\tilde{\Delta}_{tr} = 0.49145373(6)$  with  $\tilde{T}_{tr} = 0.15214439(1)$ , (equivalently  $D_{tr} = 3.2301797(2)$  and  $K_{tr} = 1.6431759(1)$ ). In the same Ref. [22], the value  $X_{tr} = 0.4549506(2)$  was proposed for the tricritical concentration. Except for the value of  $X_{tr}$ , we shall assume the validity of the cited estimates, whenever convenient.

For  $D \lesssim 0.3D_{tr}$ , the procedure of employing MRA estimator-sequences of the ordinary susceptibility to determine the critical contour, yields results that agree well with and probably are more accurate than other determinations. It was anticipated that as  $D$  gets closer to  $D_{tr}$ , the MRA sequences begin to show oscillations and at the same time also the accuracy of the PAs and of the DAs deteriorates. However, forming MRA estimator-sequences of the mixed susceptibility  $\chi_{(2,2)}(K, D; 1)$  (i.e. taking two  $D$ -derivatives of the ordinary susceptibility to modify the pattern of the unphysical singularities) and in some cases, performing a “weighted moving-average” over six terms of the sequences, smoother estimate sequences are obtained, so that the determination of the *sq* critical phase-boundary can be extended up to  $D \lesssim 0.98D_{tr}$ , keeping within  $\approx 0.01\%$  the relative deviations from the best recent estimates<sup>23,37,39</sup> obtained by transfer matrix<sup>23</sup> or MC simulations<sup>37,39</sup>. This is shown in Fig. 3. For  $D > 0.98D_{tr}$ , the *sq* critical boundary obtained from the HT expansion and represented as a solid line in Fig. 3 is only slightly higher in temperature than the cited recent estimates that for comparison are reported as full dots on the curve. For graphical clarity, this figure blows up only a small vicinity of the TCP. A more extensive comparison of the data in the literature with the series estimates obtained in our study, appears in the Tables III and IV. The MRA value of the critical temperature at  $D = 0$  (i.e. for the Ising model with spin  $S = 1$ ) to which we have attached a very generous uncertainty, also appears in this Table to give an idea of the precision of the various simulations. Similarly for higher values of  $D$ , the spread among the simulation data from the various sources suggests that, in some of the older studies, the uncertainties were

underestimated. A set of very accurate recent estimates of points in the first-order part of the phase-boundary<sup>23,37,39</sup> is also reported in Fig. 3. The series estimates of these points, indicated as small open circles in the figure, are obtained by determining the intersections of the values of the free-energies computed from LT and HT expansions. They are completely consistent with the cited results except perhaps just beneath the tricritical temperature, in the range  $0.14 \lesssim \tilde{T} \lesssim 0.15$ , in which the intersection method produces less accurate results. For this calculation, it is convenient to use the temperature-grouped  $sq$  lattice LT expansion of the free-energy, that extends to order  $u^{20}$ . Applying the intersection method of the LT and HT expansions of the free-energy for  $T > T_{tr}$ , but looking for tangency points instead of crossings, yields a critical phase-contour slightly lower in temperature than that obtained by the MRAs of the (mixed) susceptibility HT expansion, an effect which probably reflects only the need of longer LT series as  $T$  increases. A similar defect was observed in the earliest series study<sup>43</sup>.

Fig. 4 shows the phase diagram in the concentration-temperature plane  $(X, \tilde{T})$ . The concentration is defined by Eq. (8). The second-order part of this phase-contour is obtained forming the highest-order available PAs of the HT expansion of  $X(K, D; 1)$  in powers of  $K$ , evaluating them on the critical contour in the  $(\tilde{\Delta}, \tilde{T})$  plane, represented in Fig. 3 and averaging these estimates. The same prescription can be directly used also starting with the recent simulation and transfer-matrix data<sup>23,37,39</sup> for the critical phase-contour of the  $sq$  lattice in the  $(\tilde{\Delta}, \tilde{T})$  plane, thus obtaining the points indicated by black dots in the Fig. 4. The results agree with those from the series within less than 0.1%. The prescription adopted for the PA resummation of the concentration series generally converges well except for  $0.35 \lesssim X \lesssim 0.45$ . In this interval, we might have to allow for uncertainties in  $\tilde{T}$  of the order of 1%. It must be stressed that the shape of this critical phase-contour, differs markedly from its MF counterpart, unlike what is observed in the  $3d$  analysis. We are finally led to the estimate  $X_{tr} = X(K(D_{tr}), D_{tr}; 1) = 0.779(1)$ , so that the value  $X_{tr} = 0.4549506(2)$  of the critical concentration proposed in Ref. [22] and represented by a star in the Fig. 4, or a similar value suggested by an earlier simulation<sup>24</sup> should be corrected by nearly a factor 2. The right-hand branch of the first-order phase-contour, is obtained evaluating the HT expansion of  $X(K, D; 1)$  on the upper rim of the first-order phase-contour in the  $(\tilde{\Delta}, \tilde{T})$  plane, shown in Fig. 3 (these points are thus approached from the right-hand side of the  $T = T(D; 1)$  curve). The LT expansion of  $X$  should be evaluated at the same points, to represent the lower rim of the first-order line in the  $(\tilde{\Delta}, \tilde{T})$  plane and thus also the left-hand branch of the phase-boundary in the  $(X, \tilde{T})$  plane is obtained. Unfortunately this branch fails to reach the value  $X_{tr}$  and therefore to corroborate our estimate of this quantity. It is useful to add that for this last computation, a PA resummed “field grouped” LT expansion turns out to be more convenient than a PA resummed “temperature grouped” expansion.

The fluctuation of the concentration, namely the concentration susceptibility  $Y(K, D; 1)$  defined by Eq. (9), is expected from Eq. (36) to show only a mild specific-heat-like singularity along the critical phase-contour and to diverge strongly at the TCP. However, our series analysis in  $2d$  suggests in Fig. 5 that  $Y(K, D; 1)$  remains finite as  $T$  approaches the critical phase-contour from above, for all fixed  $D < D_{tr}$ . No theoretical explanation of this behavior is known<sup>69,77</sup>. The same figure shows that along the critical phase-contour,  $Y(K, D; 1)$  grows steeply as  $D \rightarrow D_{tr}$ .

For several values of  $D \ll D_{tr}$  and a few values closer to  $D_{tr}$ , Fig. 6 shows the twelve highest-order terms (out of the 24 available) in the MRA estimator-sequences of the susceptibility exponent  $\gamma^{(2;0)}(D; 1)$ . The terms in the sequences are formed with the expansions of the mixed susceptibility  $\chi_{(2;2)}(K, D; 1)$  and are plotted vs the power  $1/n^\theta$  of the number  $n$  of HT coefficients used in the computation. Whenever possible, the behavior of last few (from two to five) terms of each sequence is extrapolated to large  $n$  choosing  $\theta = 2.5$  in the Ansatz Eq. (C6). The extrapolations are indicated by dashed lines. A solid line interpolates among the symbols, to profile clearly the trend of each sequence and show when it appears to settle down in the asymptotic behavior predicted by Eq. (C5). The MRA sequences computed for  $D \lesssim 0.7D_{tr}$ , tend to flatten for sufficiently large  $n$  and thus can be convincingly extrapolated. On the contrary, for  $0.7D_{tr} < D < D_{tr}$ , the MRA sequences develop pronounced oscillations so that a simple-minded extrapolation by Eq. (C5) of their last few available terms, would lead to irregular fluctuations in the final exponent estimates. Therefore in this range of  $D$ , no extrapolations are indicated in Fig. 6.

In Fig. 7 the results of the above procedure using the expansions of the ordinary (higher) susceptibilities or their  $D$ -derivatives, are summarized by plotting vs  $\tilde{\Delta}$  the relative deviations  $rdv$  from the  $2d$  Ising exponents, of the extrapolated values of the MRA estimator-sequences for the exponents  $\gamma^{(2;0)}(D; 1)$ , and  $\gamma^{(4;0)}(D; 1)$ . These deviations are defined as  $rdv = \frac{\gamma^{(2r;0)}(D;1)}{\gamma^{(2r;0)}(0;1)} - 1$  (with  $r = 1, 2$ ), for  $D < D_{tr}$  and our estimates of them are quite small over a large range of values of  $D$  since they exceed 1% only in the crossover region for  $D \gtrsim 0.7D_{tr}$ . Also the exponent  $\nu(D; 1)$  can be simply obtained using the hyperscaling relation. The uncertainties of the exponent deviations are smaller than the size of symbols. The figure does not include points from MRA sequences in the region in which simple-minded extrapolations are not safe. These results corroborate the validity of universality over a large part of the critical boundary.

The effects of the crossover at  $D \gtrsim 0.4D_{tr}$ , show up also when studying the behavior of the first few terms  $\mathcal{I}_6^+$ ,  $\mathcal{I}_8^+$  and  $\mathcal{J}_8^+$  of the sets of universal ratios of critical amplitudes defined by Eqs. (38) and (39). These quantities, computed forming first-order DAs for the appropriate non-singular universal ratios of the higher susceptibilities, are

TABLE III: BC model with  $S = 1$  on the  $sq$  lattice in zero magnetic field. Phase-contour  $T_c = T_c(\Delta; 1)$  from MC simulations, transfer-matrix and the analysis of the expansions of the ordinary susceptibility (or of its  $D$ -derivatives). Temperatures and crystal fields are not normalized to the coordination number  $q$ , unlike elsewhere in the text.

$\Delta/J$	$T/J$							Trans.Ord.	
	This paper	Ref.[23]	Ref.[39]	Ref.[37]	Ref.[21]	Ref.[34]	Ref.[36]		Ref.[22]
0.	1.69378(4)				1.695	1.714(2)	1.693(3)		Second
0.5	1.5664(1)				1.567	1.584(4)	1.564(3)		Second
1.	1.3986(1)				1.398	1.413(1)	1.398(2)		Second
1.5	1.1467(1)				1.150	1.155(1)	1.151(1)		Second
1.7027(1)	0.994(5)	1.	1.						Second
1.75	0.950(1)						0.958(1)		Second
1.80280(6)			0.80						Second
1.87	0.812(1)				0.800	0.800(3)			Second
1.87879(3)		0.80							Second
1.9	0.766(1)					0.755(3)	0.769(1)		Second
1.92	0.7289(2)				0.700	0.713(2)			Second
1.9336(4)		0.70							Second
1.93296(2)		0.70							Second
1.9379(5)		0.69							Second
1.9421(5)		0.68							Second
1.9461(5)		0.67							Second
1.9501(2)	0.656(4)	0.66		0.66	0.650	0.651(2)	0.659(2)		Second
1.95273(1)			0.65						Second
1.9533(1)		0.65							Second
1.9534(1)				0.65					Second
1.9565(1)		0.64		0.64					Second
1.9596(2)		0.63							Second
1.95980(5)				0.63					Second
1.96270(1)				0.62					Second
1.96539(1)		0.61							Second
1.96550(1)				0.61	0.61				Second
1.9658149(2)							0.60857756(4)		TCP
1.96582(1)		0.60858(5)							TCP
1.96604(1)				0.608					TCP

biased with the series estimates of the critical boundary  $T_c = T_c(D)$ . In Fig. 8, we have plotted vs  $\tilde{\Delta}$  the relative deviations  $rdv$  of these ratios from their  $D = 0$  (i.e. pure Ising) values. They remain quite small over a wide range of values of  $D$  up to  $D \lesssim 0.4D_{tr}$ . A good consistency with the universality predictions is observed, although as  $D$  approaches  $D_{tr}$ , the convergence rate of the analysis methods deteriorates.

In the Fig. 9, we have plotted the critical amplitudes of  $\chi_{(2;0)}(K, D; 1)$  and  $\chi_{(4;0)}(K, D; 1)$  vs  $\tau$  for the  $sq$  lattice, showing that our estimates are consistent with the predictions of amplitude-scaling and with the location of the TCP determined in Ref. [22], where they should vanish. These quantities are estimated forming DAs of the effective amplitudes (see for example Eq. (37) for the the ordinary susceptibility) biased with the series estimates of the critical temperatures  $T_c = T_c(D)$  and the Ising values of the exponents, so that this calculation *must assume* that exponent universality is valid over all the critical boundary.

In conclusion, strong crossover effects are observed in the analysis of the  $sq$  lattice series. Therefore, we have not indicated extrapolations in some figures, and expect that, in this range of  $D$ , significantly extended series and/or improvements of the simple numerical methods of our analysis would be needed.

TABLE IV: (Continued from the preceding Table) BC model with  $S = 1$  on the  $sq$  lattice in zero magnetic field. Phase-contour from MC simulations, transfer-matrix and the analysis of the expansions of the ordinary susceptibility (or of its  $D$ -derivatives). Our estimates of the first-order part of the phase-contour are obtained by the LT-HT intersection method. Temperatures and crystal fields are not normalized to the coordination number  $q$ , unlike elsewhere in the text.

$\Delta/J$	$T/J$					Trans.Ord.
	This paper	Ref.[23]	Ref.[39]	Ref.[37]	Ref.[21]	
1.968174(3)			0.60			First
1.96820(3)		0.60				First
1.96825(1)				0.60		First
1.97080(5)				0.59		First
1.97072(5)		0.59				First
1.97308(4)	0.581(2)	0.58				First
1.97323(1)				0.58		First
1.97528(4)		0.57				First
1.9777(1)	0.565					First
1.97744(3)	0.5602(4)	0.56				First
1.97766(1)				0.56		First
1.97950(3)		0.55				First
1.98142(2)	0.543(4)	0.54				First
1.98490(2)	0.519(2)	0.52				First
1.98786(1)	0.502(2)	0.50				First
1.99036(1)	0.481(2)	0.48	0.48			First
1.992479(1)	0.460(1)	0.46	0.46			First
1.994232(5)	0.440(1)	0.44	0.44			First
1.99681357	0.399(2)	0.40	0.40	0.40	0.40	First
1.99842103	0.36	0.36		0.36		First
1.99932488	0.32	0.32		0.32		First
1.968174(3)			0.60			First
1.96820(3)		0.60				First
1.96825(1)				0.60		First
1.97080(5)				0.59		First
1.97072(5)		0.59				First
1.97308(4)	0.581(2)	0.58				First
1.97323(1)				0.58		First

## V. THE BC MODEL WITH SPIN $S = 1$ IN $3d$

Generally, for the BC model with spin  $S = 1$  at zero field on three-dimensional lattices, the HT analysis is numerically simpler than in the  $sq$  case, because the series expansions show smoother behaviors.

For the  $sc$  lattice, Fig. 10 shows the phase diagram in the anisotropy-temperature plane. The position of the TCP determined in the MC simulation of Ref.[30] is  $\tilde{\Delta}_{tr} = 0.474113(5)$  with  $\tilde{T}_{tr} = 0.2363(1)$ . A more recent (and probably more accurate) MC estimate<sup>32</sup>, indicated in the figure by a big open crossed circle, is  $\tilde{\Delta}_{tr} = 0.474617(16)$  with  $\tilde{T}_{tr} = 0.23365(4)$ , so that  $D_{tr} = 2.0313(4)$ . The same simulation moreover indicated the value  $X_{tr} = 0.6485(2)$  for the critical concentration.

A sample of the results from MRA extrapolations for the ordinary susceptibility  $\chi_{(2;0)}(K, D; 0)$  (to which generous error bars are attached) is reported in Table V and compared with those of earlier MC studies. Our extrapolations agree well with MC data<sup>30,33</sup> over the range of values of  $\tilde{\Delta}$  in which both analyses are available, except very close to the TCP. At  $\Delta/J = 2.82$ , a visible difference appears between the estimate of Ref. [33] and that of the series. However the latter are likely to be more accurate up to the TCP. From the Table V, an excellent agreement can be observed between the series and the simulation results, in particular at the value<sup>27,28</sup>  $D = 0.655$  or equivalently  $\Delta/J = 1.689\dots$ , in which the corrections to scaling are expected to be minimal, so that also the MC estimates can be very accurate.

A sequence of points in the first-order part of the phase-boundary is also shown in Fig. 10. As anticipated, it is obtained locating the intersections of the LT and HT expansions of the free-energies in the region in which both might be approximately valid. In this calculation, we have used the temperature-grouped *sc* lattice LT expansion of the free-energy, that extends to order  $u^{42}$ . Both the HT and the LT expansions are resummed by the highest available PAs. Except very close to the TCP, the resulting estimates appear quite reasonable, but unfortunately no independent estimates exist. The method based on the joint use of LT and HT expansions might be applied also at temperatures above  $T_{tr}$  at which the transition is continuous, to reproduce also the critical phase-boundary. One should then look for tangency points of the LT and HT free-energy curves. While such points do exist for  $\tilde{T} > \tilde{T}_{tr}$ , they yield estimates falling systematically below (in temperature) those previously obtained from the analysis of the susceptibility HT expansions. This fact is not surprising, at least because as the temperatures increase, longer LT expansions would be needed. Also in the case of the *fcc* lattice expansions<sup>43</sup>, the second-order line computed in this way suffered from the same shortcomings.

The Fig. 11, contains a bilogarithmic plot of the ordinary susceptibility evaluated along the path  $D = D_{tr} - 2.15(2)(1 - K/K_{tr})$  tangent to the phase-boundary at the TCP and suggesting the value  $\gamma_u = 2.00(5)$  of the critical exponent. This implies  $\phi_u = 2.00(5)$ .

In Fig. 12, the phase-contour is drawn in the  $(\tau, \tilde{T})$  plane to show that it continues to be very nearly a straight line down to  $\tau \approx 0.1$ .

The phase diagram in the concentration-temperature plane  $(X, \tilde{T})$  for the *sc* lattice is shown in Fig. 13. The phase-boundary is obtained averaging the highest possible PAs of the HT expansion of  $X(K, D; 1)$  evaluated along the critical contour in the anisotropy-temperature plane shown in Fig. 10. At  $(D = D_{tr}, K = K_{tr})$ , the estimate  $X_{tr} = 0.666(3)$  is obtained for the critical concentration. Unlike what is observed for the *fcc* lattice<sup>43</sup>, in this case the LT expansions are sufficiently long to show that the left-hand branch of the first-order line reaches the TCP, with good approximation.

The same considerations as for the *sq* lattice can be repeated here for the *sc* lattice. The behavior of  $Y(K, D; 1)$  observed in our series analysis is illustrated in Fig. 14 that indicates an asymptotically finite behavior along the critical phase-contour and a strong divergence as the TCP is approached from above at fixed  $D = D_{tr}$ . In  $3d$  the mild specific-heat-like divergence expected on the critical contour is not observed experimentally and no theoretical explanation of this fact is known<sup>69,77</sup>. In the following Fig. 15, this behavior is contrasted with that of the ordinary susceptibility that diverges over all the critical boundary, albeit showing a smaller exponent at the TCP.

When computing the MRA sequences for the critical exponents  $\gamma^{(2;0)}(D; 1)$  from the expansion of the ordinary susceptibility  $\chi_{(2,0)}(K, D; 1)$ , crossover effects begin to appear only at values of  $D$  significantly closer to  $D_{tr}$  than in the *sq* lattice analysis. Correspondingly our simple extrapolation procedure becomes less reliable and its results begin to deviate from the Ising value of the exponent. This effect however might partly be due to some residual upward concavity in the curves to be extrapolated, which we have not attempted to account for. The ensuing indication is that the extrapolation of longer expansions is likely to lead to a closer agreement with the Ising values. The Fig. 16 shows the smoother MRA estimator-sequences of the exponent  $\gamma^{(2;0)}(D; 1)$  computed from the mixed susceptibility  $\chi_{(2,1)}(K, D; 1)$ . The lowest curve shown in this figure shows the sequence evaluated at  $D \approx D_{tr} = 2.8446$ . Its extrapolated value is close to the expected MF tricritical exponent,  $\gamma^{(2;0)}(D_{tr}; 1) = 1$ , within an uncertainty that might be ascribed to the presence of logarithmic corrections (unaccounted for by this approach).

For several values of  $\tilde{\Delta}$  indicated on the curves, the Fig. 17 shows the behavior of high-order PAs of the effective exponent  $\gamma^{(2;0)}(D; 1)$  vs the deviation  $1 - K/K_c(\tilde{\Delta})$  from the corresponding critical temperatures. This computation uses the expansion of  $\chi_{(2,0)}(K, D; 1)$ .

Finally, still for the *sc* lattice, the Fig. 18 summarizes all these results showing the relative deviations  $rdv$  from the Ising values of the extrapolated estimator-sequences (defined as for the *sq* lattice) for the exponents  $\gamma^{(2;0)}(D; 1)$  and  $\gamma^{(4;0)}(D; 1)$  determined over a large interval of values of  $D$  nearly reaching the TCP. The two exponents have been evaluated by extrapolating the MRA estimator-sequences. Assuming the validity of the hyperscaling relation  $\gamma^{(4;0)}(D; 1) = 2\gamma^{(2;0)}(D; 1) + d\nu(D; 1)$  also the universality of  $\nu(D; 1)$  can be checked. It might be conventionally assumed that the slowdown of convergence rate and thus the crossover region begins where the deviation of the estimated exponents from the Ising values<sup>60</sup> exceeds 0.5%, namely at the value  $D \approx 0.9D_{tr}$ .

The Fig. 19 plots vs  $\tau$  the critical amplitudes  $A_{(2,0)}$  (full triangles) of  $\chi_{(2;0)}(K, D; 1)$  and  $-A_{(4,0)}$  (full circles) of  $\chi_{(4;0)}(K, D; 1)$  and shows that they vanish as the TCP is approached.

In Fig. 20 the solid lines are from a fit comparing the predictions of the amplitude-scaling property, with the behaviors the critical amplitudes  $A_{(2,0)}$  (full triangles) of  $\chi_{(2;0)}(K, D; 1)$  and  $-A_{(4,0)}$  (full circles) of  $\chi_{(4;0)}(K, D; 1)$  vs  $1 - \Delta/\Delta_{tr}$  under the assumption that  $\phi = 2$  and the position of the TCP is well determined in Ref. [32].

The LT expansions with  $H \neq 0$  for the three-dimensional lattices are used to study the expansion of the magnetization in powers of  $\mu = \exp(-H)$ . The (field-grouped) magnetization is resummed by a simple [5/6] PA that uses all available coefficients. In particular, Fig. 21 shows the spontaneous magnetization vs  $u$  for several equally spaced values of  $-1.44 \leq D \leq D_{tr} \approx 2.0313$ . In Fig. 22 the same PA is used to represent the behavior of the magnetization



TABLE V: The BC model with  $S = 1$  on the  $sc$  lattice. Phase-contour  $T_c = T_c(\Delta; 1)$  from MC simulations and from the analysis of the expansions of the ordinary susceptibility. The estimates of the first-order part of the phase-contour are obtained by the LT-HT intersection method. To retain the conventions of most authors, the data for the temperatures and the crystal fields, unlike those in the figures and in the text, are not normalized to the coordination number  $q$ .

$\Delta/J$	$T/J$						Trans.Ord.
	This paper	Ref.[33]	Ref.[30]	Ref.[32]	Ref.[38]	Ref.[28]	
0.	3.19622(2)	3.20(1)					Second
1.	2.877369(3)(1)	2.88(1)					Second
1.43474(1)	2.7						Second
1.5	2.670434(1)						Second
1.68933856...	2.57914(3)					2.5791695...	Second
1.83970(1)	2.5						Second
2.	2.407314(1)	2.42(1)					Second
2.16568(1)	2.3						Second
2.2	2.275495(1)	2.27(2)					Second
2.4	2.118974(1)	2.11(2)					Second
2.42144(1)	2.1						Second
2.523(6)					2.		Second
2.52513(1)	2.						Second
2.61361(1)	1.9						Second
2.68752(1)	1.8						Second
2.74738(1)	1.7						Second
2.79370(1)	1.6						Second
2.80		1.61(5)					Second
2.82		1.59(4)					Second
2.82693(1)	1.5						Second
2.83874(1)	1.45						Second
2.8446(3)					1.4182		TCP
2.8448(3)	1.421(3)		1.4182(55)				TCP
2.8477(1)	1.403(2)			1.4019(3)			TCP
2.8502	0.221(1)						First
2.890	0.201(1)						First
2.961	0.152(1)						First
2.994	0.108(1)						First
2.998	0.0835(2)						First

vs  $h$ , at fixed  $D = D_{tr} \approx 2.0313$  and at a few other values of  $D$  such that  $0 \leq u(D) \leq u_c(D_{tr})$ . The asymptotic behaviors of the curves shown in these figures are consistent with the expected values of the exponents  $\beta_{tr}$  and  $\delta_{tr}$ . Longer LT expansions would be needed to obtain also reliable estimates of the uncertainties.

Generally, completely similar results are obtained from the analysis of the  $bcc$  lattice, so that for brevity most of the corresponding figures are omitted. For this lattice (see the Table VI and the Fig. 23), the series analyses show a faster convergence and a narrower crossover region than in the  $sc$  case. In spite of these more favorable features, we have continued to attach quite generous error bars also to the estimates for this lattice.

A single estimate<sup>15</sup> of the TCP position for the  $bcc$  lattice:  $\tilde{\Delta}_{tr} = 3.792$ ,  $\tilde{T}_{tr} = 2.024$  (with undetermined uncertainties) can be found in the literature. Its location is indicated by a star in the Fig. 23. The results of the series analysis suggest that slightly smaller values for both coordinates might be preferred. We conjecture that  $3.7785 \leq \tilde{\Delta}_{tr} \leq 3.795$  and  $2. \geq \tilde{T}_{tr} \geq 1.90(3)$ .

The first-order part of the phase-boundary for the  $bcc$  system, obtained as in the  $sc$  lattice analysis, is also shown in this figure. We have used the temperature-grouped LT expansion of the free-energy that extends to order  $u^{56}$ . Quite reasonable estimates are obtained even very near the expected TCP. Also for the  $bcc$  lattice, as for the  $sc$  lattice, no independent results for this region of the phase-boundary are available for comparison.

Results similar to those of the Fig. 18 are obtained also in the case of the  $bcc$  lattice. For  $D \lesssim .4D_{tr}$ , the estimated limits of the MRA sequences for the exponents show relative deviations  $< 10^{-3}$  from the Ising values.

TABLE VI: The BC model with  $S = 1$  on the  $bcc$  lattice. Phase-contour  $T_c = T_c(\Delta; 1)$  the analysis of the expansions of the ordinary susceptibility (or of its  $D$ -derivatives). Our estimates of the first-order part of the phase-contour are obtained by the LT-HT intersection method. Temperatures and crystal fields are not normalized to the coordination number  $q$ , unlike elsewhere in the text. No independent estimates exist.

$\Delta/J$	$T/J$	Trans.Ord.
0.0	4.4512(1)	Second
1.36015(1)	4.	Second
1.83802(1)	3.8	Second
2.25133(1)	3.6	Second
2.60624(1)	3.4	Second
2.76339(1)	3.3	Second
2.90771(1)	3.2	Second
3.15972(1)	3.	Second
3.36555(1)	2.8	Second
3.52797(1)	2.6	Second
3.59367(1)	2.5	Second
3.64940(1)	2.4	Second
3.69547(1)	2.3	Second
3.73215(1)	2.2	Second
3.75975(1)	2.1	Second
3.778476(1)	2.	Second
		TCP
3.795	1.897(1)	First
3.865	1.610(1)	First
3.957	1.199(1)	First
3.980	0.995(1)	First
3.997	0.6892(1)	First

Moreover, in the case of the  $bcc$  lattice, properties similar to those of the  $sc$  lattice are shown in Fig. 24 for the phase diagram in the concentration-temperature plane. The series estimate  $X_{tr} = 0.69(1)$  of the critical concentration, is obtained for the  $bcc$  lattice. For brevity, no figure is devoted to the concentration susceptibility  $Y(K, D; 1)$  because its behavior is completely similar to that for the  $sc$  lattice.

The Fig. 25 shows the dependence on  $\tau$  of the critical amplitudes  $A_{(2,0)}$  (full triangles) of  $\chi_{(2,0)}(K, D; 1)$  and  $-A_{(4,0)}$  (full circles) of  $\chi_{(4,0)}(K, D; 1)$ , for  $\tau$  in a small vicinity of the TCP of the  $bcc$  lattice.

The estimates of the universal ratios of critical amplitudes  $\mathcal{I}_6^+$ ,  $\mathcal{I}_8^+$  and  $\mathcal{J}_8^+$ , are shown in the Fig. 26, for both the  $sc$  and the  $bcc$  lattices. For these ratios, it is convenient to plot vs  $\tilde{\Delta}$  the relative deviations  $rdv$  from the Ising values. They are quite small up to  $\tilde{\Delta} \lesssim 0.4$ , whereas for larger values of  $\tilde{\Delta}$ , it is the convergence rate of our methods that slows down.

## VI. THE BC MODEL WITH SPIN $S = 3/2$ ON THE $sq$ LATTICE

The phase diagram in the  $(\tilde{T}, \tilde{\Delta})$  plane for the spin  $S = 3/2$  system on the  $sq$  lattice (together with those for the  $sc$  and the  $bcc$  lattices) is shown in Fig. 27. The phase-boundary in the MF approximation, which is given by the curve highest in temperature is also reported for comparison.

Also for this value of the spin, very accurate determinations of the phase-boundary and exponents up to  $\tilde{\Delta} \lesssim 0.45$  and for  $\tilde{\Delta} \lesssim 0.55$  are obtained by forming MRAs of the HT expansion of  $\chi_{(2,0)}(K, D; 3/2)$ . In the range  $0.45 \lesssim \tilde{\Delta} \lesssim 0.55$ , the MRA sequences oscillate and thus their extrapolations are not straightforward. In Sect. IV D, this fact was related to the presence of nearby singularities accompanied by the weakening of the critical amplitudes for  $\tilde{\Delta} \approx 1/2$ . It is suggested by the MF approximation and subsequently confirmed by a MC simulation<sup>14</sup>, that a critical end-point of the first-order transition in the LT region of the phase diagram lies very close to the  $sq$  critical border, at  $\tilde{\Delta} \approx 0.492$  with  $S^2\tilde{T} \approx 0.09$ . It is then likely that the asymptotic behavior of the HT expansion coefficients of the susceptibility is sensitive also to this nearby singularity and that in a vicinity of this value of  $\tilde{\Delta}$ , it is more convenient to form the MRAs of  $\chi_{(2,1)}(K, D; 3/2)$  instead of those of  $\chi_{(2,0)}(K, D; 3/2)$  to determine the phase-boundary.

The numerical results for the phase-boundary can be used, together with the known Ising exponents, to bias the determination of the critical amplitudes of  $\chi_{(2;0)}(K, D; 3/2)$  and  $-\chi_{(4;0)}(K, D; 3/2)$ , that are plotted for graphical convenience vs  $(1 + \exp(2d))^{-1}$  in Fig. 9, together with the analogous quantities for the spin  $S = 1$  system to contrast the respective behaviors. After decreasing to a very small minimum at  $\tilde{\Delta} \approx 1/2$ , the amplitudes for  $S = 3/2$  system sharply rise. This behavior is not surprising because for large values of  $\tilde{\Delta}$ , the spin  $S = 3/2$  model reduces to a spin  $S = 1/2$  model, for which these amplitudes are sizable.

As shown in Fig. 28, only for values of  $\tilde{\Delta} \approx 0.5$ , the estimates of the exponent  $\gamma^{(2;0)}(D; 3/2)$  along the phase-boundary, obtained extrapolating the MRA sequences with the Ansatz Eq. (C7), deviate up to a few percent from the expected Ising value.

The fluctuations in a small interval around  $\tilde{\Delta} = 1/2$ , are not so strong as to indicate a violation of universality, but only a slower convergence rate of our numerical procedures.

In Fig. 29, the relative deviations  $rdv$  from the Ising values for the universal ratios of critical amplitudes  $\mathcal{I}_6^+$ ,  $\mathcal{I}_8^+$  and  $\mathcal{J}_8^+$ , are plotted vs  $\tilde{\Delta}$  in the interval  $-2. \leq \tilde{\Delta} \leq 2$  to show that they remain Ising-like over a large interval of values of  $\tilde{\Delta}$  and display no serious anomalies that might signal the presence of a TCP. At larger values of  $\tilde{\Delta}$ , we observe a slowdown of the convergence rate of the approximations rather than a failure the universality properties.

In conclusion, for this lattice, no indications appear of a TCP with its ensuing first-order line, so that the behavior of the model is Ising-like over a large range of values of  $D$  and the qualitative predictions of the MF approximation for the half-odd-spin BC models are fully confirmed.

## VII. THE BC MODEL WITH SPIN $S = 3/2$ IN $3d$

The phase-boundaries of the spin  $S = 3/2$  systems for both the *sc* and the *bcc* lattices are drawn in the same Fig. 27. For the former system, a critical-end-point at<sup>16</sup> ( $\tilde{\Delta} \approx 0.491, S^2\tilde{T} \approx 0.095$ ) or at<sup>12</sup> ( $\tilde{\Delta} \approx 0.4922, S^2\tilde{T} \approx 0.103$ , not far from the phase-contour (but less close to it than in the *sq* case) is likely to influence the convergence of the simplest MRAs formed with the expansions of the ordinary susceptibility  $\chi_{(2;0)}(K, D; 3/2)$ . A similar problem might occur for the *bcc* lattice. As observed for the *sq* lattice, in a neighborhood of  $\tilde{\Delta} = 1/2$ , a faster convergence in the determination of the critical boundary can be achieved using the HT expansions of the  $D$ -derivative of the susceptibilities.

In Fig. 30, the sequences of MRA estimators of the critical exponent  $\gamma^{(2;0)}(D; 3/2)$  are plotted vs  $1/n^\theta$  with  $\theta = 0.5$ , for the *sc* lattice. The diagram obtained for the *bcc* lattice is completely similar and therefore it needs no separate illustration. The MRA sequences are computed for several values of  $-1.5 \lesssim \tilde{\Delta} \lesssim 0.85$ , using Eq. (C4). As in the analogous figures for the other BC systems considered so far, a solid line interpolates among the terms of each sequence, while the last few points of the sequence are extrapolated to large expansion order by a fit of Eq. (C5). It is clear that in a wide range of values of  $D$ , no significant anomalies are observed all along the phase-boundary and the exponent estimates remain Ising-like within  $\approx 10^{-3}$ . The terms of the MRA sequences for  $\tilde{\Delta} \approx 0.443$  and  $\tilde{\Delta} \approx 0.507$ , are indicated by triangles.

For the *bcc* lattice, the next Fig. 31 is devoted to the effective exponent of the susceptibility. The curves are computed for various values of  $D$  by forming the highest-order, defect-free, diagonal or near-diagonal PAs of the HT expansions of the effective exponents and each one is plotted vs the corresponding deviation  $1 - K/K_c(D)$  from the critical temperature. The curves show that the effective critical exponents are Ising-like in a vicinity of  $K_c(D)$  that becomes very narrow as  $\tilde{\Delta} = 1/2$  is approached from below, while it expands for smaller or larger values of  $\tilde{\Delta}$ . The figure obtained for the *sc* lattice, is completely similar and therefore is omitted.

It is also useless to include for the *sc* and the *bcc* lattices, figures summarizing the relative deviations  $rdv$  from the Ising values of the extrapolated MRA estimator-sequences for the exponents  $\gamma^{(2;0)}(D; 3/2)$  of  $\chi_{(2;0)}(K, D; 3/2)$ , and  $\gamma^{(4;0)}(D; 3/2)$  of  $\chi_{(4;0)}(K, D; 3/2)$ . over a large range of values of  $D$ . It is enough to remark that the BC system is confirmed to remain Ising-like along the phase-boundary up to large values of  $D$ , and the few-percent fluctuations of the exponent estimates, observed in a neighborhood of  $\tilde{\Delta} = 1/2$  are certainly due only to a slowdown of the convergence rate of the approximations and should not be taken as indications of anomalies.

Similarly the figures showing the relative deviations from the Ising values for the universal ratios of critical amplitudes  $\mathcal{I}_6^+$ ,  $\mathcal{I}_8^+$  and  $\mathcal{J}_8^+$  on the *sc* and the *bcc* lattices can be omitted. Again no such anomalies are observed in the estimates that might suggest the presence of a TCP. As for the exponents, the small fluctuations in the estimates are likely to be due only to a local slowdown of the approximations convergence rate.

In the Figs. 19 and 25, the critical amplitudes of  $\chi_{(2;0)}(K, D; 3/2)$  and  $\chi_{(4;0)}(K, D; 3/2)$  are plotted vs  $(1 + \exp(2d))^{-1}$  for graphical convenience, for the *sc* and of the *bcc* lattices, to emphasize the qualitative difference of their behavior from that of the spin  $S = 1$  case. Just as observed for the *sq* lattice, after a fast decrease as  $\tilde{\Delta} \rightarrow 1/2$ , the amplitudes rise sharply with  $\tilde{\Delta}$  as they should since for large values of this field, the spin  $S = 3/2$  BC model tends to a spin  $S = 1/2$  model.

In conclusion, also in  $3d$  the behavior of the spin  $S = 3/2$  model appears qualitatively different from that of the spin  $S = 1$  model. As  $D$  varies, the exponent estimates remain Ising-like and thus consistent with the expected universality properties and with a previous MC simulation<sup>13</sup> confirming the absence of a TCP followed by a first-order line. The validity of the structural prediction of the MF approximation, at least for the model with the lowest non-trivial half-odd spin value is thereby confirmed.

## VIII. SUMMARY AND CONCLUSIONS

We have derived an extensive body of HT and LT expansions for many thermodynamical observables of the BC model with spin  $S = 1$  and  $S = 3/2$  on the  $sq$ , the  $sc$  and the  $bcc$  lattices in presence of a magnetic field. Our aim was to understand the potential of an approach to this model by long series expansions and possibly to demonstrate how it can be employed to map carefully a very wide region of the phase diagram, testing at the same time the universality properties for the critical exponents and for appropriate ratios of the critical amplitudes. The expansions of the moments of the correlation-function remain to be computed, so that only assuming the validity of hyperscaling, we had access to the correlation-length exponents, but of course not to the corresponding critical amplitudes.

Our analyses succeed in mapping the phase diagrams both in the anisotropy-temperature and in the concentration-temperature planes as well as in the verification, over large regions of the parameter space, of several expected universality properties. Moreover, although presented here only for the particular cases of spin  $S = 1$  and  $S = 3/2$  (the latter not studied in detail so far by series methods), they confirm the validity of the general indication emerging from the MF approximation, that a TCP can occur only in BC models with integer values of the spin.

Unlike what is observed for the  $3d$  lattices, for the system with spin  $S = 1$  on the  $sq$  lattice we have pointed out that the crossover region is very wide and the shape of the critical phase-contour in the concentration-temperature plane deviates markedly from the MF behavior. These remarks might be confirmed by simulations, that however have not been reported so far. Moreover, as in  $3d$ , the concentration susceptibility evaluated along the critical contour is finite and rises very steeply as  $\Delta \rightarrow \Delta_{tr}$ .

At HT, mostly in the case of the  $sq$  lattice with spin  $S = 1$ , the series-analysis approach meets with convergence problems in the tricritical region. As a result, we have not been able to improve the accuracy of the present determinations of the TCP parameters obtained by simulation or transfer-matrix methods, but we could only test their consistency with our analysis. We have conjectured that this difficulty might reflect the clustering of unphysical singularities nearby the series convergence border, accompanied by the vanishing of the critical amplitudes as the TCP is approached, (as it is prescribed by amplitude-scaling). In spite of the absence of a TCP, a similar problem arises also in the case of spin  $S = 3/2$ , in which a drastic increase of the complexity of the corrections to scaling takes place when the phase-contour approaches the critical end-point of the first-order transition line in the ordered phase. However, for both values of the spin, these convergence problems of our approximations can be alleviated by the simple prescription of studying the  $D$ - or  $K$ -derivatives of the susceptibility instead of the susceptibility to determine the phase-boundary, so that finally the range of validity of the standard single-variable methods of series analysis can be extended up to a small distance from the point  $\tilde{\Delta} \approx 1/2$ . Thus it seems that presently in this region both the transfer-matrix and the simulation methods might be more promising than the simplest series methods, because they do not need to keep a strict control of the leading singularities to determine the critical parameters.

For spin  $S = 1$ , at LT the only known method for mapping out the first-order part of the phase-boundary, based on the intersection of the LT and HT approximations of the free-energy in their expected common region of approximate validity, has given access to this part of the phase-contour also for the  $sc$  and the  $bcc$  lattices, so far not obtained by other numerical methods. The procedure however may loose precision in a small vicinity of the TCP.

In the future, it might be appropriate to return on this subject, not only because the BC models with spin  $S \geq 2$  are still unexplored by series methods, but also because several features of the behavior of the systems considered here need further illustration and moreover the simplest single-variable approximation methods employed in this study might perhaps have missed part of the information content of the expansions. In spite of all the limitations of our analysis, we are confident that the series data we have derived, might remain as a necessary tool for further extensions and for alternative analyses.

### Appendix A: Mean Field description of the phase structure

The simplest MF-like description<sup>10,51</sup> of a typical tricritical behavior is obtained starting with a Landau-Ginzburg Hamiltonian for a scalar field  $\phi(x)$  of the form

$$\mathcal{H}_{LG}(\phi) = \frac{1}{2}(\partial_k \phi)^2 + V(\phi) \quad (\text{A1})$$

with potential

$$V(\phi) = -H\phi + \frac{A_2}{2}\phi^2 + \frac{A_4}{4}\phi^4 + \frac{A_6}{6}\phi^6 \quad (\text{A2})$$

The coefficients  $A_{2i}$  are functions of the parameters that characterize the system, for example the temperature  $T$  etc. In the  $H = 0$  plane, a MF-like approximation is obtained restricting to  $x$ -independent configurations of the field  $\phi$  (i.e. neglecting its spatial fluctuations) and assuming  $A_6 > 0$  to ensure thermodynamical stability. One can then conclude<sup>51</sup> that a TCP occurs for values of the parameters such that  $A_2 = A_4 = 0$ . It separates a second-order line described by the equation  $A_2 = 0$  ( $A_4 > 0$ ), from a first-order line described by the equation  $A_2 = 3A_4^2/16A_6$ , (with  $A_4 < 0$ ).

A more realistic spin-dependent description of the essential features of the phase diagram of the BC model is formulated<sup>1,2,7</sup> turning to the standard MF approximation whereby the Hamiltonian of Eq. (1) with spin  $S$  is replaced by the solvable trial Hamiltonian

$$\mathcal{H}_0(\eta, \Delta, T; \{s_i\}) = -\frac{\eta}{S} \sum_i s_i + \frac{\Delta}{S^2} \sum_i s_i^2 \quad (\text{A3})$$

of non-interacting spins in external fields  $\eta$  and  $\Delta$ .

If  $\langle \cdot \rangle_0$  indicates the ensemble average with respect to  $\mathcal{H}_0$ , the specific magnetization  $m(\eta, \Delta, T) \equiv \langle s_0 \rangle_0$  is

$$m(\eta, \Delta, T) = \frac{S}{\beta} \frac{\partial \ln z_0(\eta, \Delta, T)}{\partial \eta} \quad (\text{A4})$$

with

$$z_0(\eta, \Delta, T) = \sum_{s=-S}^S \exp(\beta\eta \frac{s}{S} - D \frac{s^2}{S^2}) \quad (\text{A5})$$

and  $D = \beta\Delta$ .

The convexity inequality<sup>78,79</sup>

$$f(H, \Delta, T) \leq \phi(H, \eta, \Delta, T) \equiv -\frac{1}{\beta} \ln(z_0) + \frac{1}{N} \langle \mathcal{H} - \mathcal{H}_0 \rangle_0 \quad (\text{A6})$$

is used to optimize the choice of the effective magnetic field  $\eta$ . We have

$$\phi(H, \eta, \Delta, T) = -\frac{1}{\beta} \ln(z_0) - \frac{1}{2} Jq \frac{m^2}{S^2} + (\eta + H) \frac{m}{S} \quad (\text{A7})$$

with  $\phi$  interpreted as MF free-energy. The extremality condition

$$\frac{\partial \phi}{\partial \eta} = 0 \quad (\text{A8})$$

is taken as equilibrium condition of the MF theory.

Since from Eq. (A7)

$$\frac{\partial \phi}{\partial \eta} = -\frac{1}{\beta} \frac{\partial \ln z_0}{\partial \eta} + \frac{m}{S} + \frac{\partial m}{\partial \eta} \left( -\frac{qJ}{S^2} + \frac{\eta + H}{S} \right) \quad (\text{A9})$$

from Eqs.(A4) and (A8), it follows

$$\eta = \frac{Jqm}{S} - H \quad (\text{A10})$$

The dependence on  $\eta$  can be eliminated computing  $\eta(m, \Delta, T)$  from Eq. (A4) and substituting this expression in  $\phi$  to form the MF Helmholtz free-energy  $f$

$$f(H, \Delta, T) \equiv \phi(H, \eta(m, \Delta, T), \Delta, T) \quad (\text{A11})$$

which does not depend on  $m$ , since

$$\frac{\partial \phi(H, \eta(m, \Delta, T), \Delta, T)}{\partial m} = \frac{\partial \phi(H, \eta, \Delta, T)}{\partial \eta} \frac{\partial \eta(m, \Delta, T)}{\partial m} = 0 \quad (\text{A12})$$

due to Eq. (A8).

By Eq. (A7)

$$f(H, \Delta, T) = G(m, \Delta, T) + \frac{m}{S} H \quad (\text{A13})$$

and

$$G(m, \Delta, T) = -\frac{1}{\beta} \ln z_0(\eta(m, \Delta, T), \Delta, T) - \frac{1}{2} J q \frac{m^2}{S^2} + \frac{m}{S} \eta(m, \Delta, T) \quad (\text{A14})$$

denotes the Gibbs free-energy, the appropriate potential to study equilibrium at constant  $H$ . Eq. (A13) is the Legendre transformation relating the potentials  $f(H, \Delta, T)$  and  $G(m, \Delta, T)$ , that implies

$$\frac{\partial G(m, \Delta, T)}{\partial m} = -\frac{H}{S} \quad (\text{A15})$$

Eq. (A4) for  $\eta(m, \Delta, T)$  cannot be solved exactly, but for small  $m$ , we are allowed to expand  $\eta(m, \Delta, T)$  and  $G(m, \Delta, T)$  in powers of  $m$ .

Defining<sup>6</sup>  $\alpha_k = \frac{\partial^k \ln(z_0)}{\partial \eta^k} |_{\eta=0}$ , and inverting Eq. (A4)

$$\eta(m, \Delta, T) = \frac{\beta}{\alpha_2} \frac{m}{S} - \frac{\beta^3 \alpha_4}{6 \alpha_2^4} \frac{m^3}{S^3} + \beta^5 \left( \frac{\alpha_4^2}{12 \alpha_2^7} - \frac{\alpha_6}{120 \alpha_2^6} \right) \frac{m^5}{S^5} + O(m^7) \quad (\text{A16})$$

The expansion of the Gibbs free-energy for small  $m$  is

$$G = A_0 + \sum_{i=1} \frac{A_{2i}}{2i} \left( \frac{m}{S} \right)^{2i}. \quad (\text{A17})$$

Using Eq. (A14), it follows

$$A_0 = -\frac{\alpha_0}{\beta}, \quad A_2 = \frac{\beta}{\alpha_2} - Jq, \quad A_4 = -\frac{\beta^3}{6} \frac{\alpha_4}{\alpha_2^4}, \quad A_6 = \frac{\beta^5}{120 \alpha_2^7} (10 \alpha_4^2 - \alpha_2 \alpha_6) \quad (\text{A18})$$

The critical phase-boundary is obtained for  $A_2 = 0$  with  $A_4 > 0$  and so is described by the equation

$$\frac{\beta}{\alpha_2} = qJ \quad (\text{A19})$$

which is exact because along the critical line  $m = 0$ .

In the  $H = 0$  plane, the first-order part of the phase-boundary can also be studied in this expansion, but only nearby its end-point, where  $m$  is small. A first-order transition occurs where  $G(0, \Delta, T) = G(m, \Delta, T)$  with  $G'(m, \Delta, T) = 0$ . For small  $m$  with positive  $A_6$ , the  $O(m^8)$  term can be neglected in Eq. (A17), so that the first-order transition is obtained for

$$A_2 \approx \frac{3}{16} \frac{A_4^2}{A_6}, \quad \frac{m^2}{S^2} \approx -4 \frac{A_2}{A_4} \quad (\text{A20})$$

These equations are valid only for small  $m$ . As  $T$  is lowered from the end-point of the first-order line,  $m$  increases and the approximation becomes invalid.

Let us now discuss the critical lines that border the wings. Inserting Eq. (A10) in Eq. (A7)

$$f(m, H, \Delta, T) \equiv -\frac{1}{\beta} \ln(z_0(\eta = \frac{Jqm}{S} - H)) + \frac{1}{2S^2} Jqm^2 \quad (\text{A21})$$

For  $f' \equiv \frac{\partial f}{\partial m} = 0$  this is the MF free-energy. The critical lines that separate two phases are characterized by the vanishing of the first three derivatives of the free-energy with respect to  $m$ . Let us argue why it is so. At a minimum of

the potential  $f' = 0$ ,  $f'' \geq 0$ . Assume now that there are two such minima  $m_A$  and  $m_B$ . Since  $\int_{m_A}^{m_B} f''(m)dm = 0$ ,  $f''$  must take both positive and negative values. Then  $f'' > 0$  for  $m_A \leq m < m_a$  and  $f'' < 0$  for  $m_b \leq m < m_B$ , where  $m_a$  and  $m_b$  are two points at which  $f'' = 0$ . This implies that there exists a point  $m_* \in [m_a, m_b]$  at which  $f''' = 0$ . If the values  $m_A$  and  $m_B$  occur in two different phases and varying  $T$  they merge at the point  $m_A = m_a = m_* = m_b = m_B$ , then  $f' = f'' = f''' = 0$ .

This is the situation for the points on the critical lines of the wings that separate two phases. Solving the two equations  $f'' = 0$  and  $f''' = 0$  in the variables  $\eta = \frac{Jqm}{S} - H$  and  $K$  and then using  $f' = 0$ , we can write  $m$  and  $H$  in terms of  $K$ . This can be done analytically for spin  $S = 1$  and numerically for spin  $S = 3/2$ .

The previous remarks apply also to the whole critical phase-contour in the  $H = 0$  plane. In this case the equations  $f' = f''' = 0$  are trivially satisfied for  $m = H = 0$  and the equation  $f'' = 0$  must lead to the same result as using  $A_2 = 0$  in the approach outlined above that uses the expansion of the Gibbs free-energy.

### 1. The spin S=1 model

For this value of the spin, Eq. (A5) takes the form

$$z_0 = 1 + 2 \exp(-D) \cosh(\beta\eta) \quad (\text{A22})$$

so that expanding  $\ln z_0(\eta) = \ln z_0(0) + \ln(1 + \frac{1}{\delta}(\cosh(\beta\eta) - 1))$

$$\alpha_2 = \frac{\beta^2}{\delta}, \quad \alpha_4 = \beta^4 \left( \frac{1}{\delta} - \frac{3}{\delta^2} \right), \quad \alpha_6 = \beta^6 \left( \frac{1}{\delta} - \frac{15}{\delta^2} + \frac{30}{\delta^3} \right) \quad (\text{A23})$$

with  $\delta \equiv 1/\tau = 1 + \frac{1}{2} \exp(D)$ .

Using<sup>7</sup> Eqs.(A18) and (A23)

$$A_2 = \frac{\delta}{\beta} - Jq, \quad A_4 = \frac{\delta^2}{2\beta} \left( 1 - \frac{\delta}{3} \right), \quad A_6 = \frac{\delta^3}{2\beta} \left( 1 - \frac{3}{4}\delta + \frac{3}{20}\delta^2 \right). \quad (\text{A24})$$

Since  $A_6$  is strictly positive, the Landau-Ginzburg potential truncated at the sixth order is stable so that for small  $m$ ,  $G(m)$  can be approximated by

$$G(m) \approx A_0 + \frac{A_2}{2}m^2 + \frac{A_4}{4}m^4 + \frac{A_6}{6}m^6 \quad (\text{A25})$$

The MF critical phase-contour is given by  $A_2 = 0$  with  $A_4 > 0$ . In terms of the variable  $\tilde{T} \equiv \frac{T}{Jq}$  and  $\tilde{\Delta} = \frac{\Delta}{qJ}$ , this line is described by  $\tilde{\Delta} = \tilde{T} \ln[2(1/\tilde{T} - 1)]$ , with  $\frac{1}{3} < \tilde{T} < 1$  and terminates at a TCP of coordinates  $\tilde{T} = \frac{1}{3}$ ,  $\tilde{\Delta} = \frac{2}{3} \ln(2)$ , at which  $A_2 = A_4 = 0$ . The critical boundary (dashed line) and the position of the TCP (big crossed circle) are shown in Figs. 3, 10 and 23. Using Eq. (A20), the first-order line in a vicinity of the TCP is  $\tilde{T} \approx \tau + \frac{5}{16} \left( 1 - \frac{1}{3\tau} \right)^2 + O((\tau - \frac{1}{3})^3)$ , while the critical phase-contour is given by  $\tilde{T} = \tau$ . Therefore at the TCP, the two lines share the same slope, but show a different curvature.

Let us now set  $\tilde{f} \equiv f/Jq$  and consider the other critical lines. From Eq. (A21)

$$\tilde{f} = -\tilde{T} \ln(1 + 2e^{-D} \cosh(\beta Jqm - \beta H)) + \frac{1}{2}m^2 \quad (\text{A26})$$

we have

$$\frac{\partial \tilde{f}}{\partial m} = m - \frac{2 \sinh(z)}{e^D + 2 \cosh(z)} \quad \frac{\partial^2 \tilde{f}}{\partial m^2} = 1 - Kq \frac{4 + 2e^D \cosh(z)}{(e^D + 2 \cosh(z))^2} \quad (\text{A27})$$

$$\frac{\partial^3 \tilde{f}}{\partial m^3} = -2(\beta q J)^2 \sinh(z) \frac{e^{2D} - 2e^D \cosh(z) - 8}{(e^D + 2 \cosh(z))^3} \quad (\text{A28})$$

here  $z = m/\tilde{T} - \beta H$ .

We are now ready to discuss the pair of first-order phase-transition surfaces, the wings, that extend in the full  $H, D, T$  space symmetrically with respect to the  $H = 0$  plane. They separate three phases, defined by the minima  $m_0, m_{\pm}$  of the potential, that correspond to the solutions of the Eq.  $f' = 0$  with  $f'' > 0$ . In the  $H = 0$  plane, the

two wings join into a first-order transition line. As explained previously, for  $T > 0$  the wings are bordered by critical lines along which the first three derivatives of  $f$  vanish<sup>49</sup>, therefore for  $z \neq 0$  we obtain

$$\cosh(z) = \frac{Kq - 2}{\sqrt{4 - Kq}}, \quad e^D = \frac{4}{\sqrt{4 - Kq}}, \quad m_*^2 = \frac{Kq - 3}{Kq} \quad (\text{A29})$$

It follows that<sup>7</sup>

$$\tilde{\Delta} = \frac{\tilde{T}}{2} \ln\left(\frac{4\tilde{T}}{4\tilde{T} - 1}\right) \quad \frac{H}{Jq} = \pm \sqrt{1 - 3\tilde{T}} \mp \tilde{T} \ln\left(\frac{1 - 2\tilde{T} + \sqrt{1 - 3\tilde{T}}}{\sqrt{\tilde{T}(4\tilde{T} - 1)}}\right) \quad (\text{A30})$$

for  $\frac{1}{4} \leq \tilde{T} \leq \frac{1}{3}$ .

The corresponding value of the magnetization is

$$m_* = \pm \sqrt{1 - 3\tilde{T}} \quad (\text{A31})$$

These critical lines terminate at the tricritical point.

The critical phase-boundary in the  $H = 0$  plane corresponds to  $m = 0$ , so that Eq. (A27) gives

$$\Delta = T \ln\left(\frac{2}{\tilde{T}} - 2\right) \quad (\text{A32})$$

as already obtained from the equation  $A_2 = 0$ .

## 2. Critical exponents in MF

Let us now review the computation of the tricritical exponents in MF in the ordered phase<sup>49</sup>. Near the critical phase boundary,  $m$  is small and we are allowed to expand the free-energy in powers of  $m$ , as in Eq.(A17). To account for the tricritical point it is sufficient to truncate the expansion at the sixth-order in  $m$

$$f = A_0 + \frac{A_2}{2} m^2 + \frac{A_4}{4} m^4 + \frac{A_6}{6} m^6 \quad (\text{A33})$$

At equilibrium

$$H = -(A_2 + A_4 m^2 + A_6 m^4) m \quad (\text{A34})$$

In the  $H = 0$  plane, the minimum can be either  $m = 0$  or

$$m^2 = \frac{-A_4 + (A_4^2 - 4A_2A_6)^{\frac{1}{2}}}{2A_6} \quad (\text{A35})$$

which is a solution of

$$A_2 + A_4 m^2 + A_6 m^4 = 0 \quad (\text{A36})$$

In the tricritical region, the scaling fields are  $g = A_2$  and  $t = A_4$ , while in the critical region, just beneath the critical phase-border  $A_2 = 0$ ,  $A_4 > 0$ , the scaling field is  $\tilde{t} = A_2$ .

At a minimum  $m \neq 0$ , using Eqs. (A33), (A35) and (A36)

$$f = A_0 + \frac{1}{24A_6^2} \left( A_4^3 - 6A_2A_4A_6 - (A_4^2 - 4A_2A_6)^{\frac{3}{2}} \right) \quad (\text{A37})$$

The magnetic susceptibility at  $H = 0$  is computed from Eq. (A34)

$$\chi = -\frac{1}{\beta} \left( \frac{\partial m}{\partial H} \right) |_{H=0} = \frac{1}{\beta} (A_2 + 3A_4 m^2 + 5A_6 m^4)^{-1} \quad (\text{A38})$$

For  $m \neq 0$ , we use Eq.(A36) to get

$$\chi = -\frac{1}{\beta} (4A_2 + 2A_4 m^2)^{-1} = \frac{-1}{4A_2\beta} \left( 1 + \frac{A_4}{\sqrt{A_4^2 - 4A_2A_6}} \right) \quad (\text{A39})$$



Two functions related to the concentration are

$$\chi_{(0;g)} = \frac{\partial f}{\partial g} = \frac{1}{4A_6} \left( -A_4 + (A_4^2 - 4A_6A_2)^{\frac{1}{2}} \right) \quad (\text{A40})$$

$$\chi_{(0;gg)} = \frac{\partial \chi_{(0;g)}}{\partial g} = -\frac{1}{2} (A_4^2 - 4A_6A_2)^{-\frac{1}{2}} \quad (\text{A41})$$

Consider now the ordered ( $m \neq 0$ ) region with  $A_4 \neq 0$ . In this region  $f - A_0$ ,  $m$  and  $\chi$  can be written as a power of  $|t|$  times a scaling function depending on the variable  $x = \frac{g}{|t|^{\phi_u}}$ , with  $\phi_u = 2$ .

From Eq.(A35)

$$|m| = |t|^{\beta_u} \mathcal{M}^{(\pm)}(x) \quad \text{with} \quad \mathcal{M}^{(\pm)}(x) = \frac{1}{\sqrt{2A_6}} \left( \mp 1 + \sqrt{1 - 4A_6x} \right)^{\frac{1}{2}} \quad (\text{A42})$$

so that  $\beta_u = \frac{1}{2}$ . The  $\pm$  superscript corresponds to the sign of  $A_4 = t$ . From Eq.(A37)

$$f = A_0 + |t|^{2-\alpha_u} \mathcal{G}^{(\pm)}(x), \quad \text{with} \quad \mathcal{G}^{(\pm)}(x) = \frac{1}{24A_6^2} [\pm(1 - 6A_6x) - (1 - 4A_6x)^{\frac{3}{2}}] \quad (\text{A43})$$

so that  $\alpha_u = -1$ . From Eq.(A39)

$$\chi = |t|^{-\gamma_u} X^{(\pm)}(x), \quad \text{with} \quad X^{(\pm)}(x) = \frac{-1}{4\beta x} \left( 1 \pm \frac{1}{\sqrt{1 - 4A_6x}} \right) \quad (\text{A44})$$

so that  $\gamma_u = 2$ . From Eq.(A40)

$$\chi_{(0;g)} = |t|^{\beta_{2u}} X_{(0;1)}^{(\pm)}(x), \quad \text{with} \quad X_{(0;1)}^{(\pm)}(x) = \frac{1}{4A_6} (\mp 1 + (1 - 4A_6x)^{\frac{1}{2}}) \quad (\text{A45})$$

so that  $\beta_{2u} = 1$ . From Eq.(A41)

$$\chi_{(0;gg)} = |t|^{-\gamma_{(0,2)u}} X_{(0;gg)}^{(\pm)}(x), \quad \text{with} \quad X_{(0;gg)}^{(\pm)}(x) = \frac{-1}{2(1 - 4A_6x)^{\frac{1}{2}}} \quad (\text{A46})$$

so that  $\gamma_{(0,2)u} = 1$ .

$f - A_0$ ,  $m$ , ...,  $\chi_{(0;gg)}$  scale exactly under  $t \rightarrow \lambda t$ ,  $g \rightarrow \lambda^2 g$ . This reflects the fact that Eq.(A33) has degree six in  $m$ . If in the expansion of Eq.(A17), higher powers of  $m$  were kept, corrections to the tricritical scaling would appear.

In MF  $\langle s_0^2 \rangle$  is given by

$$\chi_{(0;1)} = \beta \frac{\partial f}{\partial D} = \beta \frac{\partial g}{\partial D} \frac{\partial f}{\partial g} + \beta \frac{\partial t}{\partial D} \frac{\partial f}{\partial t} \quad (\text{A47})$$

Near the tricritical point the first term behaves as  $|t|^{2-\alpha_u-\phi_u}$ , and the second term as  $|t|^{2-\alpha_u-1}$ . Therefore using Eq.(A24)

$$\chi_{(0;1)} \approx (\delta - 1) \chi_{(0;g)} \quad (\text{A48})$$

Similarly the tricritical behavior of  $\chi_{(0;2)}$  is the same as that of  $\chi_{(0;gg)}$ .

Let us now consider the MF computation of the exponents along the critical phase-contour. The scaling functions are  $A_2 = g = \dot{t} \rightarrow 0$  and  $A_4 = t$  constant. Set  $x = \frac{1}{A_4^2} \dot{t} \rightarrow 0$ . Along this path the thermodynamical quantities differ from the corresponding scaling functions by a multiplicative constant (a power of  $|A_4|$ ), so that the critical exponents are determined directly using the scaling functions.

$$\mathcal{G}^{(+)}(x) = -\frac{x^2}{4} - \frac{A_6}{6} x^3 + O(x^4) \quad (\text{A49})$$

At the leading order,

$$\mathcal{G}^{(+)}(x) = \dot{G} \dot{t}^{2-\alpha}, \quad \text{with} \quad \dot{G} = -\frac{1}{4A_4^4} \quad (\text{A50})$$

so that  $\alpha = 0$  is the critical exponent of the specific heat.

$$\mathcal{M}^{(+)}(x) = (-x)^{\frac{1}{2}}(1 + \frac{A_6}{2}x + O(x^2)) \quad (\text{A51})$$

At the leading order,

$$\mathcal{M}^{(+)}(x) = (-x)^{\frac{1}{2}} = A_4^{-1}|t|^\beta \quad (\text{A52})$$

so that  $\beta = \frac{1}{2}$  is the critical exponent of the magnetization.

$$X^{(+)}(x) = -\frac{1}{2\beta x}(1 + A_6x + O(x^2)) \quad (\text{A53})$$

and

$$X^{(+)}(x) = \dot{X}(t)|t|^{-\gamma}, \quad \text{with} \quad \dot{X}(t) = \frac{A_4^2}{2\beta}(1 + \frac{A_6}{A_4^2}t + O(t^2)) \quad (\text{A54})$$

so that  $\gamma = 1$  is the critical exponent of the susceptibility.

There are corrections to the ordinary scaling  $t \rightarrow \lambda t$ . The term in  $A_6$  is the first correction to the ordinary scaling, that would be exact if  $A_6 = 0$ .

$X_{(0;g)}^{(\pm)}(x)$  and  $X_{(0;gg)}^{(\pm)}(x)$  are regular, so that the concentration and its susceptibility diverge only at the TCP.

Consider now the region  $A_2 \neq 0$  and use the tricritical scaling fields  $g = A_2$  and  $t = A_4$ . At  $m \neq 0$ ,

$$f - A_0 = |g|^{2-\alpha_t} \mathcal{G}_t^{(\pm)}(y), \quad \text{with} \quad \mathcal{G}_t^{(\pm)}(y) = \frac{1}{24A_6^2} \left( y^3 \mp 6yA_6 - (y^2 \mp 4A_6)^{\frac{3}{2}} \right) \quad (\text{A55})$$

so that  $\alpha_t = \frac{1}{2}$  and  $y = \frac{t}{|g|^{\phi_t}}$ ,  $\phi_t = \frac{1}{2}$ .

$$|m| = |g|^{\beta_t} \mathcal{M}_t^{(\pm)}(y), \quad \text{with} \quad \mathcal{M}_t^{(\pm)}(y) = \frac{1}{\sqrt{2A_6}} \left( -y + (y^2 \mp 4A_6)^{\frac{1}{2}} \right)^{\frac{1}{2}} \quad (\text{A56})$$

so that  $\beta_t = \frac{1}{4}$ .

$$\chi = |g|^{-\gamma_t} X_t^{(\pm)}(y), \quad \text{with} \quad X_t^{(\pm)}(y) = \mp \frac{1}{4\beta} \left( 1 + \frac{y}{\sqrt{y^2 \mp 4A_6}} \right) \quad (\text{A57})$$

so that  $\gamma_t = 1$ .

$$\chi_{(0;g)} = |g|^{\beta_{2t}} X_{(0;g)t}^{(\pm)}, \quad \text{with} \quad X_{(0;g)t}^{(\pm)} = \frac{1}{4A_6} \left( -y + (y^2 \mp 4A_6)^{\frac{1}{2}} \right) \quad (\text{A58})$$

so that  $\beta_{2t} = \frac{1}{2}$

$$\chi_{(0;gg)} = |g|^{-\gamma_{(0;2)t}} X_{(0;gg)t}^{(\pm)}, \quad \text{with} \quad X_{(0;gg)t}^{(\pm)} = -\frac{1}{2}(y^2 \mp 4A_6)^{-\frac{1}{2}} \quad (\text{A59})$$

so that  $\gamma_{(0;2)t} = \frac{1}{2}$ .

To examine the critical behavior along the critical phase-boundary for  $A_2 = g = t \rightarrow 0$  with  $A_4 = t > 0$  constant, we should expand at  $y \rightarrow \infty$ .

If  $t > 0$  and  $g < 0$  one has  $y \rightarrow +\infty$ , so  $X_t^{(-)} = \frac{1}{2\beta} + O(y^{-2})$ , and  $\chi = |t|^{-\gamma} X_t^{(-)}$  with the susceptibility exponent  $\gamma = 1$ , as already found using  $X^{(+)}(x)$  and similarly for the other ordinary critical exponents.

While along a trajectory with  $y = \frac{t}{|g|^{\frac{1}{2}}}$  constant the tricritical scaling is exact, along the trajectory with  $A_4 > 0$  constant, there is a crossover from the region with  $y$  small, in which the tricritical scaling is valid, to the region with  $y$  large, in which ordinary scaling is valid. Consider for instance the magnetization scaling function in Eq.(A56). For  $y$  small

$$\mathcal{M}_t^{(-)}(y) \approx A_6^{-\frac{1}{4}}, \quad \text{with} \quad |m| \approx |g|^{\frac{1}{4}} A_6^{-\frac{1}{4}} \quad (\text{A60})$$

and the behavior is tricritical, with tricritical exponent  $\beta_t = 1/4$ .

For  $y$  large,

$$\mathcal{M}_t^{(-)}(y) \approx \frac{|g|^{\frac{1}{4}}}{A_4^{\frac{1}{2}}}, \quad |m| \approx |g|^{\frac{1}{2}} A_4^{-\frac{1}{2}} = |t|^{\frac{1}{2}} A_4^{-\frac{1}{2}} \quad (\text{A61})$$

so that ordinary critical behavior appears, with critical exponent  $\beta = 1/2$ .

### 3. The spin S=3/2 model

In this case Eq. (A5) is

$$z_0 = 2e^{-\frac{D}{9}}(\mathcal{C}_1 + d_1\mathcal{C}_3) \quad (\text{A62})$$

where we have defined  $d_1 = \exp(-\frac{8}{9}D)$ ,  $\mathcal{C}_n = \cosh(n\frac{\beta}{3}(\frac{2}{3}Jqm - H))$ ,  $\mathcal{S}_n = \sinh(n\frac{\beta}{3}(\frac{2}{3}Jqm - H))$  and  $b = \frac{4}{9}\beta Jq$ . The first Taylor coefficients of  $\ln(z_0(\eta))$  are

$$\alpha_2 = \frac{\beta^2}{9} \frac{9d_1 + 1}{1 + d_1} \quad \alpha_4 = -\frac{2\beta^4}{81} \frac{81d_1^2 - 14d_1 + 1}{(1 + d_1)^4} \quad (\text{A63})$$

From Eq. (A18), we can determine the first coefficients of the Landau-Ginzburg expansion of the potential

$$A_2 = \frac{9(d_1 + 1)}{\beta(9d_1 + 1)} - qJ \quad A_4 = \frac{27}{\beta}(1 + d_1)^2 \frac{81d_1^2 - 14d_1 + 1}{(9d_1 + 1)^4} \quad (\text{A64})$$

$A_4$  is always positive. The MF critical phase-boundary is obtained from the Eq.  $A_2 = 0$ :

$$\tilde{\Delta} = \frac{9\tilde{T}}{8} \ln\left(\frac{1 - \tilde{T}}{\tilde{T} - \frac{1}{9}}\right) \quad (\text{A65})$$

Equivalently, in terms of  $\tilde{\tau} = C(D, h = 0; 3/2) = 1/(1 + \exp(8D/9))$  the phase-contour is

$$\tilde{T} = \frac{8}{9}\tilde{\tau} + \frac{1}{9} \quad (\text{A66})$$

since the coefficient  $A_4$  is always positive, and no tricritical point<sup>6</sup> can exist.

Let us now consider the critical phase boundaries for generic  $H$ . From Eq. (A21)

$$f = -\frac{1}{\beta} \ln(2e^{-\frac{D}{9}}(\mathcal{C}_1 + d_1\mathcal{C}_3)) + \frac{2}{9}Jqm^2 \quad (\text{A67})$$

$$f' = \frac{4Jq}{9} \left(m - \frac{1}{2} \frac{\mathcal{S}_1 + 3d_1\mathcal{S}_3}{\mathcal{C}_1 + d_1\mathcal{C}_3}\right) \quad f'' = \frac{4Jq}{9} \left(1 - \frac{b\xi}{4(\mathcal{C}_1 + d_1\mathcal{C}_3)^2}\right) \quad (\text{A68})$$

where  $\xi \equiv 1 + 9d_1^2 + 6d_1\mathcal{C}_2 + 4d_1\mathcal{C}_1\mathcal{C}_3$ .

$$f''' = -\frac{Jqb^2}{18(\mathcal{C}_1 + d_1\mathcal{C}_3)^3} [(12d_1\mathcal{S}_2 + 4d_1\mathcal{S}_1\mathcal{C}_3 + 12d_1\mathcal{C}_1\mathcal{S}_3)(\mathcal{C}_1 + d_1\mathcal{C}_3) - 2\xi(\mathcal{S}_1 + 3d_1\mathcal{S}_3)] \quad (\text{A69})$$

The critical points occur at  $f' = f'' = f''' = 0$ .

For  $\frac{2}{3}Jqm - H = 0$  one has  $\mathcal{S}_i = 0$  and  $\mathcal{C}_i = 1$ , so that  $f''' = 0$  is trivially satisfied and  $f'$  gives  $m = 0 = H$ ; the equation  $f'' = 0$  gives again Eq. (A65).

Use Eq. (A68) to eliminate  $\xi$  from Eq. (A69), obtaining an equation quadratic in  $d_1$ . Eq. (A68) has the form  $N_2d_1^2 + N_1d_1 + N_0 = 0$  where  $N_2 = \frac{9}{4}b - \mathcal{C}_3^2$ ,  $N_1 = \frac{3}{2}b\mathcal{C}_2 + b\mathcal{C}_1\mathcal{C}_3 - 2\mathcal{C}_1\mathcal{C}_3$ ,  $N_0 = \frac{b}{4} - \mathcal{C}_1^2$ . From these two quadratic equations in  $d_1$

$$d_1 = \frac{N_2\mathcal{S}_1\mathcal{C}_1 - 3N_0\mathcal{C}_3\mathcal{S}_3}{3N_1\mathcal{S}_3\mathcal{C}_3 - N_2(3\mathcal{S}_3\mathcal{C}_1 - \frac{3}{2}b\mathcal{S}_2 - \frac{b}{2}\mathcal{S}_1\mathcal{C}_3 - \frac{3}{2}b\mathcal{C}_1\mathcal{S}_3 + \mathcal{S}_1\mathcal{C}_3)} \quad (\text{A70})$$

Thus we observe two first-order phase-transition surfaces. They are formed by two wings bordered by two critical lines ( for  $H > 0$  and for  $H < 0$ ), along which the first three derivatives of the free energy vanish. For  $H = 0$ , the critical lines terminate with a critical end-point at  $\tilde{T}_{cep} = 0.12941913384882\dots$ ,  $\tilde{\Delta}_{cep} = 0.4875062362287\dots$ , with  $m_{cep} = \pm 0.854170713633042$ , lying on the first-order transition surface with magnetization  $\pm m$ , the minima of the double well. At the critical end-point, these minima are flat, since  $\frac{\partial^2 \tilde{f}}{\partial m^2} = 0$ .

## Appendix B: Phenomenological Scaling

The scaling-laws approach to the crossover behavior, introduced in Ref.[53–55,70,80,81] in the context of the transition from weakly anisotropic to fully isotropic exchange-interactions in spin systems and illustrated in various other contexts can also describe the transition from Ising-like to tricritical behavior of the BC model.

First we should replace the thermodynamic fields by scaling fields appropriate to the TCP. For this purpose let us first define the reduced deviation from the tricritical temperature  $t = T/T_{tr} - 1$ , and observe that for small  $t > 0$ , the equation of the critical line (see Fig. 1) can be approximated as

$$\Delta_2(t) = \Delta_{tr} - at + b_2 t^{\psi_2} + \dots \quad (\text{B1})$$

with  $\psi_2 > 1$ , while similarly for the first-order line (small  $t < 0$ ), we have

$$\Delta_1(t) = \Delta_{tr} - at + b_1 |t|^{\psi_1} + \dots \quad (\text{B2})$$

with  $\psi_1 > 1$ . The same finite (nonuniversal) slope of the critical line is generally assumed

$$a = -T_{tr} \left( \frac{d\Delta_2(T)}{dT} \right) \Big|_{T_{tr}} = -T_{tr} \left( \frac{d\Delta_1(T)}{dT} \right) \Big|_{T_{tr}} \quad (\text{B3})$$

on both sides of the TCP (as in some physical systems and for models in the MF approximation). It is also assumed that the exponents  $\psi_1$  and  $\psi_2$  that characterize the lowest order correction to the tangent approximation, are equal  $\psi_1 = \psi_2 = \phi_u$ .

The variable

$$g \equiv \Delta - \Delta_{tr} + at \quad (\text{B4})$$

will be used as a scaling field. Along the locus  $g = 0$ , the TCP is approached along the tangent to the phase-contour as  $|t| \rightarrow 0$ . If  $t = 0$ , the TCP is approached at an angle with respect to the tangent, as  $g \rightarrow 0$ . The fields  $t$ ,  $g$  and the magnetic field  $h$  are usually adopted as tricritical scaling fields.

In terms of these fields, a ‘‘tricritical scaling’’ hypothesis for the singular part  $f_s$  of the free-energy can now be formulated as follows

$$f_s(g, t, h) \approx |t|^{2-\alpha_u} W_u^{(\pm)}(g/|t|^{\phi_u}, h/|t|^{\hat{\Delta}_u}) \quad (\text{B5})$$

for  $t, g \rightarrow 0$ , with arbitrary ratio  $g/t$ . (The phase-contour lies in the  $H = 0$  plane.) Thus, if the TCP is approached along the line  $g = 0$ , it is appropriate to refer to Eq. (B5) in which the singularity is described explicitly by a power of  $t$ , for example  $f_s \approx |t|^{2-\alpha_u} W_u(0, 0)$ . This is a natural parametrization of the TCP scaling property. The exponents that characterize the TCP, are the specific-heat exponent  $\alpha_u$ , the tricritical gap exponent  $\hat{\Delta}_u = \beta_u + \gamma_u^{(2;0)}$ , and  $\phi_u$  an additional ‘‘crossover exponent’’. (Please notice also that we have changed into  $\hat{\Delta}_u$  the symbol usually denoting the gap exponent to avoid confusion with the crystal field). In the MF approximation  $\phi_u = 2$ . The scaling function  $W_u(x, y)$  is assumed to be analytic at  $x = 0$  and thus at  $g = 0$  for fixed  $t \neq 0$ .

Defining  $W_{tr}(X, Y) \equiv |X|^{2-\alpha_u} W_u^{(\pm)}(|X|^{-\phi_u}, Y|X|^{-\hat{\Delta}_u})$ , Eq. (B5) can be written equivalently as

$$f_s(g, t, h) \approx |g|^{(2-\alpha_{tr})} W_{tr}(t/|g|^{\phi_{tr}}, h/|g|^{\hat{\Delta}_{tr}}) \quad (\text{B6})$$

with the new set of exponents  $\alpha_{tr}, \beta_{tr}, \dots, \phi_{tr}$  defined by

$$2 - \alpha_{tr} = \frac{2 - \alpha_u}{\phi_u}, \quad \beta_{tr} = \frac{\beta_u}{\phi_u}, \quad \gamma_{tr} = \frac{\gamma_u}{\phi_u}, \quad \hat{\Delta}_{tr} = \frac{\hat{\Delta}_u}{\phi_u}, \quad \phi_{tr} = \frac{1}{\phi_u}, \quad (\text{B7})$$

The expected values of these new exponents can be read in Table II. Also the scaling function  $W_{tr}(X, Y)$  is assumed to be analytic at  $X = 0$ .

If the TCP is approached along a line  $t = cg$ , crossing the critical line at a finite angle, so that we have  $t/|g|^{\phi_{tr}} \rightarrow 0$ , because  $\phi_{tr} < 1$ , it is appropriate to refer to Eq. (B6) in which the singularity appears explicitly as a power of  $g$ , for example  $f_s \approx |g|^{2-\alpha_{tr}} W_{tr}(0, 0)$ .

These remarks suggest a simple method to estimate the crossover exponent: we should simply compare the usual exponents computed along a path tangent to the phase-boundary at the TCP with those computed along a path forming an angle with it (as are naturally obtained when studying series at fixed  $D = D_{tr}$ ).

The scaling function  $W_u$  of Eq. (B5), can describe also the Ising-like ordinary scaling behavior that is observed along the critical line, provided that an appropriate singularity appears in this quantity. Let us set  $t_c(g) \equiv T_c(g)/T_{tr} - 1$ , so that  $\dot{t} \equiv t - t_c(g)$  can be taken as a distance from the critical line. Since as  $\dot{t} \rightarrow 0$  the scaling variable  $x = g/t^{\phi_u} \rightarrow \dot{x} = g/t_c(g)^{\phi_u}$ , we have precisely to assume that at  $x = \dot{x}$  the scaling function  $W_u^{(\pm)}(x, y)$  has a singularity of the form  $(1 - x/\dot{x})^{2-\alpha}$ , so that  $f_s \approx |\dot{t}|^{2-\alpha}$  as  $\dot{t} \rightarrow 0$  with  $g \neq 0$ . This assumption is actually realized<sup>81</sup> in the MF approximation.

It can be observed that for fixed small  $g \neq 0$ , as  $T$  approaches the critical temperature  $T_c(g)$ , the system will first behave as if  $T \rightarrow T_{tr}$  and only when  $T - T_c(g)$  is very small, past a ‘‘crossover temperature’’  $T^x(g)$ , i.e. for  $T^x(g) > T > T_c(g)$ , it will develop the full Ising-like critical behavior expected away from the TCP. This can be observed also in MF, see the end of Appendix A.

For a (mixed) susceptibility, the critical scaling reads

$$\chi_{(r;p)}(K, D) \approx A_{(r;p)}(K, D)|\dot{t}|^{-\gamma^{(r;p)}} \quad (\text{B8})$$

The tricritical scaling is

$$\chi_{(r;p)}(K, D) \approx A_{(r;p)tr} \left( \frac{t}{|g|^{\phi_{tr}}} \right) |g|^{-\gamma_{tr}^{(r;p)}} \quad (\text{B9})$$

Approaching the TCP along the scaling path  $g = x|t|^{\frac{1}{\phi_{tr}}}$ , with the constant  $x$  chosen small enough to be close to the critical line, Eqs. (B8) and (B9) are both valid. Therefore in this region  $g \approx \dot{t}$

$$A_{(r;p)}(K; D) \approx |x|^{\gamma^{(r;p)} - \gamma_{tr}^{(r;p)}} A_{(r;p)tr}^{(\pm)}(|x|^{-\phi_{tr}})|t|^{(\gamma^{(r;p)} - \gamma_{tr}^{(r;p)})/\phi_{tr}}. \quad (\text{B10})$$

Thus, if the estimates of the amplitudes of observables like the susceptibilities, were sufficiently accurate, the study of their  $g \rightarrow 0$  behavior might help to spot the TCP and to determine the crossover exponent. In particular, in the case of the ordinary susceptibility, as  $t \rightarrow 0$  along the line  $g = x|t|^{\frac{1}{\phi_{tr}}}$ , with  $|x| \ll 1$ , the critical amplitude will vanish as

$$A_{(2;0)}(K, D) \approx |t|^{(\gamma - \gamma_{tr})/\phi_{tr}}. \quad (\text{B11})$$

### Appendix C: Tools for the series analysis

To make the paper reasonably selfcontained, it is useful to sketch the standard numerical approximation techniques of series analyses. More detailed discussions can be found in Refs.[46–48,60,72,73].

#### 1. Coefficient-ratio based methods

To determine the location of the critical points and their critical exponents using the HT expansions, it is often convenient to resort to the unbiased *modified-ratio-approximants*(MRAs) (in the loose lattice version), which is a smoother and faster converging improvement<sup>60,72,73</sup> of the traditional methods<sup>72</sup> of extrapolation of the series-coefficient ratio-sequences.

To illustrate this prescription by an example, we can refer to the HT expansion of the magnetic susceptibility  $\chi_{(2;0)}(K, D; S) = \sum_r c_r(D; S)K^r$ . For each fixed  $D$ , a value of the inverse critical temperature can be obtained by forming the sequence of estimators  $(K_c(D; S))_n$  of  $K_c(D; S)$  defined<sup>72,73</sup> by

$$(K_c(D; S))_n = \left( \frac{c_{n-2}c_{n-3}}{c_n c_{n-1}} \right)^{1/4} \exp\left[ \frac{s_n + s_{n-2}}{2s_n(s_n - s_{n-2})} \right] \quad (\text{C1})$$

with

$$s_n = \left( \ln\left( \frac{c_{n-2}^2}{c_n c_{n-4}} \right)^{-1} + \ln\left( \frac{c_{n-3}^2}{c_{n-1} c_{n-5}} \right)^{-1} \right) / 2. \quad (\text{C2})$$

$c_n \equiv c_n(D; S)$  being an abridged notation for the  $n$ th expansion coefficient of the susceptibility. Provided that the leading correction to scaling dominates over the subleading ones, this prescription Eq. (C1) has the important advantage of providing at the same time information on  $K_c(D; S)$  and on the leading correction-to-scaling amplitude  $a_{(2;0)}(D; S)$ , defined by Eq. (33). Otherwise, it yields some ‘‘effective value’’ for this amplitude. If the critical

singularity is the nearest one to the origin of the complex  $K$  plane, the MRA estimator-sequence has the asymptotic behavior<sup>60</sup> for large order  $n$

$$(K_c(D; S))_n = K_c(D; S) \left( 1 - \frac{1}{2} \frac{C(\gamma^{(2;0)})\theta^2(1-\theta)a_{(2;0)}(D; S)}{n^{1+\theta}} + o(1/n^{1+\theta}) \right) \quad (\text{C3})$$

where  $C(\gamma^{(2;0)})$  is a known<sup>60</sup> positive function of the exponent  $\gamma^{(2;0)}$  of  $\chi_{(2;0)}$ ,  $a_{(2;0)}$  is defined in Eq. (33) and  $\theta \approx 0.52$ , in the  $3d$  Ising universality class, is the exponent of the leading correction to scaling.

A prescription<sup>60,72,73</sup> of a similar kind provides a sequence of estimators  $(\gamma^{(2;0)}(D; S))_n$  for the critical exponent

$$(\gamma^{(2;0)}(D; S))_n = 1 + \frac{2(s_n + s_{n-2})}{(s_n - s_{n-2})^2} \quad (\text{C4})$$

In this case, the asymptotic behavior of the sequence for large order  $n$  is

$$(\gamma^{(2;0)}(D; S))_n = \gamma^{(2;0)}(D; S) - \frac{C(\gamma^{(2;0)})\theta(1-\theta^2)a_{(2;0)}(D; S)}{n^\theta} + O(1/n) \quad (\text{C5})$$

In general the set of the corrections to scaling rules the convergence properties of any extrapolation method in the critical region and the MRA method of analysis can account explicitly for the leading terms. Thus, we expect that if the HT series are sufficiently long and regular, the MRA estimator-sequences have settled into their asymptotic regimes described by Eq. (C3), (C5), and only the leading correction-to-scaling have non-negligible amplitudes, then it is reasonable to determine  $(K_c(D; S))$  by fitting the simple extrapolation Ansatz

$$(K_c(D; S))_n = b_1(D; S) - b_2(D; S)/n^{1+\theta}. \quad (\text{C6})$$

to the last few terms of the estimator-sequence  $(K_c(D; S))_n$ . We can thus assume that  $K_c(D; S) \approx b_1(D; S)$ . A similar ansatz

$$(\gamma^{(2;0)})_n = \tilde{b}_1(D; S) - \tilde{b}_2(D; S)/n^\theta \quad (\text{C7})$$

can be used with the MRA estimator-sequence for the exponent  $(\gamma^{(2;0)}(D; S))_n$ , concluding that  $\gamma^{(2;0)}(D; S) \approx \tilde{b}_1(D; S)$ . An analogous prescription in which the HT expansion coefficients of  $\chi_{(4;0)}$  are employed, is adopted to estimate  $\gamma^{(4;0)}(D; S)$ . These methods are *unbiased*, i.e. no assumption on the value of the exponent is used in Eq. (C1) to compute the critical temperature and no assumption on the critical temperature in Eq. (C4) to compute the exponent. Small multiples of the uncertainties inherent in these extrapolations can be taken as a measure of the errors of the final estimates.

Using the formulas Eqs. (C6) and (C7), we can estimate also the coefficients  $b_2(D; S)$  and  $\tilde{b}_2(D; S)$ , proportional to the correction-to-scaling amplitudes, and thus get some hint of the uncertainties to be expected. Procedures of this kind were suggested long ago in Ref. [73,82] and were later pursued by several authors<sup>27,28,60,73</sup> to achieve optimal determinations of the universal critical parameters by studying a model with minimal leading corrections to scaling, singled out in a family of one-parameter-dependent models known to belong to the same universality class. In the case of the BC model, the family parameter is  $D$ .

When the structure of the correction-to-scaling terms becomes more complex and oscillations are observed in the highest-order terms of the MRA estimator-sequences, as it happens in the crossover regions, simple (but less accurate) ratio-method estimators<sup>72</sup> such as

$$(K_c(D; S))_n = \frac{n-1 + \gamma^{(2;0)}}{na_n/a_{n-1}} + o(1/n) \quad (\text{C8})$$

that is biased with some accurate value of  $\gamma^{(2;0)}$  and

$$(\gamma^{(2;0)}(D; S))_n = n + 1 - \frac{na_{n-1}}{a_n K_c(D; S)} + o(1/n) \quad (\text{C9})$$

that is biased with some accurate value of  $K_c(D; S)$ , might sometimes be more robust than the MRA approach.

## 2. Padè and differential approximant methods

In many cases the MRAs, if cautiously extrapolated to large orders of expansion, show an apparent accuracy comparable or higher than that obtained by the *differential approximants* (DAs) method for which such extrapolations are controversial.

The DA method also used in the series analysis, is a generalization<sup>72</sup> of the well known Padé approximant(PA) method and can similarly be either biased or unbiased. Both methods can be employed to evaluate either the expansions of the quantities that remain finite at the critical points or the parameters of the singularities for quantities that diverge there. The DA method uses the solution, called differential approximant, of an initial value problem for an ordinary linear inhomogeneous differential equation of the first or higher order in the expansion variable. The coefficients of the equation are polynomials in that variable such that the series expansion of the solution of the equation equals, up to some appropriate order, the series to be approximated. Truncating the series under investigation at various lengths or using series of a fixed length and choosing different degrees for the polynomial coefficients, various DAs (i.e. solutions of various differential equations) can be formed. Following this procedure, for each quantity under study, a sample of estimates can be obtained from the highest-order approximants, namely those formed using all or most available expansion coefficients, whose average and spread can be computed, after possibly discarding evident outliers. If the sample average remain essentially stable as the order of truncation of the series increases and it can be believed that stability indicates convergence, then this average can be taken as the best estimate of the parameter and a (generous) multiple of the spread of the sample may be trusted to be a reasonable measure of uncertainty. It should be stressed that the uncertainties associated with the analysis of a series either by the DAs and by the MRAs do not have such a precise statistical meaning as for MC methods, but remain subjective to some extent. Our analyses, will be corroborated by checking the consistency, within the numerical uncertainties, between the MRA and DA estimates of the critical parameters, whenever both approaches are feasible. The critical amplitudes and their ratios have to be determined by (biased) PAs and DAs.

- 
- \* Electronic address: paolo.butera@mib.infn.it  
† Electronic address: mario.pernici@mi.infn.it
- <sup>1</sup> M. Blume, Theory of the First-Order Magnetic Phase Change in UO<sub>2</sub>, Phys. Rev. **141** (1966) 517-524.  
<https://link.aps.org/doi/10.1103/PhysRev.141.517>.
  - <sup>2</sup> H.W.Capel, On the possibility of first-order phase transitions in Ising systems of triplet ions with zero-field splitting, Physica **32** (1966) 966-988.  
[https://doi.org/10.1016/0031-8914\(66\)90027-9](https://doi.org/10.1016/0031-8914(66)90027-9).
  - <sup>3</sup> Robert B. Griffiths, Thermodynamics Near the Two-Fluid Critical Mixing Point in He<sup>3</sup> - He<sup>4</sup> Phys. Rev. Lett. **24** (1970) 715-717.  
<https://link.aps.org/doi/10.1103/PhysRevLett.24.715>.
  - <sup>4</sup> Robert B. Griffiths, Proposal for Notation at Tricritical Points, Phys. Rev. B **7** (1973) 545-551.  
<https://link.aps.org/doi/10.1103/PhysRevB.7.545>
  - <sup>5</sup> G.B.Taggart and R.A.Tahir-Kheli, Phase transitions in Ising systems of doubly degenerate four-level ions, Physica **44** (1969) 321-336.  
[https://doi.org/10.1016/0031-8914\(69\)90209-2](https://doi.org/10.1016/0031-8914(69)90209-2).
  - <sup>6</sup> J.A. Plascak, J.G. Moreira and F.C. sa Barreto, Mean field solution of the general spin Blume-Capel model, Phys. Lett. A **173** (1993) 360.  
[https://doi.org/10.1016/0375-9601\(93\)90250-4](https://doi.org/10.1016/0375-9601(93)90250-4)
  - <sup>7</sup> M.Blume, V.J. Emery, R.B. Griffiths, Ising Model for the  $\lambda$  Transition and Phase Separation in He<sup>3</sup>-He<sup>4</sup> Mixtures, Phys. Rev. A **4** (1971) 1071-1077.  
<https://link.aps.org/doi/10.1103/PhysRevA.4.1071>.
  - <sup>8</sup> A. N. Berker and M. Wortis, Blume-Emery-Griffiths-Potts model in two dimensions: Phase diagram and critical properties from a position-space renormalization group, Phys. Rev. B **14** (1976) 4946-4963.  
<https://link.aps.org/doi/10.1103/PhysRevB.14.4946>.
  - <sup>9</sup> J. Adler, A. Aharony and J.Oitmaa, Renormalisation group studies of the Blume-Emery-Griffiths model in two dimensions, Journal of Physics A: Mathematical and General **11** (1978) 963-974.  
<https://doi-org/10.1088/0305-4470/11/5/026>.
  - <sup>10</sup> L.D. Landau and E. M. Lifshitz, “*Statistical Physics*”, (Pergamon Press, Oxford 1958).
  - <sup>11</sup> P.M.C. de Oliveira, Finite-Size Scaling Renormalization Group, Europhys. Lett. **20** (1992) 621-626. <https://doi-org/10.1209/0295-5075/20/7/008>
  - <sup>12</sup> V. Ilkovic, Cluster expansion for the spin=3/2 Blume-Capel model, Physica A **234** (1996) 545-553.  
[https://doi.org/10.1016/S0378-4371\(96\)00289-0](https://doi.org/10.1016/S0378-4371(96)00289-0).
  - <sup>13</sup> D. Peña Lara and J.A. Plascak, The Critical Behavior of the General Spin Blume-Capel Model, Int. J. Mod. Phys. B **12** (1998) 2045-2061.  
<https://doi-org/10.1142/S0217979298001198>.
  - <sup>14</sup> J.C. Xavier, F.C. Alcaraz, D. Peña Lara and J.A. Plascak, Critical behavior of the spin- $\frac{3}{2}$  Blume-Capel model in two dimensions, Phys. Rev. B **57** (1998) 11575-11581.  
<https://link.aps.org/doi/10.1103/PhysRevB.57.11575>.
  - <sup>15</sup> S. Grollau, E. Kierlik, M.L. Rosinberg and G. Tarjus, Thermodynamically self-consistent theory for the Blume-Capel model,

TABLE VII: BC model with spin  $S = 1$  on a simple-cubic lattice, subject to a magnetic field  $H$  and a crystal field  $D$ . The coefficients  $L_n(u, x; 1)$  of the LT series expansion in powers of  $\mu = \exp(h)$  for the free-energy density Eq. (6) are expressed in terms of the LT variable  $u = \exp(-\beta)$  and of the crystal-field variable  $x = \exp(D)$ .

$$\begin{aligned}
L_1 &= +xu^6 \\
L_2 &= -7/2x^2u^{12} + 3x^2u^{11} + u^{12} \\
L_3 &= +64/3x^3u^{18} - 36x^3u^{17} + 15x^3u^{16} - 7xu^{18} + 6xu^{16} \\
L_4 &= -651/4x^4u^{24} + 405x^4u^{23} - 657/2x^4u^{22} + 83x^4u^{21} + 3x^4u^{20} + 64x^2u^{24} - 36x^2u^{23} - 72x^2u^{22} \\
&\quad + 30x^2u^{21} + 15x^2u^{20} - 7/2u^{24} + 3u^{20} \\
L_5 &= +7031/5x^5u^{30} - 4608x^5u^{29} + 5532x^5u^{28} - 2804x^5u^{27} + 426x^5u^{26} + 48x^5u^{25} - 651x^3u^{30} \\
&\quad + 810x^3u^{29} + 567x^3u^{28} - 828x^3u^{27} - 57x^3u^{26} + 126x^3u^{25} + 32x^3u^{24} + 64xu^{30} - 72xu^{28} - 21xu^{26} \\
&\quad + 30xu^{24} \\
L_6 &= -39452/3x^6u^{36} + 53370x^6u^{35} - 84738x^6u^{34} + 64574x^6u^{33} - 44289/2x^6u^{32} + 1575x^6u^{31} \\
&\quad + 496x^6u^{30} + 18x^6u^{29} + 7031x^4u^{36} - 13824x^4u^{35} - 471x^4u^{34} + 14020x^4u^{33} - 5091x^4u^{32} \\
&\quad - 2496x^4u^{31} + 421x^4u^{30} + 348x^4u^{29} + 63x^4u^{28} - 1953/2x^2u^{36} + 405x^2u^{35} + 1620x^2u^{34} - 486x^2u^{33} \\
&\quad - 423x^2u^{32} - 48x^2u^{31} - 360x^2u^{30} + 126x^2u^{29} + 129x^2u^{28} + 12x^2u^{27} + 64/3u^{36} - 36u^{32} + 15u^{28} \\
L_7 &= +909434/7x^7u^{42} - 628236x^7u^{41} + 1240035x^7u^{40} - 1261904x^7u^{39} + 674652x^7u^{38} \\
&\quad - 157380x^7u^{37} - 1360x^7u^{36} + 3888x^7u^{35} + 378x^7u^{34} + 8x^7u^{33} - 78904x^5u^{42} + 213480x^5u^{41} \\
&\quad - 103104x^5u^{40} - 172268x^5u^{39} + 170994x^5u^{38} - 2724x^5u^{37} - 27700x^5u^{36} - 2568x^5u^{35} + 1779x^5u^{34} \\
&\quad + 900x^5u^{33} + 114x^5u^{32} + 14062x^3u^{42} - 13824x^3u^{41} - 24435x^3u^{40} + 22128x^3u^{39} + 10551x^3u^{38} \\
&\quad - 6018x^3u^{37} + 817x^3u^{36} - 3348x^3u^{35} - 1233x^3u^{34} + 750x^3u^{33} + 456x^3u^{32} + 96x^3u^{31} - 651xu^{42} \\
&\quad + 810xu^{40} + 567xu^{38} - 808xu^{36} - 117xu^{34} + 186xu^{32} + 12xu^{30} \\
L_8 &= -10690323/8x^8u^{48} + 7496787x^8u^{47} - 35373351/2x^8u^{46} + 22521935x^8u^{45} - 65448621/4x^8u^{44} \\
&\quad + 6392769x^8u^{43} - 1895165/2x^8u^{42} - 106113x^8u^{41} + 44793/2x^8u^{40} + 4622x^8u^{39} + 306x^8u^{38} + x^8u^{36} \\
&\quad + 909434x^6u^{48} - 3141180x^6u^{47} + 2963502x^6u^{46} + 1262118x^6u^{45} - 3515763x^6u^{44} + 1363200x^6u^{43} \\
&\quad + 407264x^6u^{42} - 201462x^6u^{41} - 54135x^6u^{40} - 1836x^6u^{39} + 6702x^6u^{38} + 1938x^6u^{37} + 219x^6u^{36} \\
&\quad - 197260x^4u^{48} + 320220x^4u^{47} + 261486x^4u^{46} - 571648x^4u^{45} - 31320x^4u^{44} + 257250x^4u^{43} \\
&\quad - 21338x^4u^{42} + 15330x^4u^{41} - 33027/2x^4u^{40} - 18840x^4u^{39} - 1887x^4u^{38} + 2196x^4u^{37} \\
&\quad + 1932x^4u^{36} + 372x^4u^{35} + 18x^4u^{34} + 14062x^2u^{48} - 4608x^2u^{47} - 27648x^2u^{46} + 6426x^2u^{45} \\
&\quad + 5091x^2u^{44} + 2172x^2u^{43} + 16912x^2u^{42} - 4560x^2u^{41} - 7092x^2u^{40} - 420x^2u^{39} - 2232x^2u^{38} \\
&\quad + 834x^2u^{37} + 777x^2u^{36} + 144x^2u^{35} + 144x^2u^{34} - 651/4u^{48} + 405u^{44} - 657/2u^{40} + 83u^{36} + 3u^{32} \\
L_9 &= +127579807/9x^9u^{54} - 90480828x^9u^{53} + 248294610x^9u^{52} - 379686836x^9u^{51} + 348702921x^9u^{50} \\
&\quad - 190517760x^9u^{49} + 54753064x^9u^{48} - 3978300x^9u^{47} - 1368954x^9u^{46} + 60804x^9u^{45} + 40050x^9u^{44} \\
&\quad + 5544x^9u^{43} + 127x^9u^{42} + 24x^9u^{41} - 10690323x^7u^{54} + 44980722x^7u^{53} - 61926729x^7u^{52} \\
&\quad + 9022472x^7u^{51} + 54503559x^7u^{50} - 45973002x^7u^{49} + 4829245x^7u^{48} + 6738564x^7u^{47} - 896967x^7u^{46} \\
&\quad - 490174x^7u^{45} - 142017x^7u^{44} + 22500x^7u^{43} + 17479x^7u^{42} + 4278x^7u^{41} + 384x^7u^{40} + 8x^7u^{39} \\
&\quad + 2728302x^5u^{54} - 6282360x^5u^{53} - 1062648x^5u^{52} + 11093040x^5u^{51} - 4277985x^5u^{50} - 5268780x^5u^{49} \\
&\quad + 2597970x^5u^{48} + 381708x^5u^{47} + 289224x^5u^{46} - 3732x^5u^{45} - 154596x^5u^{44} - 42816x^5u^{43} - 16392x^5u^{42} \\
&\quad + 11136x^5u^{41} + 6456x^5u^{40} + 1344x^5u^{39} + 132x^5u^{38} - 789040/3x^3u^{54} + 213480x^3u^{53} + 600072x^3u^{52} \\
&\quad - 419688x^3u^{51} - 326820x^3u^{50} + 110796x^3u^{49} - 141215x^3u^{48} + 187176x^3u^{47} + 162291x^3u^{46} \\
&\quad - 72954x^3u^{45} - 27303x^3u^{44} - 25044x^3u^{43} - 6391x^3u^{42} + 4506x^3u^{41} + 1188x^3u^{40} + 2016x^3u^{39} \\
&\quad + 828x^3u^{38} + 72x^3u^{37} + 7031xu^{54} - 9216xu^{52} - 10611xu^{50} + 15310xu^{48} + 5058xu^{46} - 8040xu^{44} \\
&\quad - 917xu^{42} + 1254xu^{40} + 84xu^{38} + 48xu^{36}
\end{aligned}$$

Phys. Rev. E **63**, 041111 (2001).

<https://link.aps.org/doi/10.1103/PhysRevE.63.041111>.

<sup>16</sup> S. Grollau, Phase diagram of the spin- $\frac{3}{2}$  Blume-Capel model in three dimensions, Phys. Rev. E **65** (2002) 056130.

<https://link.aps.org/doi/10.1103/PhysRevE.65.056130>.

<sup>17</sup> E. Costabile, J.R. Viana, J. R. de Sousa and J.A. Plascak, The general-spin Blume-Capel model: A study of the multicritical behavior using effective-field theory, Physica A **393**, 297 (2014).

<https://doi.org/10.1016/j.physa.2013.09.003>.

<sup>18</sup> Li-Ping Yang, and Zhi-Yuan Xie, Tensor Renormalization Group Study of the General Spin-S Blume-Capel Model, J. Phys. Soc. Jpn. **85** (2016) 104602.



TABLE VIII: (Continued from the preceding Table) BC model with spin  $S = 1$  on a simple-cubical lattice, subject to a magnetic field  $H$  and a crystal field  $D$ . The coefficients  $L_n(u, x; 1)$  of the LT series expansion in powers of  $\mu = \exp(h)$  for the free-energy density Eq. (6) are expressed in terms of the LT variable  $u = \exp(-\beta)$  and of the crystal field variable  $x = \exp(D)$ .

$$\begin{aligned}
L_{10} = & -1540944687/10x^{10}u^{60} + 1102444428x^{10}u^{59} - 3449297064x^{10}u^{58} + 6156900766x^{10}u^{57} \\
& - 6835882485x^{10}u^{56} + 23965701903/5x^{10}u^{55} - 2018275270x^{10}u^{54} + 414942978x^{10}u^{53} \\
& + 2839656x^{10}u^{52} - 12412763x^{10}u^{51} - 614784x^{10}u^{50} + 236808x^{10}u^{49} + 67267x^{10}u^{48} + 4131x^{10}u^{47} \\
& + 396x^{10}u^{46} + 24x^{10}u^{45} + 127579807x^8u^{60} - 633365796x^8u^{59} + 1136891808x^8u^{58} - 633220552x^8u^{57} \\
& - 611949780x^8u^{56} + 1042711956x^8u^{55} - 432968505x^8u^{54} - 65933616x^8u^{53} + 73586991x^8u^{52} \\
& + 977856x^8u^{51} - 2551188x^8u^{50} - 1745292x^8u^{49} - 155650x^8u^{48} + 87072x^8u^{47} + 45669x^8u^{46} + 8348x^8u^{45} \\
& + 849x^8u^{44} + 24x^8u^{43} - 74832261/2x^6u^{60} + 112451805x^6u^{59} - 40853013x^6u^{58} - 174019476x^6u^{57} \\
& + 326069793/2x^6u^{56} + 52714461x^6u^{55} - 94539076x^6u^{54} + 8386548x^6u^{53} + 11536857/2x^6u^{52} + 4477701x^6u^{51} \\
& + 1683855x^6u^{50} - 1249242x^6u^{49} - 181277x^6u^{48} - 297030x^6u^{47} - 28746x^6u^{46} + 40770x^6u^{45} + 20220x^6u^{44} \\
& + 4716x^6u^{43} + 562x^6u^{42} + 24x^6u^{41} + 4547170x^4u^{60} - 6282360x^4u^{59} - 9825078x^4u^{58} + 14528896x^4u^{57} \\
& + 5447442x^4u^{56} - 8416140x^4u^{55} + 626182x^4u^{54} - 2440008x^4u^{53} - 945117x^4u^{52} + 2950388x^4u^{51} \\
& + 456423x^4u^{50} - 204420x^4u^{49} - 332881x^4u^{48} - 141396x^4u^{47} + 24819x^4u^{46} - 16444x^4u^{45} + 6561x^4u^{44} \\
& + 10980x^4u^{43} + 4220x^4u^{42} + 744x^4u^{41} + 24x^4u^{40} - 197260x^2u^{60} + 53370x^2u^{59} + 426960x^2u^{58} - 80736x^2u^{57} \\
& - 18732x^2u^{56} - 51564x^2u^{55} - 476312x^2u^{54} + 102984x^2u^{53} + 384921/2x^2u^{52} + 17103x^2u^{51} + 162828x^2u^{50} \\
& - 43710x^2u^{49} - 76855x^2u^{48} - 4608x^2u^{47} - 21024x^2u^{46} + 5982x^2u^{45} + 6633x^2u^{44} + 918x^2u^{43} \\
& + 888x^2u^{42} + 240x^2u^{41} + 396x^2u^{40} + 36x^2u^{39} + 7031/5u^{60} - 4608u^{56} + 5532u^{52} - 2804u^{48} + 426u^{44} + 48u^{40} \\
L_{11} = & + 18794572864/11x^{11}u^{66} - 13540389348x^{11}u^{65} + 47569139712x^{11}u^{64} - 97076564452x^{11}u^{63} \\
& + 126406988784x^{11}u^{62} - 108143883564x^{11}u^{61} + 59739201959x^{11}u^{60} + 14304038720x^9u^{60} \\
& - 2477592492x^9u^{59} - 19491928200x^{11}u^{59} + 2620578876x^{11}u^{58} + 306005260x^{11}u^{57} - 86214999x^{11}u^{56} \\
& - 12635748x^{11}u^{55} + 423644x^{11}u^{54} + 602928x^{11}u^{53} + 70275x^{11}u^{52} + 6656x^{11}u^{51} + 660x^{11}u^{50} + 24x^{11}u^{49} \\
& - 1540944687x^9u^{66} + 8819555424x^9u^{65} - 19439069532x^9u^{64} + 17599284188x^9u^{63} + 2383226190x^9u^{62} \\
& - 18579302220x^9u^{61} + 14304038720x^9u^{60} - 2477592492x^9u^{59} - 1744972041x^9u^{58} + 620343152x^9u^{57} \\
& + 70418718x^9u^{56} + 2196588x^9u^{55} - 14062078x^9u^{54} - 3441096x^9u^{53} - 111972x^9u^{52} + 314324x^9u^{51} \\
& + 98685x^9u^{50} + 18228x^9u^{49} + 1828x^9u^{48} + 72x^9u^{47} + 510319228x^7u^{66} - 1900097388x^7u^{65} \\
& - 108143883564x^{11}u^{61} + 59739201959x^{11}u^{60} + 1598116578x^7u^{64} + 2151778972x^7u^{63} - 3985693602x^7u^{62} \\
& + 589317072x^7u^{61} + 2069817648x^7u^{60} - 946297212x^7u^{59} - 162915150x^7u^{58} + 9669012x^7u^{57} \\
& + 40864122x^7u^{56} + 38590740x^7u^{55} - 11288488x^7u^{54} + 653808x^7u^{53} - 2042730x^7u^{52} - 981400x^7u^{51} \\
& - 21864x^7u^{50} + 129864x^7u^{49} + 63514x^7u^{48} + 14892x^7u^{47} + 2220x^7u^{46} + 168x^7u^{45} - 74832261x^5u^{66} \\
& + 149935740x^5u^{65} + 117115302x^5u^{64} - 368112532x^5u^{63} + 13494099x^5u^{62} + 268457844x^5u^{61} \\
& - 67818484x^5u^{60} - 13818084x^5u^{59} - 8156250x^5u^{58} - 48587000x^5u^{57} + 18009936x^5u^{56} + 14417604x^5u^{55} \\
& + 4763664x^5u^{54} - 2262660x^5u^{53} - 2736036x^5u^{52} + 301952x^5u^{51} - 149535x^5u^{50} - 123420x^5u^{49} \\
& + 30794x^5u^{48} + 43992x^5u^{47} + 20628x^5u^{46} + 4280x^5u^{45} + 396x^5u^{44} + 24x^5u^{43} + 4547170x^3u^{66} \\
& - 3141180x^3u^{65} - 12064851x^3u^{64} + 6959616x^3u^{63} + 6816114x^3u^{62} - 1299924x^3u^{61} + 6726046x^3u^{60} \\
& - 5978568x^3u^{59} - 7517436x^3u^{58} + 2638500x^3u^{57} + 208077x^3u^{56} + 1763880x^3u^{55} + 1676511x^3u^{54} \\
& - 747330x^3u^{53} - 290739x^3u^{52} - 260484x^3u^{51} - 123447x^3u^{50} + 49494x^3u^{49} + 16420x^3u^{48} \\
& + 11232x^3u^{47} + 4140x^3u^{46} + 3720x^3u^{45} + 2508x^3u^{44} + 504x^3u^{43} + 32x^3u^{42} - 78904xu^{66} + 106740xu^{64} \\
& + 173112xu^{62} - 252388xu^{60} - 135885xu^{58} + 214710xu^{56} + 46144xu^{54} - 75192xu^{52} - 6654xu^{50} + 7104xu^{48} \\
& + 288xu^{46} + 852xu^{44} + 72xu^{42}
\end{aligned}$$

<https://doi-org/10.7566/JPSJ.85.104602>.

- <sup>19</sup> J. Strečka and M. Jaščur, A brief account of the Ising and Ising-like models: mean-field, effective field and exact results, *acta physica slovacica* **65** (2015) 235-367.  
No doi n.
- <sup>20</sup> Y. Yüksel, Ü. Akinçi and H. Polat, An introduced effective-field approximation and Monte Carlo study of a spin-1 Blume-Capel model on a square lattice, *Physica Scripta* **79** (2009) 045009.  
<https://doi-org/10.1088/0031-8949/79/04/045009>.
- <sup>21</sup> P.D. Beale, Finite-size scaling study of the two-dimensional Blume-Capel model, *Phys. Rev. B* **33** (1986) 1717-1720.  
<https://link.aps.org/doi/10.1103/PhysRevB.33.1717>.
- <sup>22</sup> Qian, Xiaofeng and Deng, Youjin and Henk W. J. Blöte, Dilute Potts model in two dimensions, *Phys. Rev. E* **72** (2005)

TABLE IX: The first nine expansion coefficients  $g_n(D, h)$  of the HT series expansion in powers of  $K$  for the free-energy density Eq. (3) of the BC model with spin  $S = 1$  and nearest-neighbor interaction on a simple-cubic lattice, in a reduced crystal field  $D = K\Delta/J$  and a reduced magnetic field  $h = KH/J$ . The coefficients of higher order, which are too long to be reproduced here, can be found in Ref. [67]. Notice that in this Table we have set for brevity  $A \equiv A(D, h; 1)$  and  $B \equiv B(D, h; 1)$ , omitting the functional dependence of these quantities on  $D$  and  $h$ , while  $x = \exp(D)$  and  $y = \exp(h)$  as in the text.

---


$$\begin{aligned}
g_0 &= \ln(1 + y/x + 1/xy) = -\ln(1 - B) \\
g_1 &= 3A^2 \\
g_2 &= 3B^2/2 + 15BA^2 - 33A^4/2 \\
g_3 &= A^2/2 + 15BA^2 + 117B^2A^2/2 + 20A^4 - 240BA^4 + 146A^6 \\
g_4 &= B^2/8 + 15B^3/4 - 9B^4/8 + 5BA^2 + 105B^2A^2 + 243B^3A^2 + 32A^4 + 75BA^4 - 4401B^2A^4/2 \\
&\quad - 420A^6 + 3753BA^6 - 6381A^8/4 \\
g_5 &= A^2/40 + 15BA^2/4 + 885B^2A^2/8 + 531B^3A^2 + 1035B^4A^2 + 10A^4 + 573BA^4 - 960B^2A^4 \\
&\quad - 16623B^3A^4 - 805A^6/2 - 7293BA^6 + 111591B^2A^6/2 + 7572A^8 - 60012BA^8 + 98298A^{10}/5 \\
g_6 &= B^2/240 + 5B^3/8 + 211B^4/16 - 6B^5 + 41B^6/4 + 2BA^2/3 + 187B^2A^2/4 + 3339B^3A^2/4 + \\
&\quad 10737B^4A^2/4 + 17241B^5A^2/4 + 1967A^4/120 + 2321BA^4/4 + 16941B^2A^4/4 - 71087B^3A^4/4 \\
&\quad - 899127B^4A^4/8 + 572A^6 - 16118BA^6 - 62856B^2A^6 + 632166B^3A^6 + 1192A^8 + 225204BA^8 \\
&\quad - 1250433B^2A^8 - 132208A^{10} + 981858BA^{10} - 261941A^{12} \\
g_7 &= A^2/1680 + 3BA^2/8 + 2917B^2A^2/80 + 3111B^3A^2/4 + 39189B^4A^2/8 + 13482B^5A^2 \\
&\quad + 141453B^6A^2/8 + 13A^4/6 + 1705BA^4/4 + 17699B^2A^4/2 + 64725B^3A^4/4 - 372027B^4A^4/2 \\
&\quad - 703539B^5A^4 + 82283A^6/120 + 6767BA^6/4 - 2176275B^2A^6/8 - 248049B^3A^6 + 6051543B^4A^6 \\
&\quad - 23672A^8 + 228360BA^8 + 3578184B^2A^8 - 19113288B^3A^8 + 95961A^{10} - 5566386BA^{10} \\
&\quad + 26486325B^2A^{10} + 2296224A^{12} - 16374696BA^{12} + 25804572A^{14}/7 \\
g_8 &= B^2/13440 + 3B^3/64 + 2371B^4/640 + 423B^5/8 - 461B^6/32 + 1689B^7/16 - 45B^8/64 + BA^2/21 \\
&\quad + 75B^2A^2/8 + 17319B^3A^2/40 + 50583B^4A^2/8 + 219345B^5A^2/8 + 258183B^6A^2/4 + 145161B^7A^2/2 \\
&\quad + 5897A^4/1680 + 2529BA^4/8 + 187383B^2A^4/20 + 611243B^3A^4/8 - 466653B^4A^4/16 \\
&\quad - 3130035B^5A^4/2 - 8319465B^6A^4/2 + 639A^6 + 217141BA^6/10 - 187287B^2A^6 - 6076527B^3A^6/2 \\
&\quad + 1757556B^4A^6 + 51507546B^5A^6 - 69649A^8/5 - 652824BA^8 + 28766757B^2A^8/4 + 78201879B^3A^8/2 \\
&\quad - 478585635B^4A^8/2 + 562028A^{10} - 68391BA^{10} - 124741005B^2A^{10} + 512545839B^3A^{10} - 3813290A^{12} \\
&\quad + 125336223BA^{12} - 1088156373B^2A^{12}/2 - 39985236A^{14} + 277367829BA^{14} - 432195261A^{16}/8 \\
g_9 &= A^2/120960 + 85BA^2/4032 + 5375B^2A^2/896 + 2497B^3A^2/8 + 190767B^4A^2/32 + 165681B^5A^2/4 \\
&\quad + 4821229B^6A^2/32 + 1195431B^7A^2/4 + 2383713B^8A^2/8 + 205A^4/756 + 67849BA^4/504 + \\
&\quad 21511B^2A^4/3 + 977359B^3A^4/8 + 922845B^4A^4/2 - 2478237B^5A^4/2 - 11566918B^6A^4 - 23547948B^7A^4 \\
&\quad + 2052793A^6/3024 + 701845BA^6/24 + 3152285B^2A^6/16 - 8477493B^3A^6/2 - 51566121B^4A^6/2 \\
&\quad + 48392016B^5A^6 + 803230243B^6A^6/2 + 31357A^8/3 - 1034012BA^8 - 7019841B^2A^8 + 131377442B^3A^8 \\
&\quad + 307273428B^4A^8 - 2598632472B^5A^8 - 2972317A^{10}/20 + 52005649BA^{10}/2 - 392748291B^2A^{10}/4 \\
&\quad - 1959609677B^3A^{10} + 15939623007B^4A^{10}/2 - 30528358A^{12}/3 - 121326545BA^{12} + 3609445080B^2A^{12} \\
&\quad - 12781309029B^3A^{12} + 210342571A^{14}/2 - 2686363629BA^{14} + 21942403551B^2A^{14}/2 + 699783404A^{16} \\
&\quad - 4758350316BA^{16} + 2450507294A^{18}/3
\end{aligned}$$


---

056132.

<https://link.aps.org/doi/10.1103/PhysRevE.72.056132>.

- <sup>23</sup> M. Jung and D.H. Kim, First-order transitions and thermodynamic properties in the 2D Blume-Capel model: the transfer-matrix method revisited, *The European Physical Journal B* **90** (2017) 245.  
<https://doi.org/10.1140/epjb/e2017-80471-2>.
- <sup>24</sup> B.L. Arora and D.P. Landau, Monte Carlo Studies of Tricritical Phenomena, *AIP Conference Proceedings* **10** (1973) 870-874.  
<https://doi-org/10.1063/1.2947039>.
- <sup>25</sup> A. K. Jain and D.P. Landau, Monte Carlo study of the fcc Blume-Capel model, *Phys. Rev. B* **22** (1980) 445-452.  
<https://link.aps.org/doi/10.1103/PhysRevB.22.445>.
- <sup>26</sup> C.M. Care, Microcanonical Monte Carlo study of a two-dimensional Blume-Capel model, *J. Phys. A* **26** (1993) 1481-1492.  
<https://doi-org/10.1088/0305-4470/26/7/010>.
- <sup>27</sup> H.W.J. Blöte, E.Lujitens and J.R. Heringa, Ising universality in three dimensions: a Monte Carlo study, *J.Phys. A* **28** (1995) 6289-6313.  
<https://doi-org/10.1088/0305-4470/28/22/007>.

- <sup>28</sup> M. Hasenbusch, Finite size scaling study of lattice models in the three-dimensional Ising Universality class, *Phys. Rev. B* **82** (2010) 174433.  
<https://link.aps.org/doi/10.1103/PhysRevB.82.174433>.
- <sup>29</sup> N.B. Wilding and P. Nielaba, Tricritical universality in a two-dimensional spin fluid, *Phys. Rev. E* **53** (1996) 926-934.  
<https://link.aps.org/doi/10.1103/PhysRevE.53.926>.
- <sup>30</sup> M. Deserno, Tricriticality and the Blume-Capel model: A Monte Carlo study within the microcanonical ensemble, *Phys. Rev. E* **56** (1997) 5204-5210.  
<https://link.aps.org/doi/10.1103/PhysRevE.56.5204>.
- <sup>31</sup> J.A. Plascak and D.P. Landau, Universality and double critical end points, *Phys. Rev. E* **67** (2003) 015103.  
<https://link.aps.org/doi/10.1103/PhysRevE.67.015103>.
- <sup>32</sup> Y. Deng and H. W. J. Blöte, Red-bond exponents of the critical and the tricritical Ising model in three dimensions, *Phys. Rev. E* **70** (2004) 056132.  
<https://link.aps.org/doi/10.1103/PhysRevE.70.056132>.
- <sup>33</sup> A. Özkan, N. Seferoglu and B. Kutlu, Critical exponents of the three-dimensional Blume-Capel model on a cellular automaton, *Physica A* **362** (2006) 327-337.  
<https://doi.org/10.1016/j.physa.2005.08.065>.
- <sup>34</sup> C.J. Silva, A.A. Caparica and J.A. Plascak, Wang-Landau Monte Carlo simulation of the Blume-Capel model, *Phys. Rev. E* **73** (2006) 036702.  
<https://link.aps.org/doi/10.1103/PhysRevE.73.036702>.
- <sup>35</sup> J.A. Plascak and P.H.L. Martins, Probability distribution function of the order parameter: Mixing fields and universality, *Comput. Phys. Comm.* **184** (2013) 259-269.  
<https://doi.org/10.1016/j.cpc.2012.09.014>.
- <sup>36</sup> A. Malakis, A. Nihat Berker, I. A. Hadjiagapiou, N. G. Fytas and T. Papakonstantinou, Scaling and universality in the phase diagram of the 2D Blume-Capel model, *Phys. Rev. E* **81** (2010) 041113.  
<https://link.aps.org/doi/10.1103/PhysRevE.81.041113>.
- <sup>37</sup> W. Kwak, J. Jeong, J. Lee and D.H. Kim, First-order phase transition and tricritical scaling behavior of the Blume-Capel model: A Wang-Landau sampling approach, *Phys. Rev. E* **92** (2015) 022134.  
<https://link.aps.org/doi/10.1103/PhysRevE.92.022134>.
- <sup>38</sup> J. Zierenberg, N.G. Fytas and W. Janke, Parallel multicanonical study of the three-dimensional Blume-Capel model, *Phys. Rev. E* **91** (2015) 032126.  
<https://link.aps.org/doi/10.1103/PhysRevE.91.032126>.
- <sup>39</sup> J. Zierenberg, N.G. Fytas, M. Weigel, W. Janke and A. Malakis, Scaling and universality in the phase diagram of the 2D Blume-Capel model, *Eur. Phys. J. Spec. Top.* **226** (2017) 789-804.  
<https://doi.org/10.1140/epjst/e2016-60337-x>.
- <sup>40</sup> J. Oitmaa, High temperature series expansions for a lattice model of critical behavior in multicomponent systems, *J. Phys. C* **4** (1971) 2466-2474.  
<https://doi-org/10.1088/0022-3719/4/16/012>.
- <sup>41</sup> J. Oitmaa, Critical behavior of a generalized Ising model, *J. Phys. C* **5** (1972) 435-449.  
<https://doi-org/10.1088/0022-3719/5/4/010>.
- <sup>42</sup> J. G. Brankov, J. Przystawa and E. Praveczi, Effect of crystal field anisotropy on the Curie temperature of an Ising ferromagnet: HTS expansion method, *J. Phys. C* **5** (1972) 3387-3396.  
<https://doi-org/10.1088/0022-3719/5/23/011>.
- <sup>43</sup> D.M. Saul, M. Wortis and D. Stauffer, Tricritical behavior of the Blume-Capel model, *Phys. Rev. B* **9** (1974) 4964-4980.  
<https://link.aps.org/doi/10.1103/PhysRevB.9.4964>.
- <sup>44</sup> R.L. Joseph and R.A. Farrel, High-temperature series for the spin-one Ising model for arbitrary biquadratic exchange, field, and anisotropy, *Phys. Rev. B* **14** (1976) 5121-5124.  
<https://link.aps.org/doi/10.1103/PhysRevB.14.5121>.
- <sup>45</sup> Y.L. Wang and F. Lee, Linked-cluster series analysis of the Blume-Capel model, *Phys. Rev. B* **29** (1984) 5156-5164.  
<https://link.aps.org/doi/10.1103/PhysRevB.29.5156>.
- <sup>46</sup> P. Butera and M. Pernici, free-energy in a magnetic field and the universal scaling equation of state for the three-dimensional Ising model, *Phys. Rev. B* **83** (2011) 054433.  
<https://link.aps.org/doi/10.1103/PhysRevB.83.054433>.
- <sup>47</sup> P. Butera and M. Pernici, Triviality problem and high-temperature expansions of higher susceptibilities for the Ising and scalar-field models in four-, five-, and six-dimensional lattices, *Phys. Rev. E* **85** (2012) 021105.  
<https://link.aps.org/doi/10.1103/PhysRevE.85.021105>.
- <sup>48</sup> P. Butera and M. Pernici, Yang-Lee edge singularities from extended activity expansions of the dimer density for bipartite lattices of dimensionality  $2 \leq d \leq 7$ , *Phys. Rev. E* **86** (2012) 011104.  
<https://link.aps.org/doi/10.1103/PhysRevE.86.011104>.
- <sup>49</sup> I.D. Lawrie and S. Sarbach, in *"Phase Transitions and Critical Phenomena"* edited by C. Domb and J. Lebowitz, (Academic Press, New York 1984), Vol. 9 pag. 1.
- <sup>50</sup> F. Harbus and H.E. Stanley, Ising-Model "Metamagnet" and Tricritical Susceptibility Exponent, *Phys. Rev. Lett.* **29** (1972) 58-62.  
<https://link.aps.org/doi/10.1103/PhysRevLett.29.58>.

- <sup>51</sup> A. Aharony, in “*Critical Phenomena*”, edited by F.J.W. Hahne, (Springer, Berlin 1983), Lecture Notes in Physics, Vol.186, pag 210.
- <sup>52</sup> J. Bernasconi and F. Rys, Critical Behavior of a Magnetic Alloy, Phys. Rev. B **4** (1971) 3045-3048.  
<https://link.aps.org/doi/10.1103/PhysRevB.4.3045>.
- <sup>53</sup> E. K. Riedel, Scaling Approach to Tricritical Phase Transitions, Phys. Rev. Lett. **28** (1972) 675-678.  
<https://link.aps.org/doi/10.1103/PhysRevLett.28.675>.
- <sup>54</sup> E.K. Riedel and F. J. Wegner, Tricritical Exponents and Scaling Fields, Phys. Rev. Lett. **29** (1972) 349-352.  
<https://link.aps.org/doi/10.1103/PhysRevLett.29.349>.
- <sup>55</sup> F.J. Wegner and E.K. Riedel, Logarithmic Corrections to the Molecular-Field Behavior of Critical and Tricritical Systems, Phys. Rev. B **7** (1973) 248-256.  
<https://link.aps.org/doi/10.1103/PhysRevB.7.248>.
- <sup>56</sup> R. Bausch, Ginzburg criterion for tricritical points, Z. Phys. **254** (1972) 81-88.  
<https://doi.org/10.1007/BF01379692>.
- <sup>57</sup> J. Cardy, in “*Phase Transitions and Critical Phenomena*”, Vol. 11 pag. 1, edited by C. Domb and J. Lebowitz (Academic, New York,1987).
- <sup>58</sup> M. Lässig, G. Mussardo and J. Cardy, The scaling region of the tricritical Ising model in two dimensions, Nucl. Phys. B **348** (1991) 591-618.  
[https://doi.org/10.1016/0550-3213\(91\)90206-D](https://doi.org/10.1016/0550-3213(91)90206-D).
- <sup>59</sup> M. Henkel, “*Conformal invariance and critical phenomena*”, Springer, Berlin 1999.
- <sup>60</sup> P. Butera and M. Comi, Critical universality and hyperscaling revisited for Ising models of general spin using extended high-temperature series, Phys.Rev. B **65** (2002) 144431.  
<https://link.aps.org/doi/10.1103/PhysRevB.65.144431>.
- <sup>61</sup> C. Domb, in “*Phase Transitions and Critical Phenomena*”, Vol. 3, pag.357, edited by C. Domb and M. S. Green, (Academic, New York 1974).
- <sup>62</sup> M. Wortis, in “*Phase Transitions and Critical Phenomena*”, Vol. 3, pag.113, edited by C. Domb and M. S. Green, (Academic, New York 1974).
- <sup>63</sup> P. Butera and M. Pernici, Ising low-temperature polynomials and hard-sphere gases on cubic lattices of general dimension, Physica A **444** (2016) 220-234.  
<https://doi.org/10.1016/j.physa.2015.09.103>.
- <sup>64</sup> P.F. Fox and A.J. Guttmann, Low temperature critical behaviour of the Ising model with spin  $S > 1/2$ , J. Phys. C **6** (1973) 913-931.  
<https://doi-org/10.1088/0022-3719/6/5/020>.
- <sup>65</sup> P.F. Fox and D.S. Gaunt, Critical isotherm of the Ising ferromagnet with spin  $S > 1/2$ , J. Phys. C **5** (1972) 3085-3096.  
<https://doi-org/10.1088/0022-3719/5/21/013>.
- <sup>66</sup> D.Saul and M. Ferer, Derivation of a low-temperature expansion for the general-spin Ising model, Phys. Rev. B **11** (1975) 387-398.  
<https://link.aps.org/doi/10.1103/PhysRevB.11.387>.
- <sup>67</sup> P.Butera and M. Pernici, unpublished.
- <sup>68</sup> W. A. Stein et al., Sage Mathematica Software, to be freely downloaded at <http://www.sagemath.org>  
doi:<http://dx.doi.org/10.1063/1.3141831>.
- <sup>69</sup> E.K. Riedel, H. Meyer and R.P. Behringer, Thermodynamic properties of liquid 3He-4He mixtures near the tricritical point. II. Data analysis by the scaling-field method, J. Low. Temp. Phys. **22** (1976) 369-402. <https://doi.org/10.1007/BF00654713>.
- <sup>70</sup> E.K. Riedel and F. J. Wegner, Scaling approach to anisotropic magnetic systems statics, Z. Phys. **255** (1969) 195-215.  
<https://doi.org/10.1007/BF01392215>.
- <sup>71</sup> P. G. Watson, Formation of invariants from critical amplitudes of ferromagnets, J. Phys. C **2** (1969) 1883.  
<https://doi-org/10.1088/0022-3719/2/10/124>.
- <sup>72</sup> A. J. Guttmann, in “*Phase Transitions and Critical Phenomena*”, edited by C. Domb and J. Lebowitz (Academic Press, New York 1989), vol. 13, pag.1.
- <sup>73</sup> J. Zinn-Justin, Analysis of high temperature series of the spin S Ising model on the body-centred cubic lattice, J. Physique **42** (1981) 783-792.  
<https://doi.org/10.1051/jphys:01981004206078300>.
- <sup>74</sup> I.G. Enting and R. J. Baxter, An investigation of the high-field series expansions for the square lattice Ising model, J. Phys. A **13** (1980) 3723-3734.  
<https://doi-org/10.1088/0305-4470/13/12/022>.
- <sup>75</sup> V. Privman and L.S. Schulman, Analytic continuation at first-order phase transitions, J. Stat. Phys. **29** (1982) 205-229.  
<https://doi.org/10.1007/BF01020783>.
- <sup>76</sup> J.S. Kouvel and M.E. Fisher, Detailed Magnetic Behavior of Nickel Near its Curie Point, Phys. Rev. **136 A** (1964) 1626-1632.  
<https://link.aps.org/doi/10.1103/PhysRev.136.A1626>.
- <sup>77</sup> E.K. Riedel, Crossover Phenomena, Critical and Tricritical Phase Transitions, AIP Conf. Proc. **18** (1974) 834.  
<https://doi-org/10.1063/1.3141831>.
- <sup>78</sup> N.N. Bogolubov, On a Variational Principle in the Many Body Problem, Dokl.Akad.Nauk SSR **119** (1958) 244.  
no DOI.
- <sup>79</sup> R. Peierls, On a Minimum Property of the Free Energy, Phys. Rev. **54** (1958) 918-919.  
<https://link.aps.org/doi/10.1103/PhysRev.54.918>.

- <sup>80</sup> A. Hankey, H.E. Stanley and T.S. Chang, Geometric Predictions of Scaling at Tricritical Points, *Phys. Rev. Lett.* **29** (1972) 278-281.  
<https://link.aps.org/doi/10.1103/PhysRevLett.29.278>.
- <sup>81</sup> P. Pfeuty, D. Jasnow and M.E. Fisher, Crossover scaling functions for exchange anisotropy, *Phys. Rev. B* **10** (1974) 2088-2112.  
<https://link.aps.org/doi/10.1103/PhysRevB.10.2088>.
- <sup>82</sup> M. E. Fisher and J. H. Chen, The validity of hyperscaling in three dimensions for scalar spin systems, *J. Physique (France)* **46** (1985) 1645-1654.  
<https://doi.org/10.1051/jphys:0198500460100164500>.

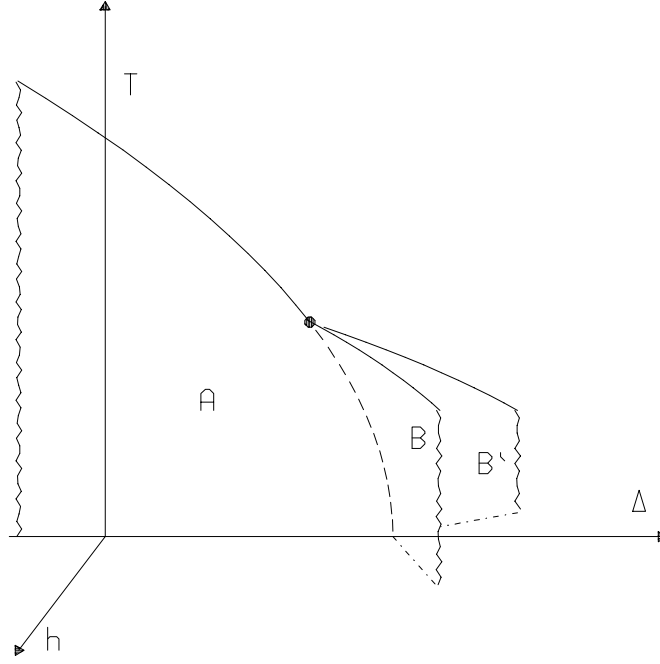


FIG. 1: Schematic<sup>3</sup> phase diagram in the  $\Delta, T, h$  space for a BC model with spin  $S = 1$ . First-order transitions occur across the surfaces  $A$ ,  $B$  and  $B'$ . The long-dashed line is a first-order line in the  $h = 0$  plane. The solid lines that meet at the TCP (full circle) are critical lines bounding the surfaces. The surface  $A$  extends to  $\Delta = -\infty$ , but in the figure is cut along the wavy line. Also the surfaces  $B$  and  $B'$ , called “wings”, extend to large  $\Delta$  and  $|h|$ , but are cut along the wavy lines. The dot-dashed lines are the wing intersections with the  $T = 0$  plane. Phases with opposite values of  $\langle s \rangle$  coexist in the  $A$ -plane while phases with different values of  $\langle s^2 \rangle$  coexist in the planes  $B'$  and  $B$ , so that three phases coexist along the first-order line.

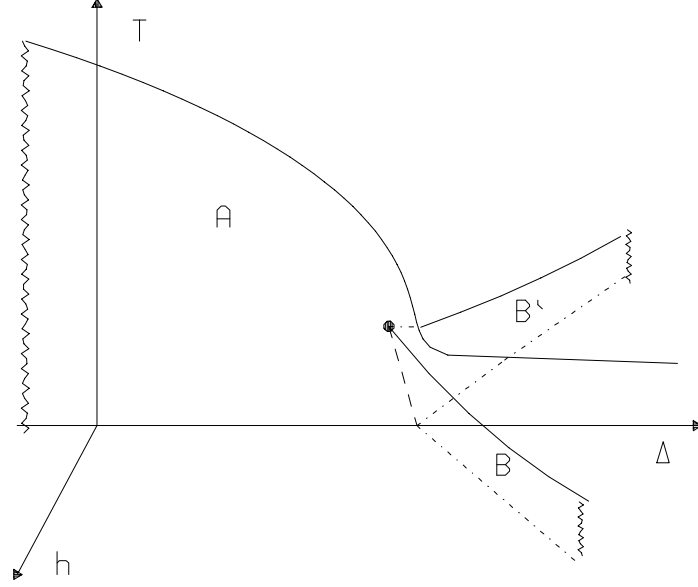


FIG. 2: Schematic<sup>31</sup> phase diagram in the  $\Delta, T, h$  space for a BC model with spin  $S = 3/2$ . First-order transitions occur across the surfaces  $A$ ,  $B$  and  $B'$ . Phases with opposite values of  $\langle s \rangle$  coexist in the  $A$ -plane and phases with different values of  $\langle s^2 \rangle$  coexist in the planes  $B'$  and  $B$ . Four phases coexist on a first-order line in the  $h = 0$  plane, that is the long-dashed line terminating at a “double critical endpoint” (full circle). Solid lines bounding the surfaces  $B$  and  $B'$  are critical transitions that meet at the “double critical endpoint”. The surface  $A$  extends to  $\Delta = -\infty$ , but is cut along the wavy line. Also the surfaces  $B$  and  $B'$ , called “wings”, extend to large  $\Delta$  and  $|h|$ , but are cut along the wavy lines. Short dashed lines are the wing intersections with the  $T = 0$  plane.

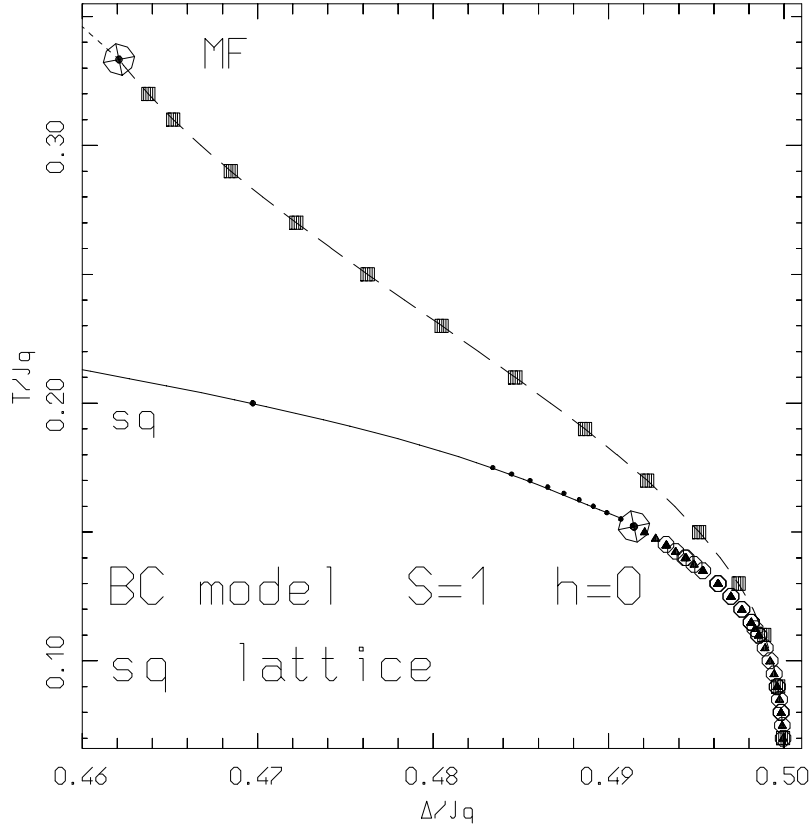


FIG. 3: BC model with spin  $S = 1$  for  $h = 0$  on the  $sq$  lattice. Phase diagram in the  $(\Delta/Jq, T/Jq)$  plane, in the MF approximation and from series analysis. Big crossed open circles are TCPs. The short-dashed line is the MF critical phase-contour. Full squares connected by a long-dashed line are the MF first-order line. The solid curve is the critical phase-contour from series, ending with a TCP computed<sup>22</sup> by transfer-matrix. Full dots on this line are from MC or transfer-matrix. Small black triangles are MC points<sup>23,37,39</sup> on the first-order line. The small open circles around the triangles are obtained by intersecting the LT and HT expansions of the lattice free-energy.



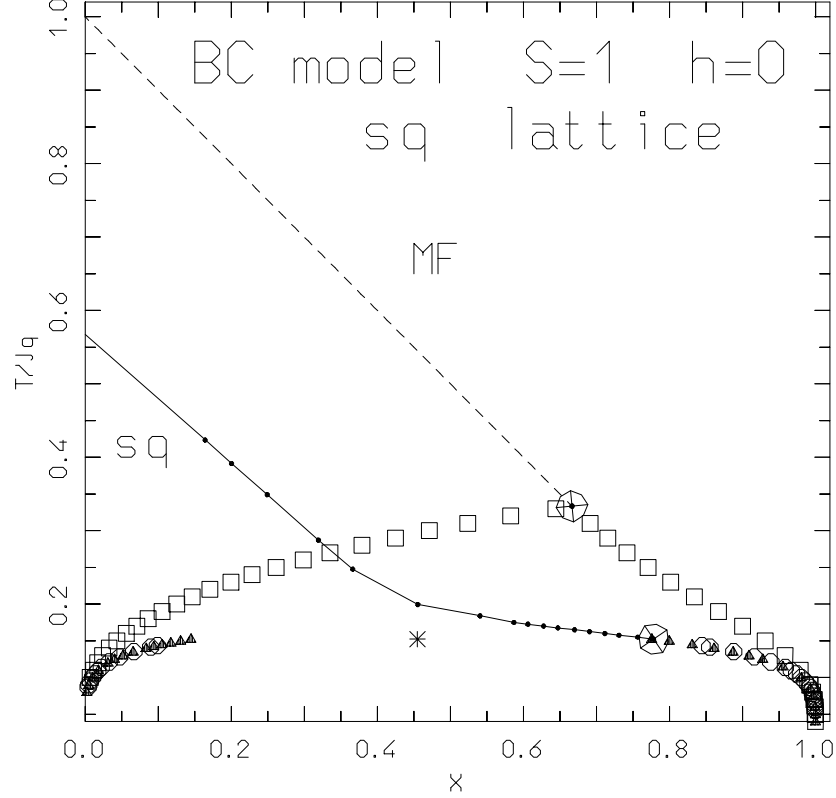


FIG. 4: BC model with spin  $S = 1$  on the  $sq$  lattice for  $h = 0$ . Phase diagram in the concentration-temperature plane. The dashed line is the MF approximation of the critical phase boundary. Sequences of open squares are the two branches of the MF first-order contour. The solid line is the critical contour from series, the black dots on it and the full triangles are the branches of the first-order contour from Refs. [23,37,39]. The small open circles surrounding the full triangles are obtained by intersecting the LT and HT expansions of the free-energy. Big crossed circles are tricritical concentrations. The star is a transfer-matrix estimate<sup>22</sup> of  $X_{tr}$ .

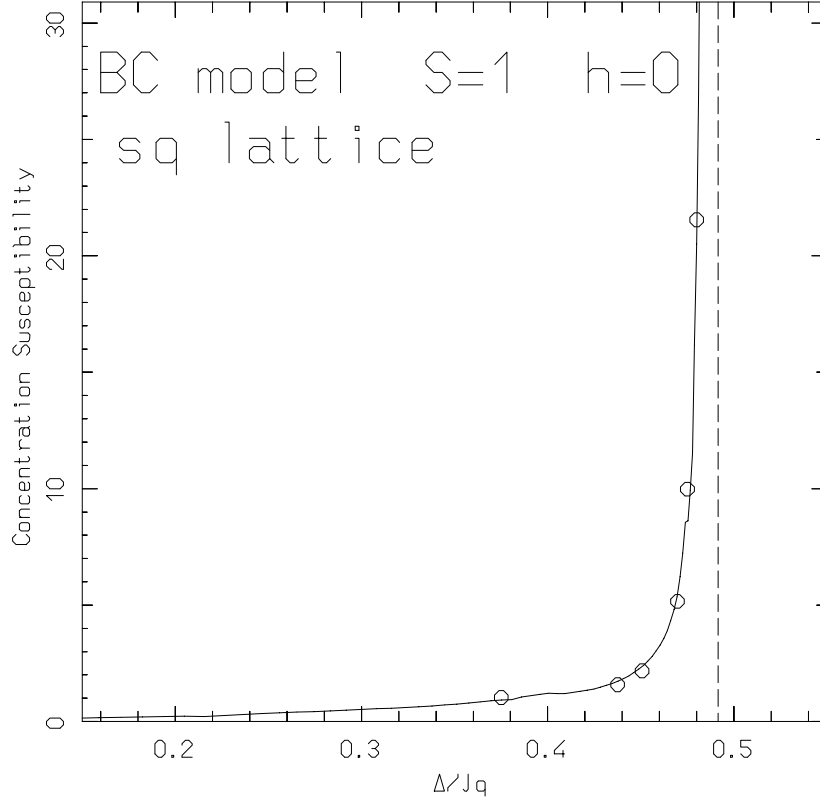


FIG. 5: BC model with spin  $S = 1$  for  $h = 0$  on the  $sq$  lattice. The HT expansion of the concentration susceptibility  $Y(K, D; 1)$  evaluated along the critical phase-boundary (solid line) vs  $\Delta/Jq$ . Open circles are obtained evaluating  $Y(K, D; 1)$  on high-precision estimates of critical points<sup>23,37,39</sup>. The vertical dashed line is the value<sup>22</sup> of  $\Delta_{tr}/Jq$ .

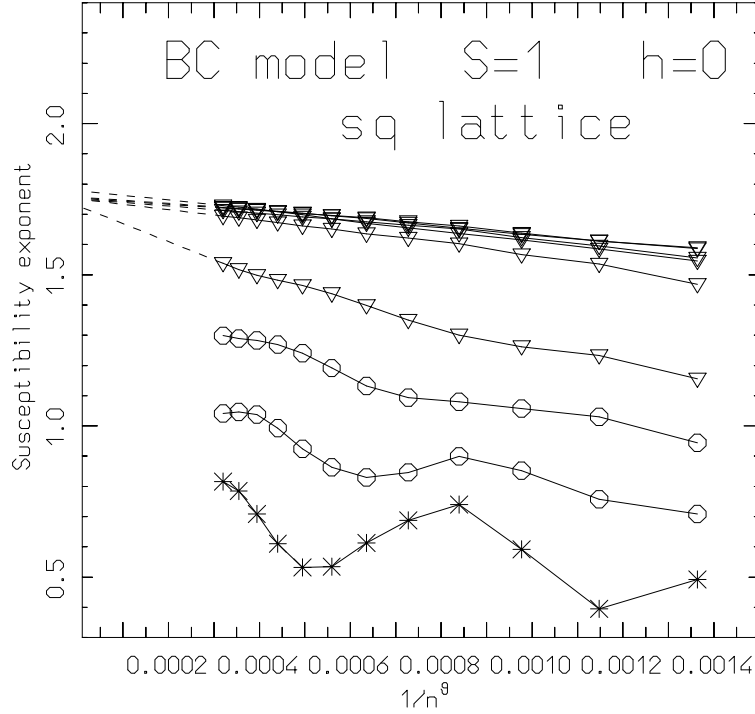


FIG. 6: BC model with spin  $S = 1$  on the  $sq$  lattice, for  $h = 0$ . The twelve highest-order terms of several MRA estimator-sequences for the critical exponent  $\gamma^{(2;0)}(D; 1)$ , obtained from the mixed susceptibility  $\chi_{(2;2)}(K, D; 1)$ , vs  $1/n^\theta$ , with  $n$  the number of terms included in the series and  $\theta = 2.5$ . The lowermost MRA sequence (stars) is computed for  $D \approx D_{tr}$ , the successive two (open circles) for  $D = 0.9D_{tr}$  and  $0.8D_{tr}$ , the remaining ones (open triangles) for  $0.7D_{tr}$ ,  $D = 0.4D_{tr}$ ,  $0.25D_{tr}$ ,  $0.15D_{tr}$ , etc. The symbols of the successive terms are connected by segments to profile the behavior of each sequence. Extrapolations to large  $n$ , indicated only for  $D < 0.8D_{tr}$ , are dashed lines.

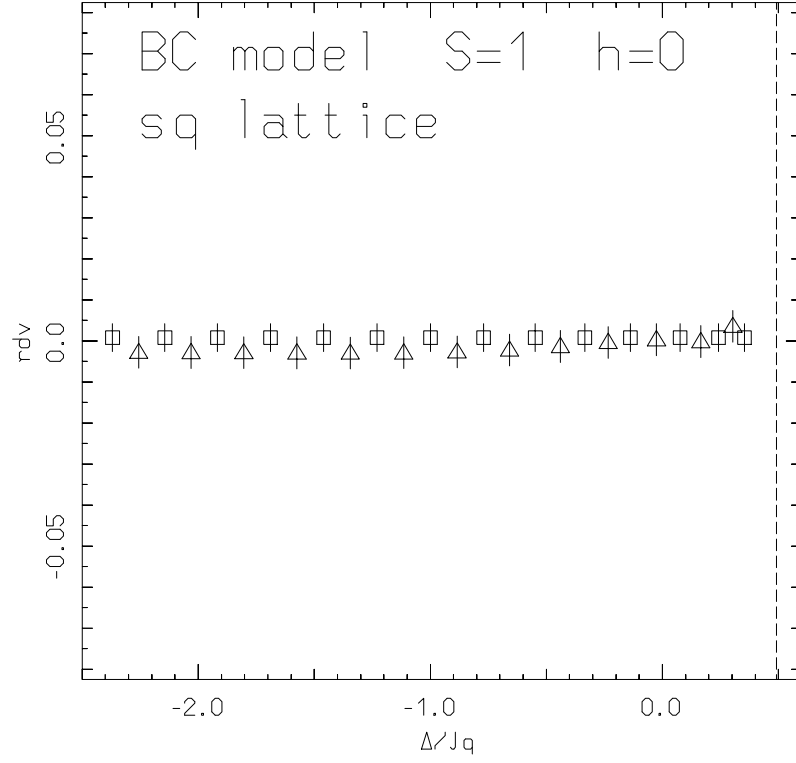


FIG. 7: BC model with spin  $S = 1$  on the  $sq$  lattice for  $h = 0$ . The relative deviations  $rdv$  from the Ising values for the exponents  $\gamma^{(2;0)}(D; 1)$  from  $\chi_{(2;1)}(K, D; 1)$  (open triangles), and  $\gamma^{(4;0)}(D; 1)$  from  $\chi_{(4;0)}(K, D; 1)$  (open squares) vs  $\Delta/Jq$ . The vertical dashed line indicates the tricritical value<sup>22</sup>  $\Delta_{tr}/Jq$  of the crystal field.

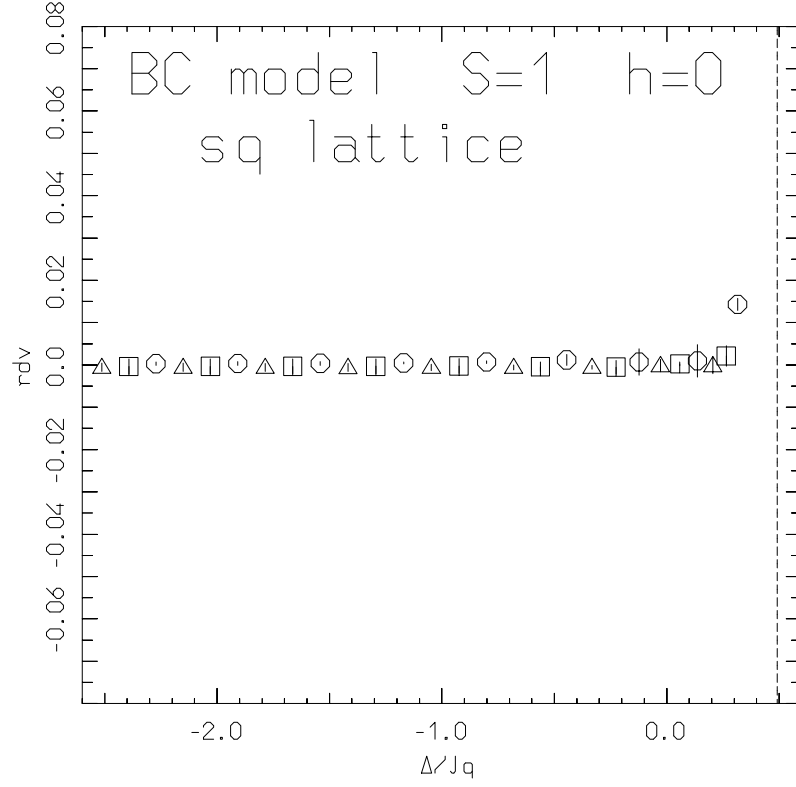


FIG. 8: BC model with spin  $S = 1$  on the  $sq$  lattice for  $h = 0$ . The relative deviations  $rdv$  from the  $2d$  Ising values for the universal ratios of critical amplitudes  $\mathcal{I}_6^+$  (open circles),  $\mathcal{I}_8^+$  (open triangles) and  $\mathcal{J}_8^+$  (open squares) vs  $\Delta/Jq$ . The vertical dashed line indicates the tricritical value<sup>22</sup>  $\Delta_{tr}/Jq$  of the crystal field.

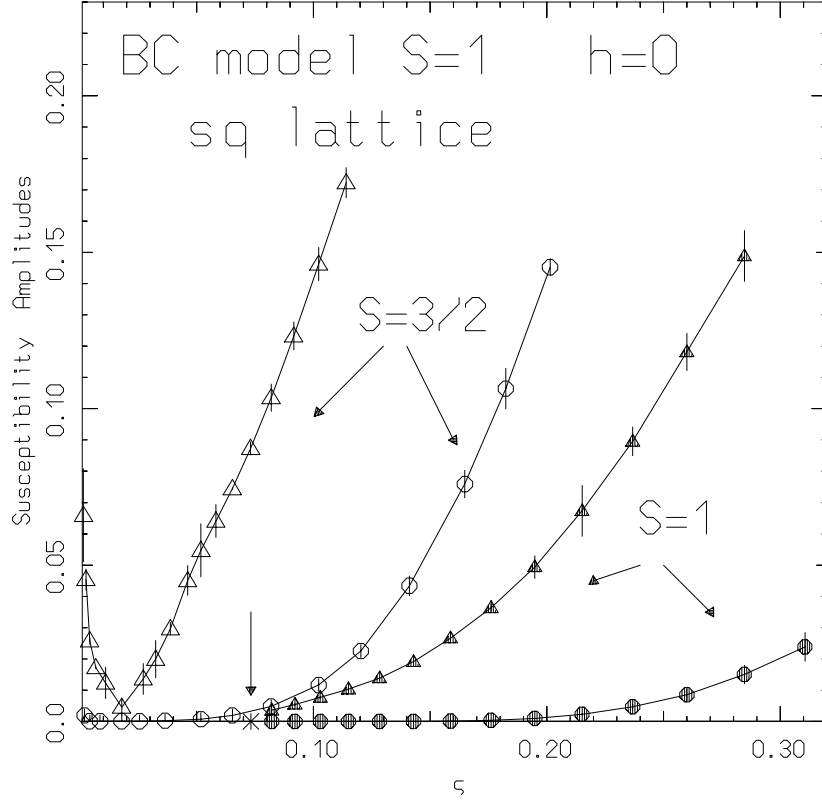


FIG. 9: BC model with spin  $S = 1$  and  $S = 3/2$  on the  $sq$  lattice, for  $h = 0$ . The critical amplitudes  $A_{(2,0)}$  of  $\chi_{(2;0)}(K, D; S)$  and  $-A_{(4,0)}$  of  $\chi_{(4;0)}(K, D; S)$  vs  $\zeta$ . The variable  $\zeta$  is  $\tau$  in the  $S = 1$  case, while for graphical convenience  $\zeta = (1 + \exp(2d))^{-1}$  in the  $S = 3/2$  case. For  $S = 1$  the amplitudes are full triangles and full circles, respectively and for  $S = 3/2$ , they are the analogous open symbols. A vertical arrow points to the expected location (star)<sup>22</sup> of the TCP. The minima in the curves of the  $S = 3/2$  susceptibility amplitudes occur at  $\Delta/Jq \approx 1/2$ .

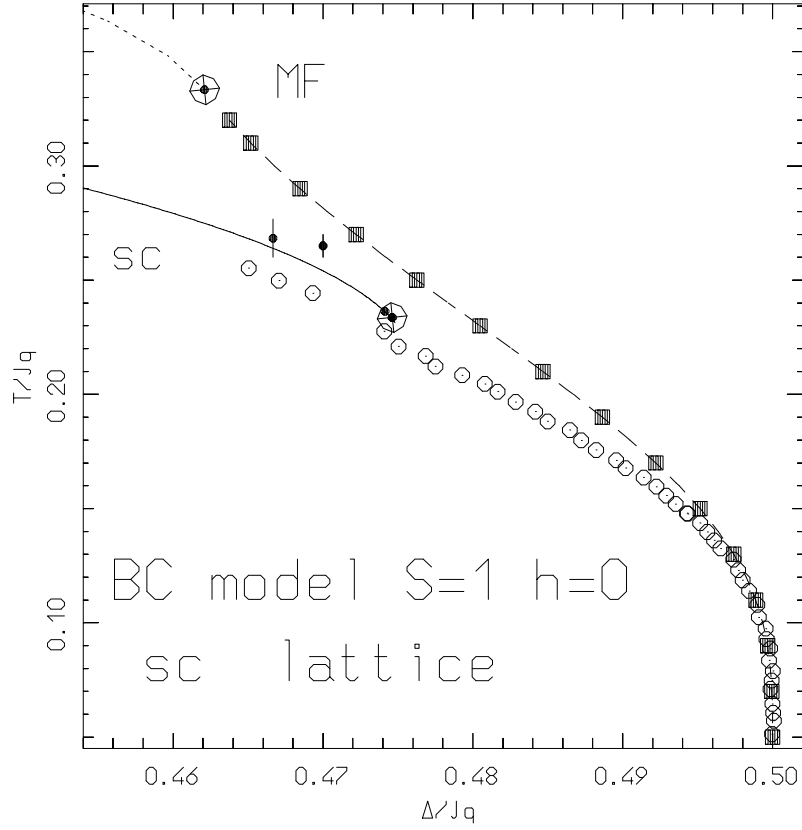


FIG. 10: BC model with spin  $S = 1$ , in the  $h = 0$  plane for the *sc* lattice. Phase diagram in the anisotropy-temperature plane, by series and in the MF approximation. Big crossed open circles are TCPs. The upper short-dashed line is the MF critical phase-contour and full squares connected by long-dashed line are the MF first-order contour. The solid curve is the critical phase-boundary from series and the TCP is taken from a simulation<sup>32</sup>. The black dots nearby the solid curve are MC points<sup>33</sup>. Open circles are points of the first-order (and the second-order) part of the phase-boundary from intersections of the LT and HT expansions of the free energy.

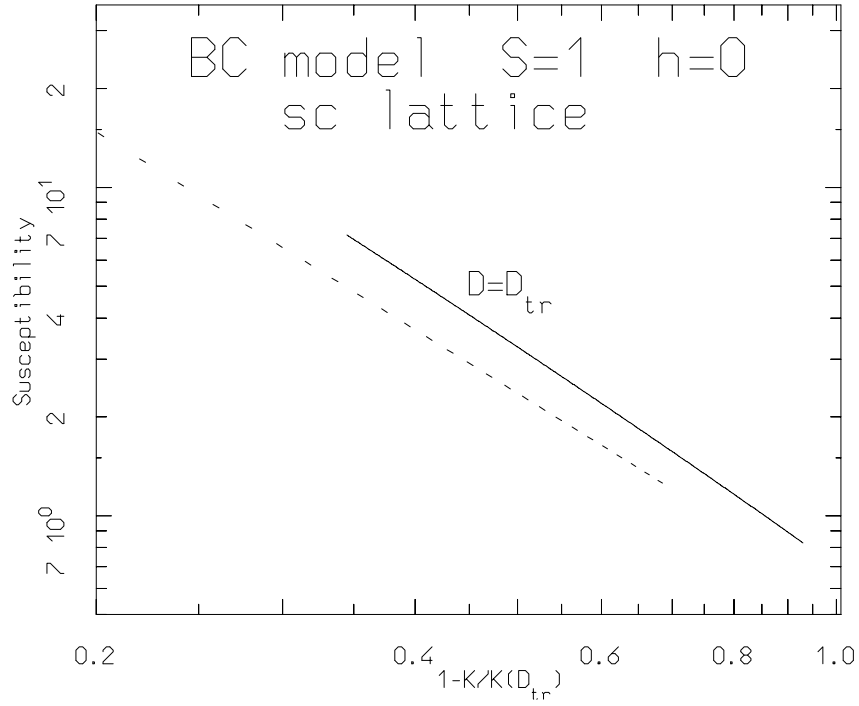


FIG. 11: BC model with spin  $S = 1$  for  $h = 0$  on the *sc* lattice. The solid line is a bilog plot of the HT expansion of the susceptibility  $\chi_{(2;0)}(K, D; 1)$  computed along the tangent to the phase-contour at  $D = D_{tr}$ . The dashed line is a simple power behavior with exponent  $\gamma_{tr} = 2$ .



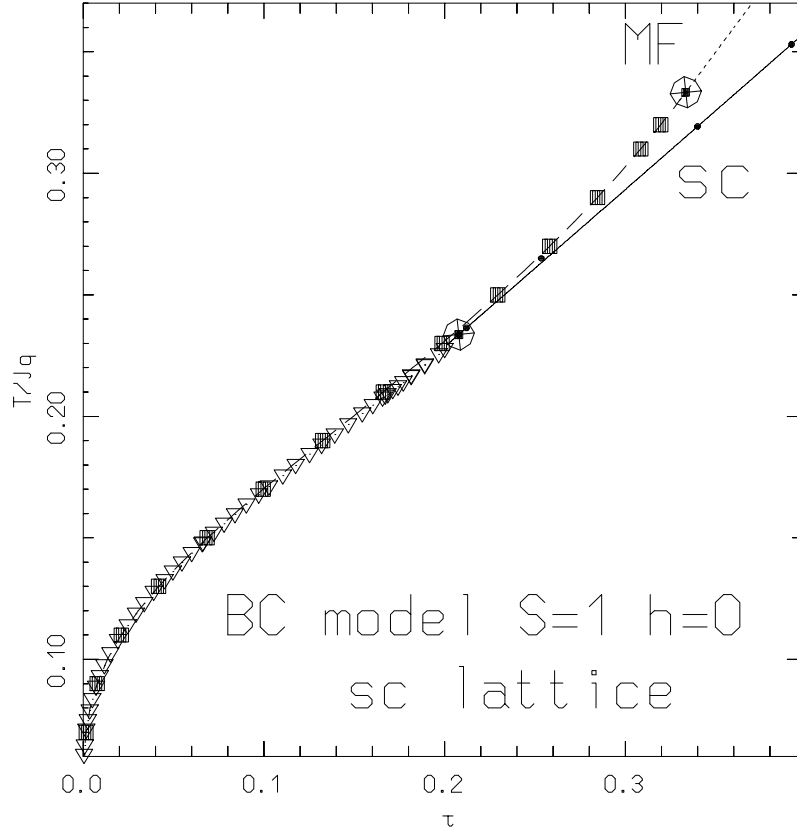


FIG. 12: BC model with spin  $S = 1$ , on the  $sc$  lattice for  $h = 0$ . Phase diagram in the  $(\tau, T/Jq)$  plane by series and in the MF approximation. Big crossed open circles are the TCPs from MF and a simulation<sup>32</sup>. The upper short-dashed line is the MF critical phase-contour and full squares connected by a long-dashed line are the MF first-order boundary. The solid curve shows the critical phase-boundary from series. Open triangles are the first-order part of the phase-boundary from intersections of the LT and HT expansions of the free energy.

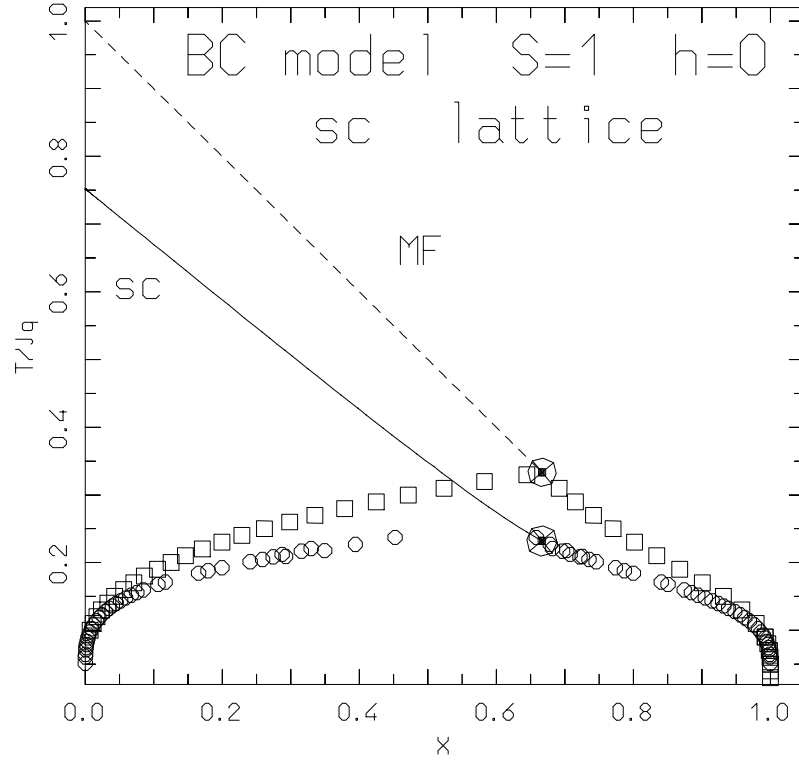


FIG. 13: BC model with spin  $S = 1$  for  $h = 0$  on the *sc* lattice. Phase diagram in the concentration-temperature plane. The dashed line is the MF approximation of the critical phase-contour. Sequences of open squares are the two branches of the phase-contour associated with the HT and the LT sides of the MF first-order line. The open circles are the corresponding branches from the series. Big crossed circles are TCPs.

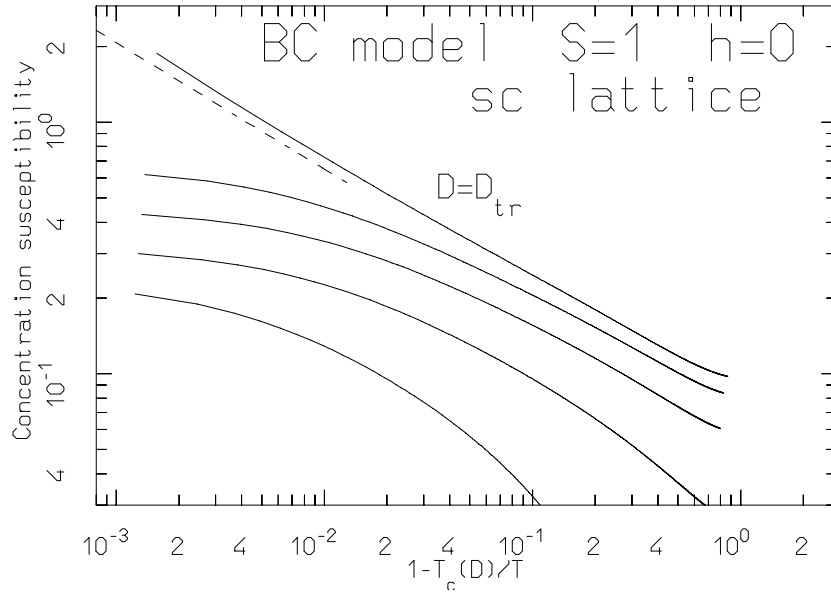


FIG. 14: BC model with spin  $S = 1$  for  $h = 0$  on the  $sc$  lattice. The uppermost solid line is a bilog plot of the PA resummed HT expansion of the concentration susceptibility  $Y(K, D; 1)$  along the path  $D = D_{tr}$  vs  $1 - T(D_{tr})/T$ . The dashed line has a simple power behavior with exponent  $\lambda = -0.5$ . The lower curves show the same quantity evaluated for  $D$  taking the sequence of four values  $0.74D_{tr}$ ,  $0.59D_{tr}$ ,  $0.44D_{tr}$ ,  $0.30D_{tr}$  and for each of them the abscissa is  $1 - T_c(D)/T$ .

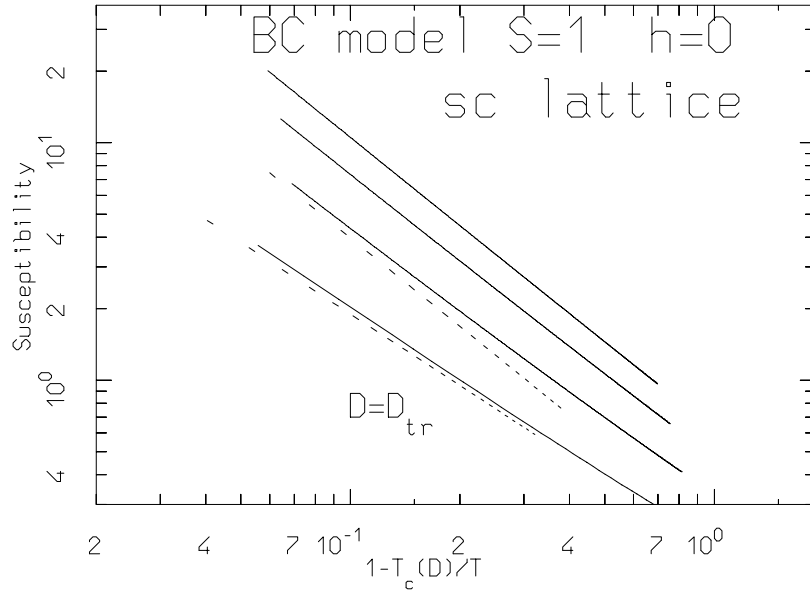


FIG. 15: BC model with spin  $S = 1$  for  $h = 0$  on the *sc* lattice. The lowermost solid line is a bilog plot of the resummed HT expansion of the ordinary susceptibility  $\chi_{(2;0)}(K, D; 1)$  along the path  $D = D_{tr}$  vs  $1 - T(D_{tr})/T$ . The lowermost dashed line has a simple power behavior with exponent  $\gamma_{tr} = 1$ . The upper curves show the same quantity evaluated for  $D$  taking the sequence of three values  $0.69D_{tr}$ ,  $0.4D_{tr}$ ,  $0.1D_{tr}$  and for each of them the abscissa is  $1 - T_c(D)/T$ . The uppermost dashed line has a simple power behavior with exponent  $\gamma = 1.237$ .

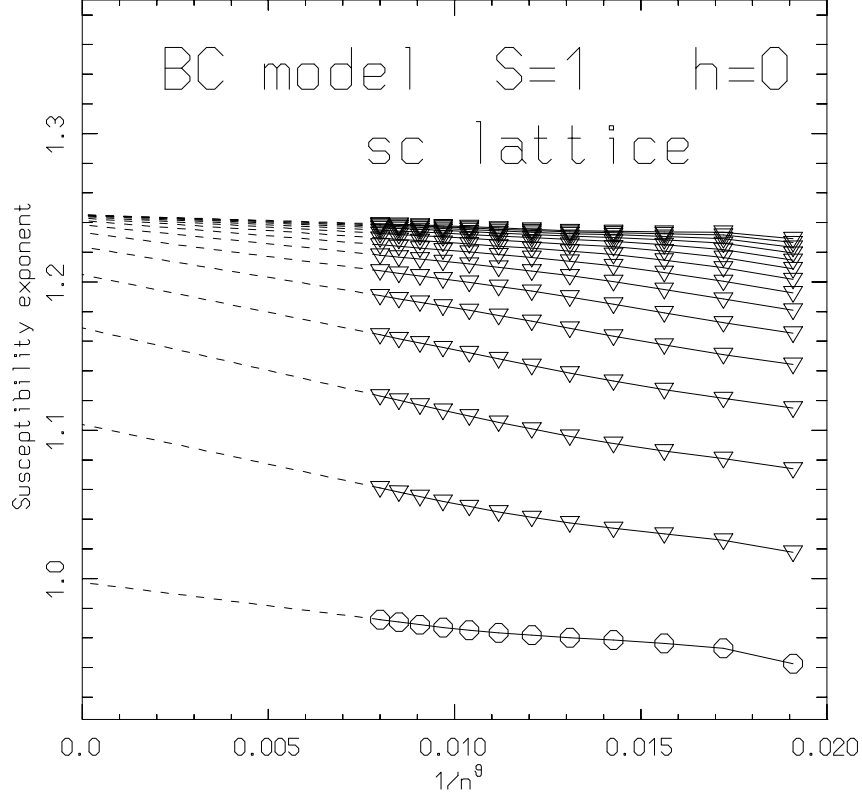


FIG. 16: BC model with  $S = 1$  on the *sc* lattice, for  $h = 0$ . MRA estimator-sequences for the exponent  $\gamma^{(2;0)}(D_{tr}; 1)$  from the mixed susceptibility  $\chi_{(2;1)}(K, D; 1)$ , vs  $1/n^\theta$  with  $\theta = 1.5$ , for several fixed values of  $D$ . The lowermost sequence (open circles) computed for  $D \approx D_{tr}$ , can be extrapolated to a value compatible with a (logarithmically corrected) MF approximation value  $\gamma^{(2;0)}(D_{tr}; 1) = 1$ . The other sequences (open triangles) are evaluated for values of  $D$  smaller by 10%, 20%, etc.

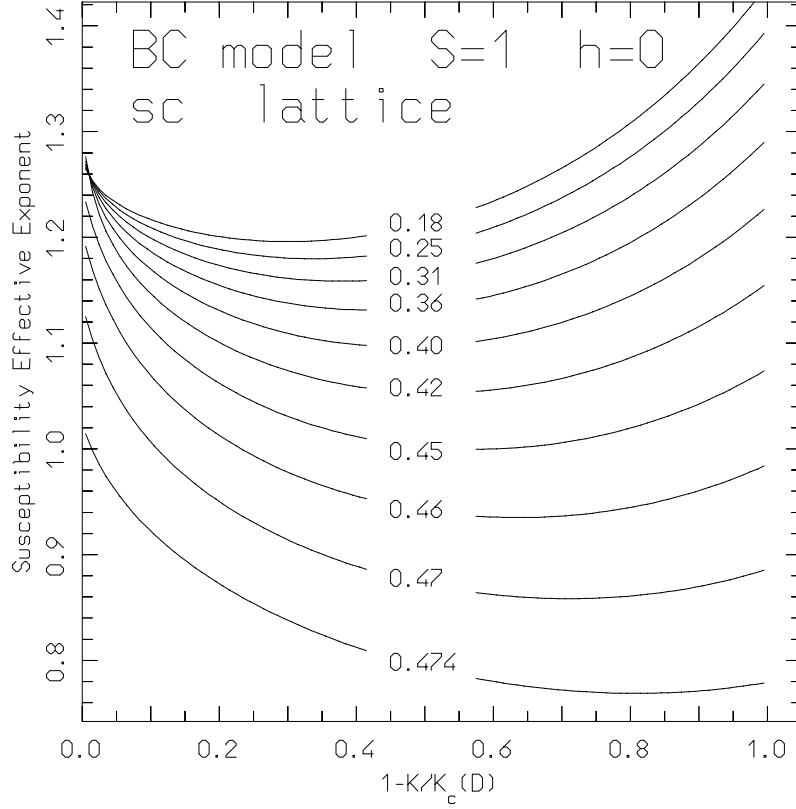


FIG. 17: BC model with spin  $S = 1$  on the  $sc$  lattice, for  $h = 0$ . The effective exponents of the susceptibility  $\chi_{(2,0)}(K, D; 1)$  vs the deviation  $1 - K/K_c(D)$  from the corresponding critical temperatures, for the values of  $\Delta_t/Jq$  indicated on the curves. The lowermost curve, computed for  $\Delta_t/Jq \approx 0.4743$ , can be extrapolated to a value of  $\gamma_t^{(2)}(D_t; 1) \approx 1.02$  compatible with the (logarithmically corrected) MF approximation value  $\gamma^{(2)}(D_t; 1) = 1$ .

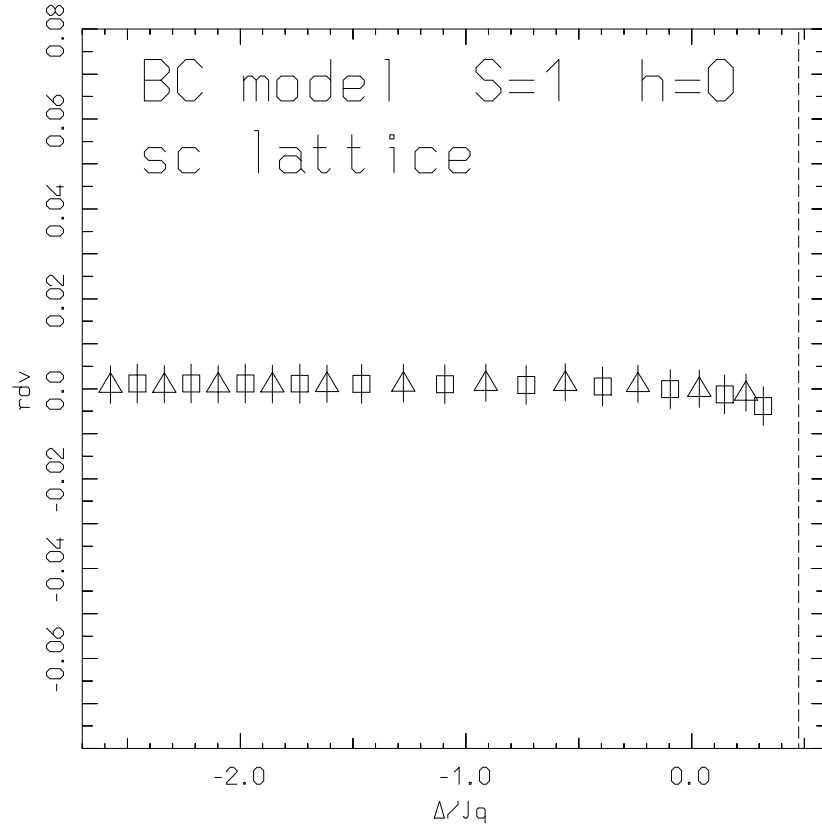


FIG. 18: BC model with spin  $S = 1$  on the  $sc$  lattice, for  $h = 0$ . The relative deviations  $r_{dv}$  from the Ising values of the extrapolated MRA estimator-sequences for the exponents  $\gamma^{(2;0)}(D;1)$  (open triangles) of  $\chi_{(2,0)}(K, D; 1)$ , and  $\gamma^{(4;0)}(D; 1)$  (open squares) of  $\chi_{(4,0)}(K, D; 1)$ . The vertical dashed line is the tricritical value  $\Delta_{tr}/Jq$  of the crystal field.

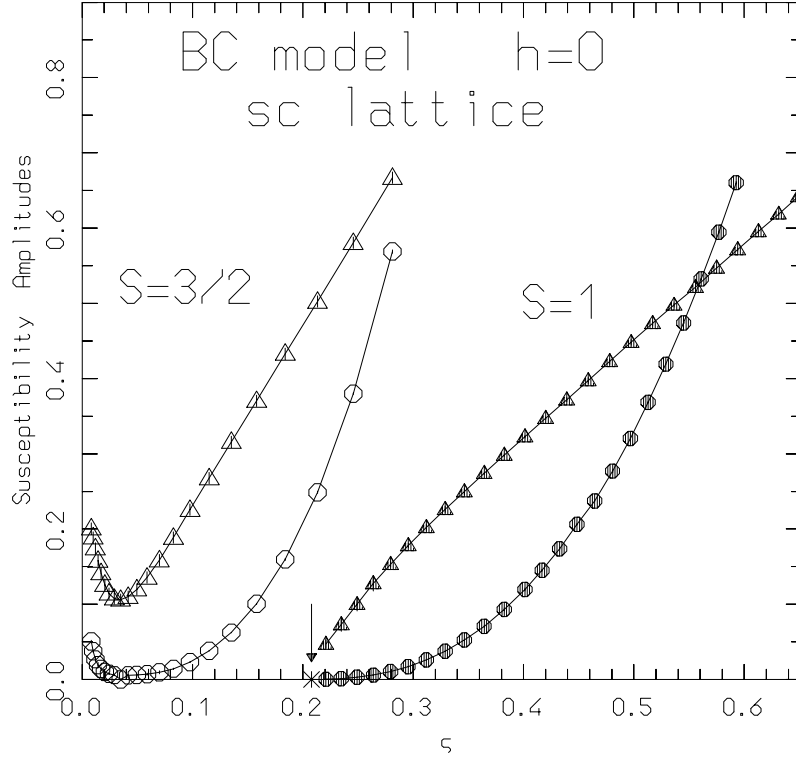


FIG. 19: BC model with spin  $S = 1$  and  $S = 3/2$  on the  $sc$  lattice, for  $h = 0$ . The critical amplitudes  $A_{2,0}$  of  $\chi_{(2;0)}(K, D; S)$  and  $-A_{4,0}$  of  $\chi_{(4;0)}(K, D; S)$  vs  $\zeta$ . The variable  $\zeta$  stands for  $\tau$  in the  $S = 1$  case, while for graphical convenience is  $(1 + \exp(2d))^{-1}$  in the  $S = 3/2$  case. For  $S = 1$  these quantities are full triangles and full circles respectively, and for  $S = 3/2$  are the analogous open symbols. In the  $S = 1$  case, a vertical arrow points to the expected location (star) of the tricritical point. The minima in the curves of  $A_{2,0}$  and  $-A_{4,0}$  for  $S = 3/2$  occur at  $\Delta/Jq \approx 1/2$ .



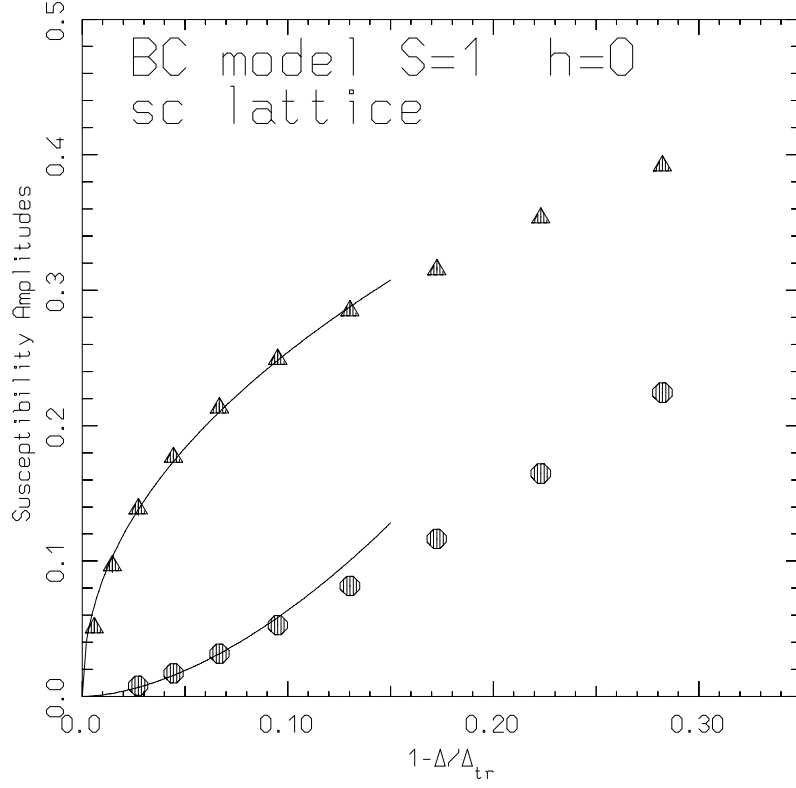


FIG. 20: BC model with spin  $S = 1$  on the  $sc$  lattice, for  $h = 0$ . The critical amplitudes  $A_{2,0}$  of  $\chi_{(2;0)}(K, D; 1)$  (full triangles), and  $-A_{4,0}$  of  $\chi_{(4;0)}(K, D; 1)$  (full circles) vs  $1 - \Delta/\Delta_{tr}$ . The solid curves are the behaviors of the amplitudes near the TCP predicted by the amplitude-scaling property with  $\phi_u = 2$ .

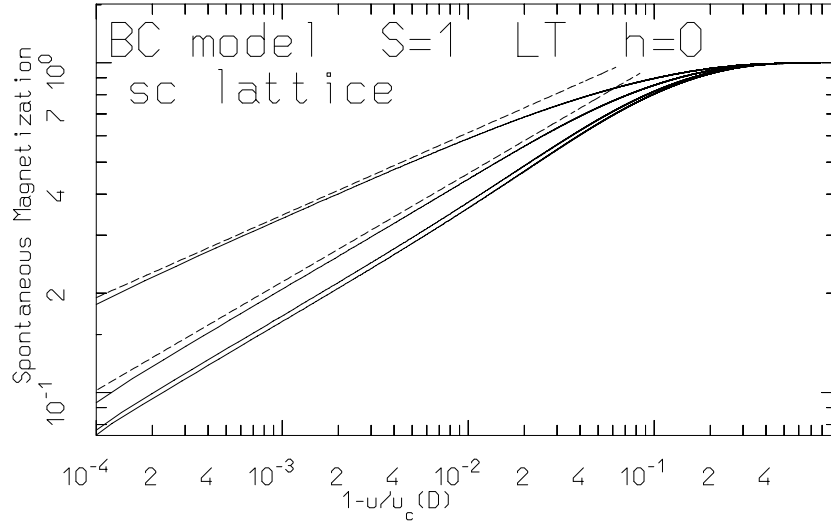


FIG. 21: BC model with  $S = 1$  on the  $sc$  lattice, for  $h = 0$ . A bilog plot of the spontaneous magnetization vs  $1 - u/u_c(D)$ . The uppermost curve is computed for  $D = D_{tr} \approx 2.031$ , while the others for the values  $D = D_{tr} - 0.35$ ,  $D = D_{tr} - 0.70$ , etc. The various curves are obtained by a [5/6] PA of the LT expansion of the spontaneous magnetization. The uppermost dashed line indicates an asymptotic value characterized by the exponent  $\beta = 0.25(1)$ , as expected at the TCP. The lowermost dashed line indicates pure power behavior with exponent  $\beta = 0.33(1)$ , shared by the curves associated to the values of  $D \ll D_{tr}$ .

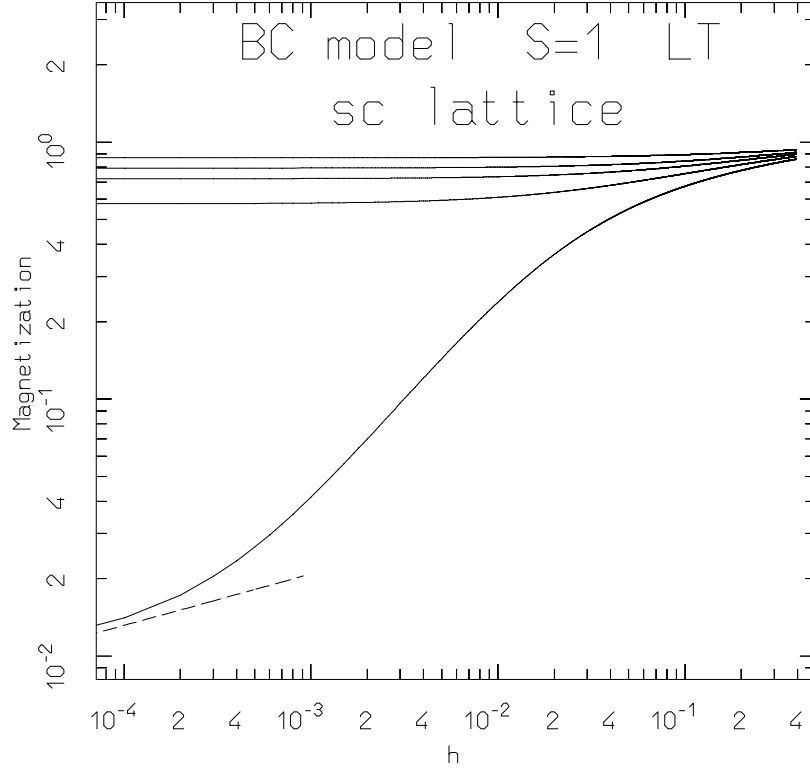


FIG. 22: BC model with  $S = 1$  on the  $sc$  lattice. A bilog plot of the magnetization at fixed  $u(D)$ , vs  $h$ . The asymptotic behavior of the lowermost curve characterized by an exponent  $\delta_{tr} \approx 5$ , is computed along the tricritical isotherm i.e. for  $u = u_c(D_{tr})$ . The other curves correspond to a sequence of decreasing values of  $u(D)$ .

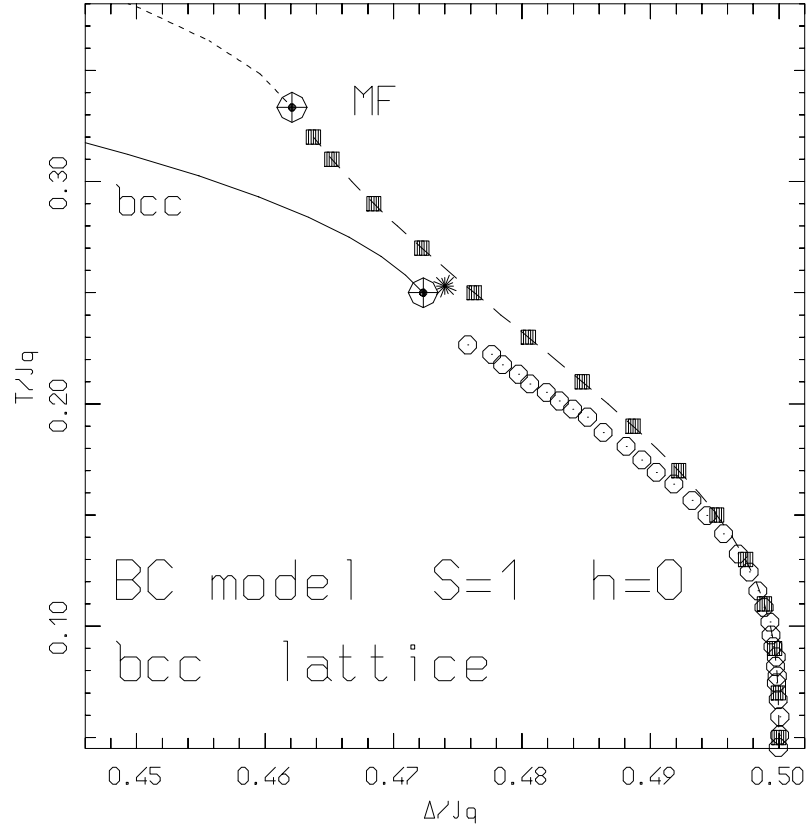


FIG. 23: BC model with spin  $S = 1$ , on the *bcc* lattice for  $h = 0$ . Phase diagram in the  $(\Delta/Jq, T/Jq)$  plane, computed by series and in the MF approximation. Big crossed open circles are TCPs, the star is taken from Ref. [15]. The upper short-dashed line is the MF critical border. Full squares connected by a long-dashed line are the MF first-order contour. The solid curve is the series result for the critical phase-contour. Open circles are points of the first-order part of the phase-contour.

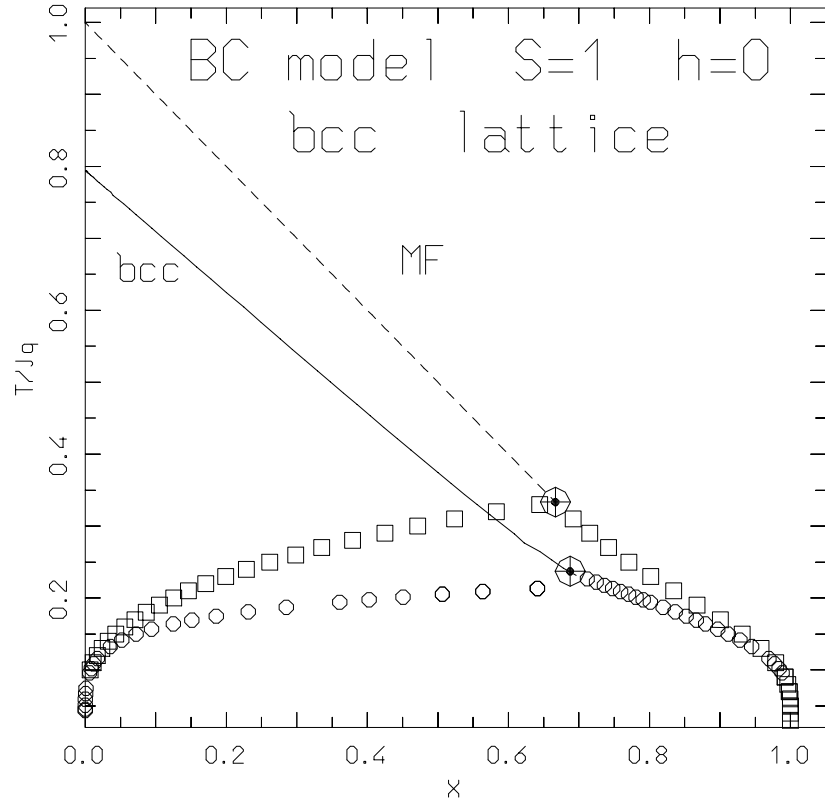


FIG. 24: BC model with spin  $S = 1$  on the *bcc* lattice for  $h = 0$ . The phase diagram in the concentration-temperature plane, computed by series and in the MF approximation. The dashed line is the MF approximation of the critical border, while sequences of open squares are the HT and the LT branches of the first-order contour. The open circles are the two branches of this line computed by series. Big crossed circles are TCPs.

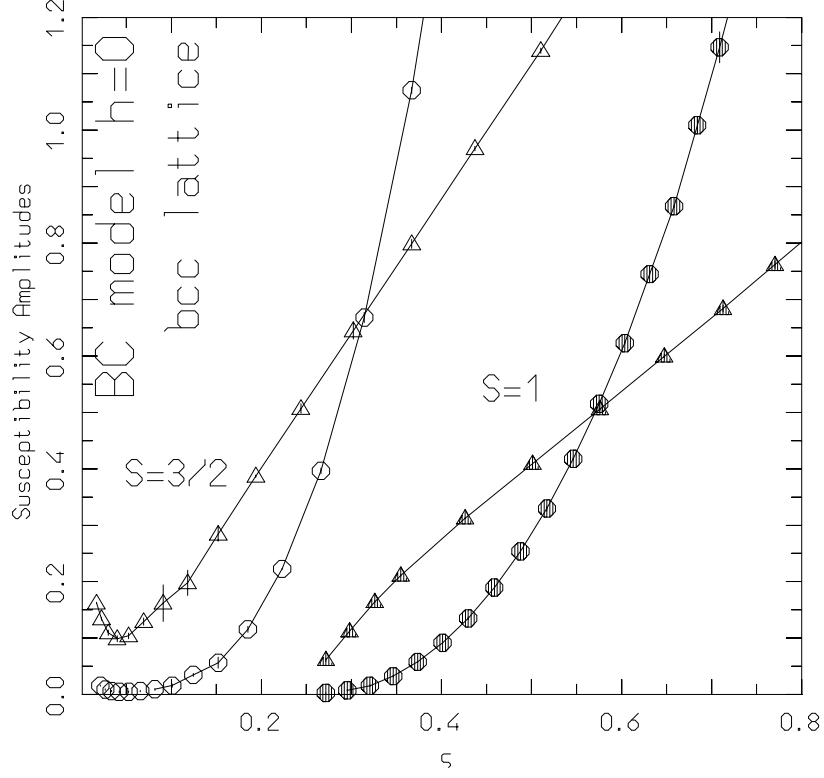


FIG. 25: BC model with spin  $S = 1$  and  $S = 3/2$  on the *bcc* lattice, for  $h = 0$ . The critical amplitudes  $A_{2,0}$  of  $\chi_{(2;0)}(K, D; S)$ , and  $-A_{(4,0)}$  of  $\chi_{(4;0)}(K, D; S)$  plotted vs  $\zeta$  that stands for  $\tau$  in the  $S = 1$  case, while for graphical convenience is  $(1 + \exp(2d))^{-1}$  in the  $S = 3/2$  case. For  $S = 1$  these quantities are full triangles and full circles, respectively. For  $S = 3/2$ , they are the analogous open symbols. The minima in the curves of  $A_{2,0}$  and  $-A_{(4,0)}$  for  $S = 3/2$  occur at  $\Delta/Jq \approx 1/2$ .

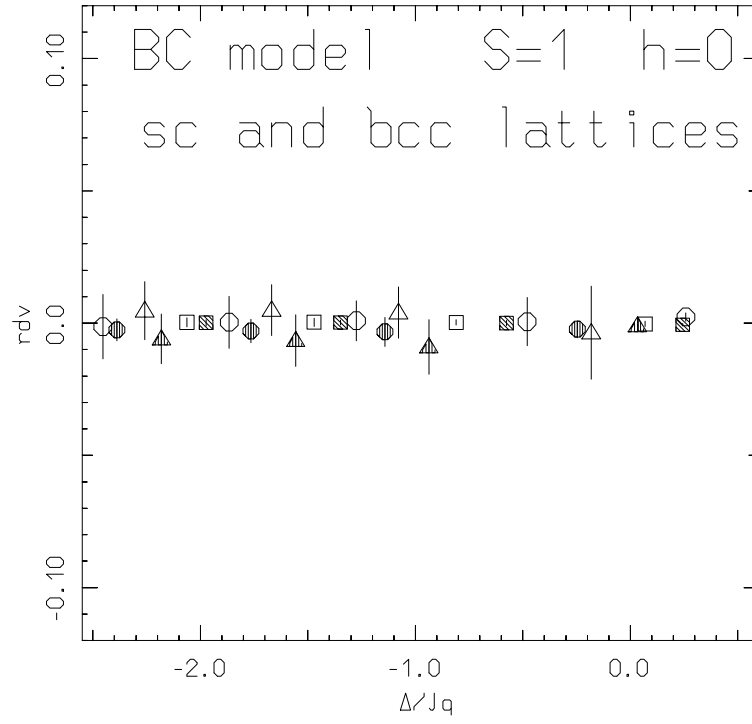


FIG. 26: BC model with spin  $S = 1$  on the *sc* and the *bcc* lattices, for  $h = 0$ . The relative deviations  $r_{dv}$  from the Ising values for the estimates of the universal ratios of critical amplitudes  $\mathcal{I}_6^+$ ,  $\mathcal{I}_8^+$  and  $\mathcal{J}_8^+$  vs  $\Delta/Jq$ . These quantities are open circles, open triangles and open squares respectively, in the case of the *sc* lattice. The analogous full symbols show the same ratios for the *bcc* lattice.

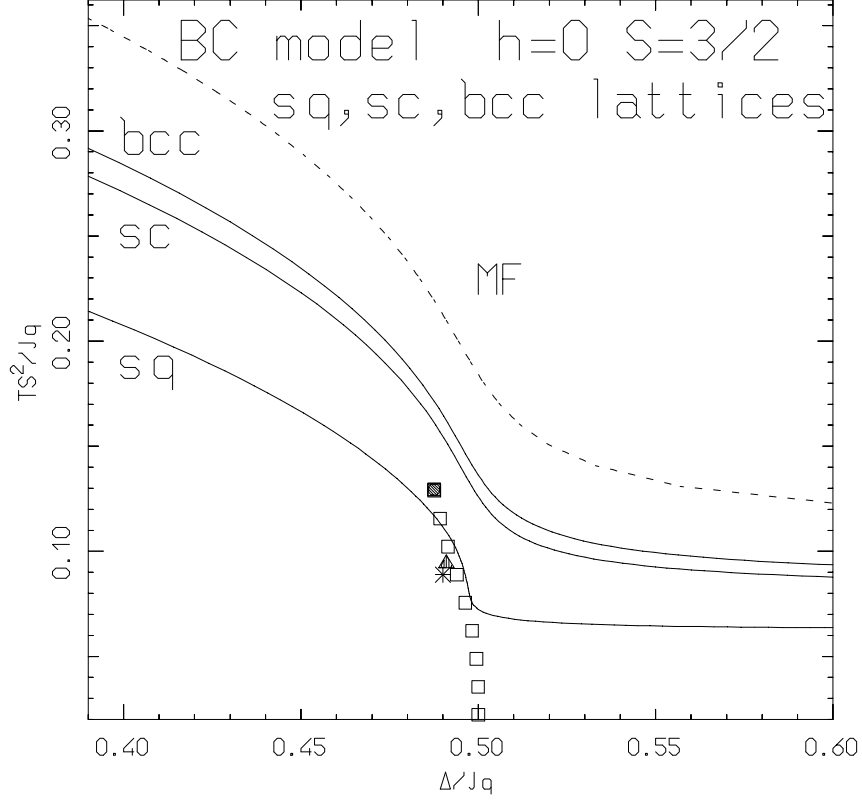


FIG. 27: BC model with spin  $S = 3/2$  in the  $h = 0$  plane. Phase diagrams in the anisotropy-temperature plane for the  $sq, sc$  and  $bcc$  lattices. The MF critical border is the upper dashed-line. The MF first-order contour is a sequence of open squares ending with a full square and not joining the critical border. The lowermost solid line is the critical phase-boundary for the  $sq$  lattice, the intermediate one for the  $sc$  lattice and the uppermost one for the  $bcc$  lattice. There is no evidence of a TCP for these lattices. A star is the end-point<sup>14</sup> of a first-order line rooted at the point  $(\tilde{\Delta} = 1/2, \tilde{T} = 0)$  for the  $sq$  lattice, and similarly a black triangle for the  $sc$  lattice<sup>16</sup>.



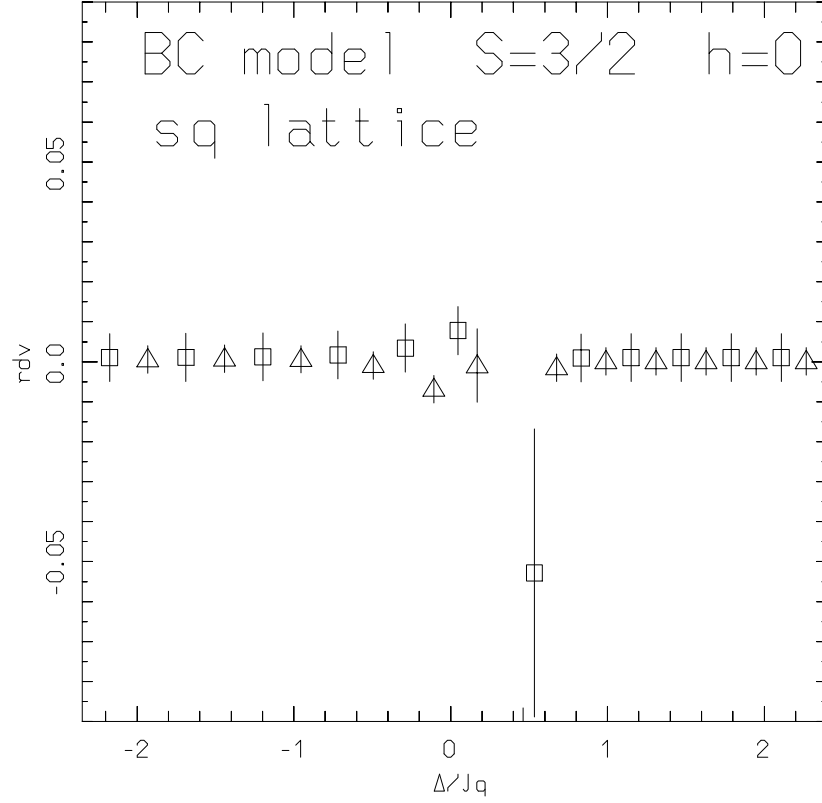


FIG. 28: BC model with spin  $S = 3/2$  on the  $sq$  lattice for  $h = 0$ . The relative deviation  $rdv$  of the extrapolated MRA estimator-sequences from the Ising values for the exponents  $\gamma^{(2;0)}(D; 3/2)$  (open triangles) of  $\chi_{(2;0)}(K, D; 3/2)$  and  $\gamma^{(4;0)}(D; 3/2)$  (open squares) of  $\chi_{(4;0)}(K, D; 3/2)$  vs  $\Delta/Jq$ .

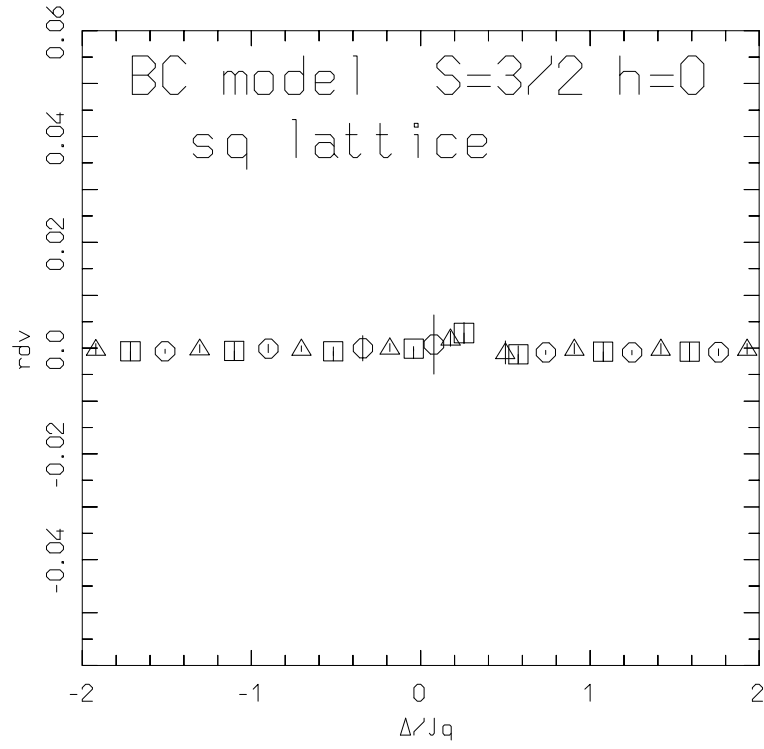


FIG. 29: BC model with spin  $S = 3/2$  on the  $sq$  lattice for  $h = 0$ . The relative deviations  $rdv$  of the universal ratios of critical amplitudes  $\mathcal{I}_6^+$  (open circles),  $\mathcal{I}_8^+$  (open triangles) and  $\mathcal{J}_8^+$  (open squares) from the corresponding  $2d$  Ising values vs  $\Delta/Jq$  in the range  $-2 < \Delta/Jq < 2$ .

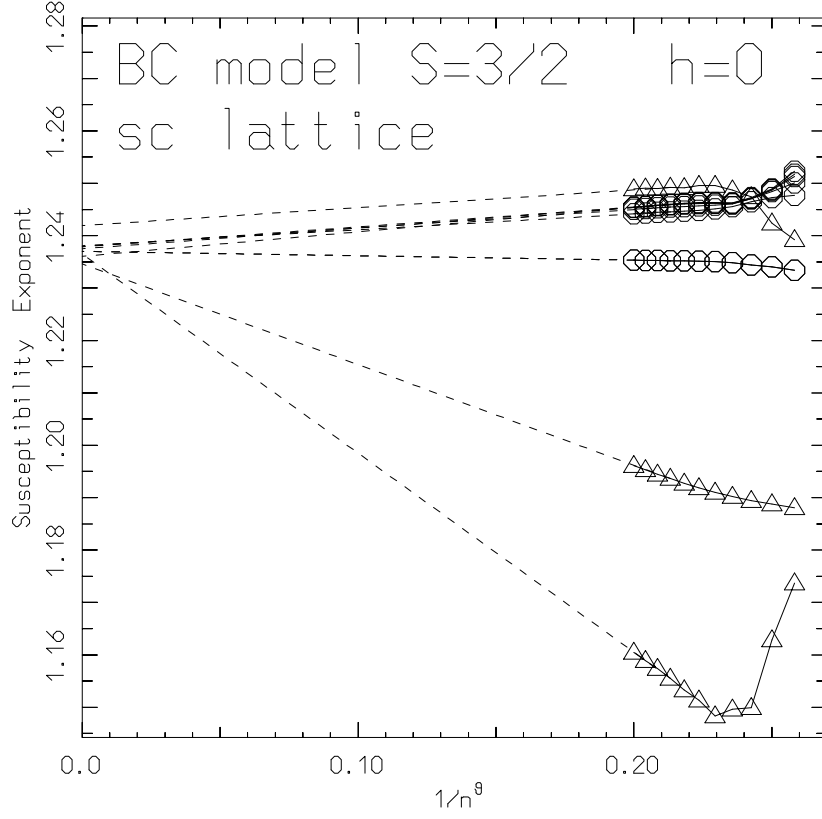


FIG. 30: BC model with spin  $S = 3/2$  on the  $sc$  lattice, for  $h = 0$ . The MRA estimator-sequences for the exponent  $\gamma^{(2;0)}(D; 3/2)$  vs  $1/n^\theta$ , with  $n$  the number of terms included in the series and  $\theta = 0.5$ , for several values of  $-1.5 \lesssim \Delta/Jq \lesssim 0.85$ . The terms of the sequences are in general indicated by open circles, except those with  $0.44 \lesssim \Delta/Jq \lesssim 0.57$  indicated by open triangles. To profile the behavior of each sequence, the symbols of the successive terms are connected by segments. The dashed lines are the sequence extrapolations to large  $n$ .

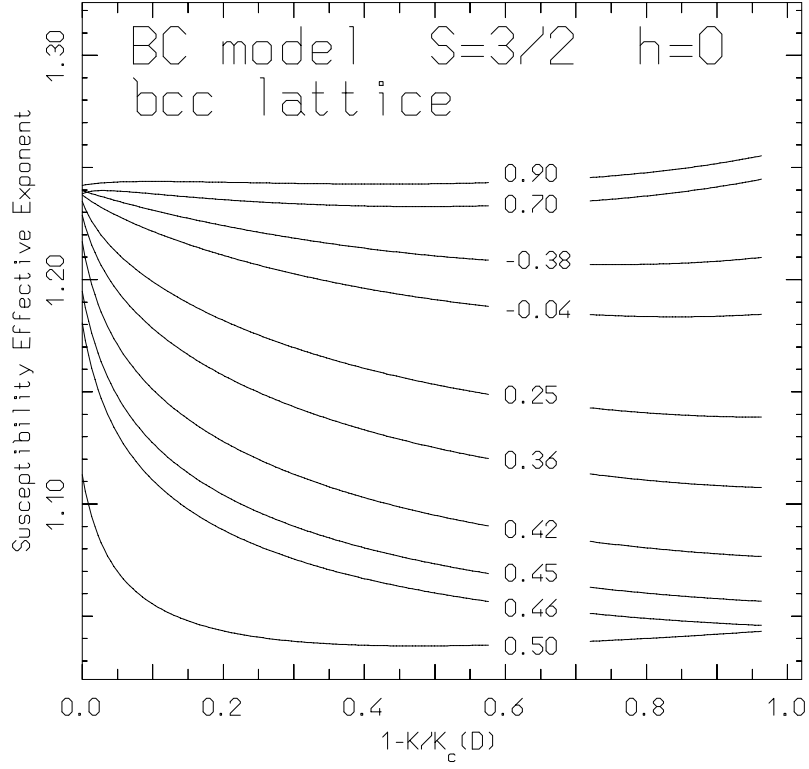


FIG. 31: BC model with spin  $S = 3/2$  on the *bcc* lattice, for  $h = 0$ . The effective exponents of the susceptibility  $\chi_{(2,0)}(K, D; 1)$ , for several fixed values of  $\Delta_c/Jq$ , vs the deviation  $1 - K/K_c(D)$  from the corresponding critical temperatures. The value of  $\Delta_c/Jq$  is indicated on each curve.